Synthesis and immobilization of linked Wnt-signaling pathway inhibitor on organic monoliths as a proof-of-concept of a *capti remedium ad monolitus* reactor for online drug deconvolution

Christine Olsen

Thesis for the Master's degree in Chemistry

60 credits

Department of Chemistry
Faculty of Mathematics and Natural Sciences

UNIVERSITY OF OSLO

24/01-2019

Synthesis and immobilization of linked Wnt-signaling pathway inhibitor on organic monoliths as a proof-of-concept of a *capti remedium ad monolitus* reactor for online drug deconvolution

The big search for tankyrase

Christine Olsen

Thesis for the Master's degree in Chemistry

60 credits

Department of Chemistry

Faculty of Mathematics and Natural Sciences

University of Oslo

24. January 2019

2018

Synthesis and immobilization of linked Wnt-signaling pathway inhibitor on organic monoliths as a proof-of-concept of a *capti remedium ad monolitus* reactor for online drug deconvolution.

Christine Olsen

http://www.duo.uio.no/

Print: Reprosentralen, University of Oslo

Abstract

A challenge in drug discovery is the identification of the drug target, called drug deconvolution. Additionally, off-target effects are considered as one of the reasons many developed drugs fail in the clinical trials. The goal of this work was to develop a solid support, displaying low secondary interactions, for immobilization of drugs (named by author as a CRAM reactor) suitable for incorporation online liquid chromatography mass spectrometry set-ups. The hypothesis was that selective purification on the online reactor would allow identification of low abundant drug targets as a consequence of reduced handling time, contamination and loss of the sample.

As a proof-of-concept, an ethylene dimethacrylate-co-vinyl azlactone (EDMA-co-VDM) monolith, prepared in 180 µm inner diameter (ID) or 250 µm ID polyimide-coated fused silica capillaries, would be immobilized with Wnt-signaling pathway inhibitor 161. The 161-immobilized CRAM reactor would then attempt to selectively trap and release a low abundant protein target, tankyrase 2 (TNKS2).

The EDMA-co-VDM monolith was successfully prepared in 250 µm ID capillaries. The Wnt-inhibitor 161 was rejected based on MS characterization and LDW639, a structural analogue of Wnt-inhibitor XAV939, was successfully synthesized by the author. To improve availability of LDW639 after immobilization, a linker was attached to LDW639 during synthesis. The linked LDW639 showed 50% inhibition of the Wnt-signaling pathway at a concentration of 11 µM after 24 hours incubation in cells.

The EDMA-co-VDM monolith showed secondary interactions towards proteins, but the issues were resolved by quenching the reactive VDM monomer with either monoethanolamine (MEA) or an excess of linked LDW639. Immobilization of the linked LDW639 was found to be successful based on measured UV-Vis absorbance of solutions containing LDW639 was reduced by flushing a monolith, but not by monoliths already flushed with MEA (MEA monolith).

The linked LDW639-immobilized CRAM reactors and the MEA monolith were not able to trap and release TNKS1/2 from human embryonic kidney 293 cells after cell lysis with a non-denaturing buffer. Showing that the identification of the drug target from complex matrices remained a challenge, even with tailored materials.

Preface

The work presented in this thesis was mainly performed at the Bioanalytical Chemistry research group at the Department of Chemistry, University of Oslo from January 2017 to January 2019. First and foremost, I would like to express my gratitude to my supervisors for their excellent guidance and support; Associate Professor Steven Ray Haakon Wilson, PhD candidate Frøydis Sved Skottvoll, Dr. Ole Kristian Merkesvik Brandtzæg, Professor Pål Rongved and Professor Elsa Lundanes. Especially Steven for his crazy suggestion of synthesizing a Wnt-inhibitor from scratch, and Ole for his continuous support and help with monoliths since my Bachelor project. Furthermore, a thanks to Dr. Hanne Røberg-Larsen and PhD candidate Henriette Engen Berg for answering all of my questions and providing interesting discussions. Thanks to Inge Mikalsen for all technical support and troubleshooting. To the previous and present Master students; thank you for a motivating environment and productive collaborations.

Secondly, thanks to Professor Pål Rongved and Dr. Christian Schnaars at the section of Pharmaceutical Chemistry at the School of Pharmacy for allowing me to use your space and equipment for synthesis. Thank you for all your help and guidance, and making the experience with synthesis a great one. Thanks to Senior Engineer Dirk Petterson for your help with NMR. Thanks to Engineer Osamu Sekiguchi for providing MS characterization during synthesis.

Thank you to the Unit of Cell Signaling at Oslo University Hospital for their help with evaluation of the synthesized inhibitor and for letting me use their equipment for western blotting. Especially to Dr. Petter Angell Olsen and Dr. Nina Therese Solberg for all their help with cells and discussions of western blot, and Dr. Jo Waaler and Technician Eric Maximilian Lycke for help with determination of the activity of the synthesized inhibitor.

To my family and Therese Katrina, a huge thank you, and appreciation of your everlasting support. Thanks to my brother for reading my thesis and offering feedback.

A multitude of techniques in analytical chemistry were used to characterize the reactors that were under development in this study. The background of these analytical techniques have been covered in course curriculum in both bachelor studies in chemistry and master studies in analytical chemistry, and will therefore not be elaborated upon in the introduction part of this thesis. For the sake of brevity, the thesis focuses on the chemistry of the reactors, not the "biological methods" used for assessment of the trapping potential of these reactors.

Abbreviations

AIBN	α,α‘-Azobisisobutyronitrile
ABC	Ammonium bicarbonate
ACN	Acetonitrile
AGC	Automatic gain control
AmAc	Ammonium acetate solution with pH 7.2
APC	Adenomatous polyposis coli
ARC	Ankyrin repeat cluster
ARTD	ADP-ribosyltransferase
BCA	Bicinchoninic acid
Bis-tris	2-Bis (2-hydroxyethyl) amino-2-(hydroxymethyl) propane-1,3-diol
BSA	Bovine serum albumin
CRAM	*Capti remedium ad monolitus*
DARTS	Drug affinity response target stability
DCM	Dichloromethane
dd	Data dependant
DMF	N,N-Dimethylformamide
DMSO	Dimethyl sulfoxide
DPPH	2,2-Diphenyl-1-picrylhydrazyl
DTT	Dithiothreitol
ECL	Enhanced chemiluminescence
EDMA	Ethylene dimethacrylate
EDTA	Ethylenediaminetetraacetic acid
ELISA	Enzyme-linked immunosorbent assay
ESI	Electrospray ionization
FA	Formic acid
FDA	U.S. food and drug administration
GMA	Glycidyl methacrylate
GSK	Glycogen synthase kinase 3
HATU	2-(7-Aza-1H-benzotriazole-1-yl)-1,1,3,3-tetramethyluronium hexafluorophosphate

HCD	Higher-energy collision dissociation
HEK293	Human embryonic kidney 293 cells
HEK293-EGFP-TNKS1	Human embryonic kidney 293 cells treated with enhanced green fluorescence protein for overexpression of tankyrase 1
HESI	Heated electrospray ionization
HPLC	High performance liquid chromatography
HPR	Horseradish peroxidase
HPS	Histidine-Serine-Proline rich domain
HSA	Human serum albumin
IAM	Iodoacetamide
ID	Inner diameter
IMER	Immobilized enzyme reactor
IUPAC	International union of pure and applied chemistry
LC	Liquid chromatography
LC-MS	Liquid chromatography mass spectrometry
LDS	Lithium dodecyl sulfate
MBA	Methylene-bis-acrylamide
MEA	Monoethanolamine
MeOH	Methanol
MoA	Mechanism of action
MOPS	3-Morpholinopropane-1-sulfonic acid
MS	Mass spectrometry
NL	Normalized level
NMM	4-Methylmorpholine
^{1}H-NMR	Proton nuclear magnetic resonance
OD	Outer diameter
OT	Open tubular
PAGE	Polyacrylamide gel electrophoresis
PARP	Poly (ADP-ribose) polymerase
PDD	Phenotype-based drug discovery
PEEK	Polyetheretherketone
PEG	Polyethylene glycol
PLOT	Porous layer open tubular

PTM	Post-translational modifications
PVDF	Polyvinylidene difluoride
rcf	Relative centrifugal force
REN	Renilla
RIPA	Radioimmunoprecipitation assay
RP	Reversed phase
RT	Room temperature
SAM	Sterile alpha motif
SAR	Structure-activity relationship
SDS	Sodium dodecyl sulfate
SEM	Scanning electron microscopy
SP	Stationary phase
STF-Luc	SuperTOPFlash – luciferase
SPROX	Stability of proteins from rates of oxidation
t-BOC	*Tert*-butyloxycarbonyl
TBS-T	Tris buffered saline with Tween™
TDD	Target-based drug discovery
TFA	Trifluoroacetic acid
TICC	Target identification by chromatographic co-elution
TLC	Thin layer chromatography
TNKS	Tankyrase
UV	Ultraviolet
UV-Vis	Ultraviolet-visible
VDM	4,4-Dimethyl-2-vinyl-2-oxazolin-5-one (Vinyl azlactone)
WB	Western blot
ɣ-MAPS	3-(Trimethoxysilyl)propylmethacrylate

Table of contents

1 Introduction

1.1 Drugs and their functionalities

In all organisms the chemical reactions occurring in the cells are responsible for communication, signaling and coordination of cell activities. These chemical reactions are dependent on small molecules, but also on large molecules (macromolecules) *i.e.* proteins and nucleic acids. By affecting these macromolecules, changes may occur in the different physiological systems in the human body, such as the cardiovascular system or the endocrine system. In the instance of a disease (*e.g.* a disturbance in the function of a physiological system), a drug may be introduced to repair the occurring disorder in the cellular reactions. That means drugs are by definition compounds that interact with a biological system to produce a biological response [1, 2] ([1] p.1-3, [2] p. 43-45).

Drugs cause the beneficial response by affecting *e.g.* enzymes, receptors, transport proteins, DNA and RNA, and may be classified according to their mechanism of action (MoA). An overall description in medicinal chemistry is that drugs are either an agonist or an antagonist. An agonist, **Figure 1A,** is designed to bind to *e.g.* a receptor in the same manner as the natural substrate and activate the reaction. On the other hand, an antagonist, **Figure 1B**, binds to the *e.g.* receptor, blocks the natural substrate and prevents the reaction from proceeding [1] (p. 88-119).

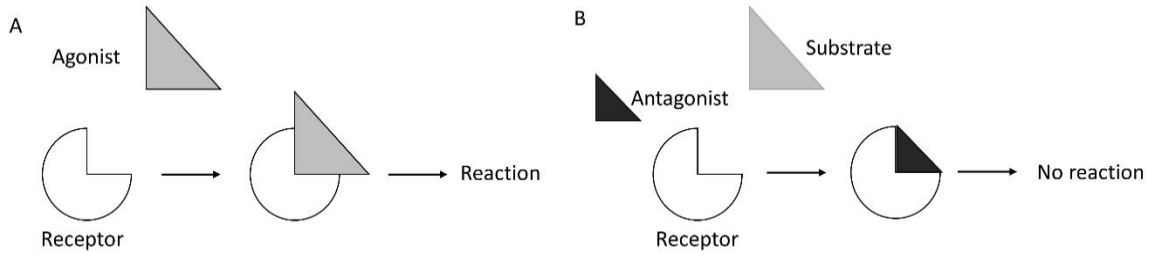

Figure 1: A, mechanism of an agonist. B, mechanism of an antagonist. The receptor is an example of a target molecule.

The binding site for the drug-target interaction is often a cave or a pocket on the surface of the target macromolecule. Here, the drug may form temporary intermolecular bonds or more permanent covalent bonds with the binding regions (*i.e.* specific binding partners within the binding site) on the target macromolecule. The small side chains on the main structure on the drug, *i.e.* the ligands, can recognize and bind to the specific regions. The affinity of the binding

is a measure of the strength at which the ligands bind to its target region. The covalent bonds may have a bond strength of 200-400 $kJmol^{-1}$, while the weaker intermolecular bonds (*e.g.* ionic interactions and hydrogen bonds) have bonds strength of 16-60 $kJmol^{-1}$. An equilibrium arises between target bound to the drug and target not bound, this equilibrium depends on the strength of the interaction between drug and target. In order to have an effective drug, the bonding strength must be sufficiently high for the drug to be able to affect the target, but the bonding strength should not be too high as the drug might not release the target after its job is done [1] (p. 4-11). For an antagonist, a measure of efficiency is the IC_{50} value (*i.e.* the concentration of the antagonist required to inhibit *e.g.* an enzyme by 50%).

The functionality of the drug does not only depend on the chemical functionalities of the ligands, but also on how they are sterically placed on the main structure of the drug and their interaction with each other [3, 4] ([4] p. 1-2). The complexity of the interaction between the ligands and the binding regions of the target macromolecules is revealed from the definition of the pharmacophore by the International Union of Pure and Applied Chemistry (IUPAC); "A pharmacophore is the ensemble of steric and electronic features that is necessary to ensure the optimal supramolecular interactions with a specific biological target structure and to trigger (or to block) its biological response".

In modern drug discovery, the interaction between the binding pocket of the target and the ligands on the drugs has been important for innovation of new drugs. X-ray crystallography has been used for determination of the atomic and molecular structure of biological molecules, and cocrystallization of drugs has revealed binding sites [5-8]. The chemical structure of the drug and their functional ligands has been optimized concerning the drugs ability to fit and bind into the binding pocket (*i.e.* docking), and the affinity of the ligands by several computation methods [9-13]. These studies can be called structure-activity relationship studies (SARs), and aim to optimize the pharmacophore.

1.2 Drug discovery based on target or phenotype

The process of drug discovery and development from initial tests to an approved drug on the marked is a very complex and costly venture, with a low possibility of success and high time consumption [14, 15]. As a consequence, the decisions of what kind of drug a pharmaceutical company want to produce not only relies on the present medical needs, but on how to maximize

the probability of success in the drug approval process and economic pay-off in the end [1] (p. 274-281).

The two main strategies for drug discovery are target-based drug discovery (TDD) and phenotype-based drug discovery (PDD). The difference between the two strategies is whether or not the biological target for the drug-in-development is known (TDD) or not (PDD), shown in **Figure 2**.

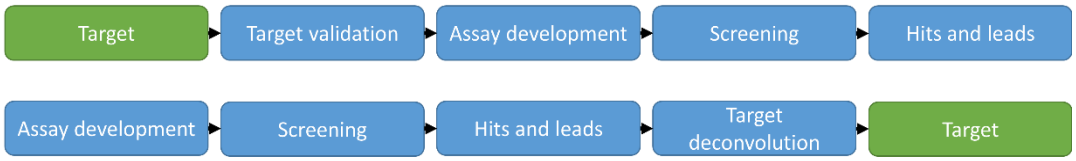

Figure 2: Scheme of target-based (Top) and phenotype-based (Bottom) drug discovery. In the target-based strategy, molecular targets are validated and used in assays and screens to find a possible structure of the drug. In the phenotype-based strategy, the drug is selected first, and the possible targets causing the observable phenotype in assays and screens need to be identified. Adapted from [16].

An identified target and an understanding of the MoA of the drug is a prerequisite for using TDD. This strategy is based on a high throughput computational assay, which screens libraries of compounds for drugs showing the needed characteristics to affect the target, often with a knowledge of a fitting MoA. Due to the cost of developing drugs, the industry has classified targets as novel, established, or validated [2] (p. 43-45). This classification is based on how certain it is that a target is involved in the disease and that by affecting this target, the positive effects outweigh the negative risks from the treatment, giving a positive net clinical benefit. Novel targets are speculated to be important to a disease, and the clinical benefit from treatment through this target is unknown. Established targets are understood both in a healthy and a disease-ridden physiology, and there have been developed prototypic drugs, but the clinical benefit still remains unknown. Validated targets have confirmed beneficial therapeutic effect on the disease when affected by a drug. When developing new drugs for validated targets, the goal is to make a more efficient treatment by *e.g.* reducing dosages and side effects.

For drugs targeting proteins, an average of 18 new drugs were approved by the U.S. Food and Drug administration (FDA) annually [17]. Of these 18, only 4.3 drugs targeted novel targets. The classification of drug targets was meant to provide the industry with a higher success rate for newly developed drugs reaching the marked, but it has also been considered as one of the reasons for the failure of TDD as a strategy of drug discovery. The failure is due to several developers selecting the same target and MoA, giving a very narrow selection of drugs being

developed in the same time periode. Another debated reason for the failure of TDD is that many developed drugs show low efficiency, and issues with toxicity during the clinical trials. This comes from a too limited consideration of the developed drugs having interaction with macromolecules besides the target and affecting other cellular reactions, this is called off-target effects [17-19].

PDD relays on observable traits caused by potential compounds affecting a relevant physiological environment, *e.g.* mammalian cell lines or small animal models. These unbiased phenotypic screens searches for the most efficient and least toxic treatment, without knowledge of the drugs target or MoA. An issue with PDD has been the degree of translatability from animal models to the human biology. However, other models are under development (*e.g.* organ-on-a-chip, human organoids on microfluidic chips), and the hope is that animal models will become redundant and that findings in the new models will have an effective predictability of how drugs affect the entire human body [20].

The phenotypic screens also have the advantage of revealing several targets causing an observable trait. The screens may also identify possible biological pathways and drug MoA causing a beneficial response linked to the disease. At the same time PDD can showcase potential toxicity issues and side effects at different dosages. However, the massive output of information becomes a critical challenge when searching for the molecular target of active hits (screens showing the desired phenotype). The molecular target must be identified and confirmed to cause the beneficial response in the phenotypic screening. Only then can the optimization of the drug continue, and the MoA of the drug be understood. This process of target identification has been called “target deconvolution” and is considered as the bottleneck of PDD [16, 21, 22].

1.3 Target deconvolution in phenotypic drug discovery

The drugs in development may target one or several nucleic acids, carbohydrates, lipids or proteins in the cellular system. To progress the development of drugs, an efficient, high-throughput and accurate target identification from phenotypic screens is needed [23, 24].

As there are a multitude of deconvolution methods available, this project will focus on methods confirming cellular targets, and most importantly proteins. This is due to the fact that as of

2013, 44% and 29% of all drug targets are protein receptors and enzymes, respectively [2] (p. 46-49). Examples of deconvolution methods are drug affinity response target stability (DARTS), target identification by chromatographic co-elution (TICC), stability of proteins from rates of oxidation (SPORX) and affinity chromatography. The three former techniques are presented as examples of label-free techniques, while affinity chromatography is in focus in the present study.

The strategies mentioned above utilizes high performance liquid chromatography-mass spectrometry (HPLC-MS) for detection of the proteins. Briefly explained, HPLC-MS or more commonly notated LC-MS is a technique for separation and detection of compounds in a mixture by applying small samples onto an analytical column for separation prior to MS detection. The separation on the analytical column occurs due to interactions between the stationary phase (often hydrophobic) on the column and the compounds. The compounds are subsequently detected and identified due to their size and charge by MS [13, 25-27]. A more detailed description of LC-MS is given in **Introduction 1.5.4**.

1.3.1 Drug affinity response target stability

DARTS was developed by Lomenich *et al.* [25] as a universally applicable technique that did not need to modify the drugs, and to be independent of the MoA of the drugs. The strategy of DARTS is that a protein is less susceptible to proteolysis when it is bound to a drug compared to existing in free form. This means that the protein target of the drug will remain intact after digestion with a protease [13, 25]. Proteins resistant to digestion can be determined by *e.g.* gel electrophoresis (*i.e.* separation of macromolecules on a gel according to size and charge in an electric field). By protease digestion of a piece of this gel, the proteins present may be identified with MS and database searches [28, 29].

1.3.2 Target identification by chromatographic co-elution

Another strategy that does not depend on modification of the drug is TICC, which monitors interactions between drug and target with LC-MS. TICC is based on considerations of retention time (*i.e.* time from application of sample to the compound elutes from the column). The key aspect is that drugs not bound to the target have a different retention time compared to drug bound by the target. The drug-target interaction will affect the drug in such a way that it will experience a shift in retention and be eluted as a drug-target complex at the expected retention

time of the large target molecule. The fractions with drug-target complexes are measured by MS to identify the co-eluting targets [26].

1.3.3 Stability of proteins from rates of oxidation

West *et al.* [27] described SPROX as a technique that compares oxidation rates of drug-protein complexes and free unbound proteins. The advantage of this technique is that the oxidation taking place at methionine residues on proteins are irreversible, meaning that the products are chemically stable and not dependent on an equilibrium during detection. A key point to SPROX is that drug-protein complexes experience less oxidation than free unbound proteins when exposed to the same amount of oxidant and denaturant (*i.e.* a substance which causes denaturation of proteins). The amount of peptides with oxidized and non-oxidized methionine residues from an array of solutions with increasing concentration of oxidant and denaturant are quantified by MS after digestion. By plotting amount of peptides with oxidized and non-oxidized methionine residues against concentration of denaturant, drug-protein complexes have a transition midpoint shifted to higher concentrations of denaturant than free proteins [13, 30-32].

1.3.4 Affinity chromatography

A direct approach for identification of drug targets is affinity chromatography, which uses solid supports for immobilization of drugs to isolate the drug target. The support can be agarose beads [33], sepharose beads [34, 35], tosyl activated magnetic beads [36], or polymeric beads [37]. The purification principle behind affinity chromatography is that the targets are trapped to the beads by bonding to the drug, while non-bonding molecules are washed off. This technique allows for purification of the target protein from complex mixtures *e.g.* cell lysates from cells or tissue.

Traditionally, assessment of the selectivity of the drug and the off-target liabilities are done using screens comprised of purified recombinant proteins representing the protein family of the protein target, not the entire proteome as expressed in the target cell or tissue [38]. The use of purified recombinant proteins is due to the difficulty of extracting a sufficient amount of proteins in their native conformation from cells using non-denaturing chemicals and methods. However, the production of recombinant proteins also experiences difficulties with obtaining the correct protein folding and inactivity of the protein [39]. The assessment of selectivity and

off-target effects of the drug by recombinant proteins depends on the selected proteins present in the assay, and how well the recombinant proteins represent the characteristic of the native protein. This biased selection of proteins is discussed as one of the reasons why many developed drugs fail the clinical trials, as the drug does not show a high enough efficiency in animal models (or humans) or have off-target effects causing issues with toxicity [38].

Contrary to DARTS, TICC and SPROX, affinity chromatography requires modification to most drugs to be able to immobilize them to the support [13]. This is due to the need for specific functional groups, *e.g.* amines, hydroxyls or thiols, present on the drug to allow covalent bonding to the support [37, 38]. By changing the chemical synthesis of the drug, one such group may be added to the drug. An important part in this procedure is to ensure that the biological activity of the pharmacophore is not inhibited by sterically hindrance or that the attached group has disturbed the drug-target interaction. To avoid steric hindrance and increasing the availability of the drugs attachment to the support, a linker (or spacer) is often added to the drugs by chemical synthesis[40]. A linker can for instance be a polyethylene glycol (PEG) group. The linker can also be attached on the support prior to binding of the drug [41].

A common characteristic of the mentioned techniques (DARTS, SPROX, TICC and affinity chromatography) utilized for drug deconvolution is the multiple, and often manual steps that are needed before the target can be identified by LC-MS. The need for target identification is of immense importance, making it beneficial to have a method that is completed in a single workflow. For this purpose, affinity chromatography has the potential to adopt a different support for immobilization of drugs, making it possible to create an online and automated LC-MS method. Combining affinity purification with LC-MS may allow for detection of low abundance proteins and unbiased discovery of targets from target cells or tissue. Online methods may reduce contamination compared to the many manual steps in the current techniques.

1.4 Alternative solid support for affinity chromatography

With the recent advances in LC and MS, sample preparation is often the largest contributor to the analytical error and the most time-consuming part of the entire method. Sample preparation may be separated into two main categories: offline procedures and online procedure. In an

offline procedure (*e.g.* affinity chromatography with beads) the samples are prepared separately from the detection of the analyte (compound of interest). In online techniques, however, the samples are prepared and measured in the same workflow in a closed system. Comparing online and offline methods, the efficiency of the online method is increased due to reduced time-consumption, and accuracy is improved because of reduction in loss of sample and in possibility of contamination. With decreased operation time, the human error is reduced, and with automation, the reproducibility of the sample preparation can be improved [42-44].

The traditional up front affinity chromatography procedures using beads are not compatible with online LS-MS. However, the efficiency and accuracy of affinity chromatography may be improved by exchanging the beads with a solid support that is directly compatible with online coupling to LC-MS set-up. There are different column formats in LC that are suitable for online sample preparation. The most common formats are particle packed, open tubular or monolithic columns made in cylindrical column bodies shown in **Figure 3** [45]. Particles in LC-MS and the beads used in affinity chromatography are made out of the same materials, but traditionally the beads have a large diameter than the particles used in LC-MS.

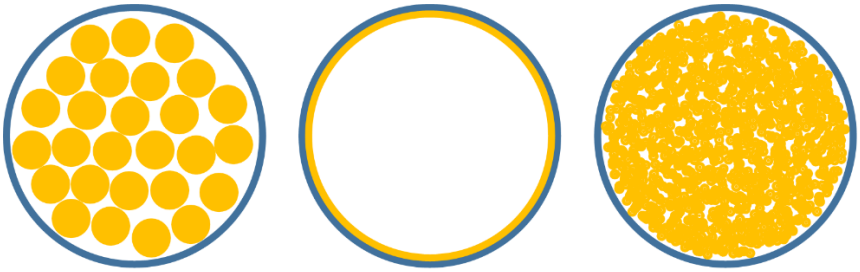

Figure 3: The most common column formats in LC: (Left) Particle packed column, (Middel) porous layer open tubular column and (Right) monolithic column.

Particle packed columns are packed with either fully porous, core-shell (*i.e.* a non-porous core with a porous shell) or non-porous particles. Traditionally, the particles size in the packing material is 3 to 5 µm, with pore sizes ranging from 10 to 30 nm [46]. The column bodies are commercially available at 4.6 mm inner diameter (ID), but packed columns can be prepared in 30 µm ID to 250 µm ID fused-silica capillaries [47, 48]. Due to the small size of the particles and the pores, the particle packed columns generates a high backpressure (*i.e.* pressure exerted by the liquid in resistant to motion through the column). It also causes the flow to go around the particles instead of into the pores, reducing the amount of surface in contact with the liquid flow. Another important feature of these column are filters, or frits, in the ends of the capillary to keep the particles inside the column, which increases dead-volumes in the connections.

Open tubular (OT) columns in LS-MS are narrow columns (ID in µm range) with a thin porous layer covering the walls of the capillary, so called porous layer open tubular (PLOT) columns. Comparing a particle packed column and a PLOT column of the same length and ID, both the surface area and the backpressure would be greatly reduced on the PLOT columns. To apply these PLOT columns for affinity chromatography with immobilization of ligands in the porous layer, a longer column or a thick coating is essential in order to have a sufficient amount of active sites. However the production of longer PLOT columns or an increase of the thickness of the porous layer frequently experiences issues with clogging [49, 50]. Another format of PLOT columns that increases the number of active sites are multichannel columns (*i.e.* a single piece of capillary with several channels) [51].

The last format, monolithic polymer columns will be the focus of this study as they may have the highest potential for immobilization of ligands due to their characteristics of: low backpressure, stability in most solvents, accessibility of the active sites due to pore sizes and structure, and the possibilities of tailoring the functionality of the polymer [52].

1.4.1 Monolithic support

The monolithic structure is a single-piece of porous material, with a multitude of channels caused by pores formed during production, and the porous structure is maintained in solvents and in dry state [53, 54]. Opposite to particle packed capillary columns, capillary monoliths do not depend on frits because the rigid porous structure fills the entire cavity of the vessel and is covalently attached to the column wall in the capillary format.

The first attempt of a different structure than beads in the chromatographic columns were made by Hjerten *et al.* [55]. A gel was made by co-polymerization of acrylic acid and N,N‘-methylenebisacrylamide, resulting in a porous sponge like material inside a mold (*i.e.* the vessel the polymerization occurred). This gel did not have a solidified distribution of pores, as the material were liable to swelling in solvent and thereby changing the pore distribution. The structure was removed from the mold, diluted in water, compressed and packed inside a column body to achieve the monolith-like structure.

The idea of a continuous porous column was further developed by Svec and Frechet [56] to form a rigid porous material based on the balance of globules and void spaces (pores). The material was formed during the co-polymerization of organic monomers (*i.e.* small molecules

that may form a network) taking place inside the column body, so called *in-situ* polymerization. The pore distribution consists of micropores, which are smaller than 2 nm, mesopores in the ranges from 2 to 50 nm, and macropores larger the 50 nm [53]. Due to the macropores being interconnected, the backpressure over the monolithic columns is greatly reduced compared to particle packed columns as resistance to mass transfer is almost absent [57, 58].

In the 1990s, Tanaka *et al.* [48] developed porous silica monoliths, also called inorganic monoliths. The structure of these silica rods is a porous skeleton network with round pores, offering a total porosity of over 80% [48, 59]. The skeleton network and the large interconnected pores result in the silica monoliths having a high permeability of fluids and low backpressure throughout the column. This can be presented based on through-pore/skeleton size ratio, which are from 3 to 5 for silica monolith while between 0.25 to 0.4 for particle packed columns [60]. A drawback for using silica monoliths is that the silica structure is not chemically stable in basic environment, and that the preparation of these inorganic monoliths has shown to be more difficult than organic monoliths [61, 62].

1.4.2 Characteristics of organic monoliths

Organic monoliths are made by *in-situ* co-polymerization of monomer and crosslinking monomer, in the presence of an initiator and a pore-forming solvent (*i.e.* porogen). During polymerization, globules are formed from the monomers being tightly bound and crosslinked, while polymer chains covering the globules are formed due to less crosslinking shown in **Figure 4**. The rigidness of the structure is due to the stability of the globules, as the globules resist swelling in different solvents. The macropores are proportional to the size of the globules, where large pores are associated with large globules [56]. The morphology (*i.e.* distribution of pores and globules) of the monolith depends on the rate of polymerization and may be adjusted through amount and type of porogen(s), amount of initiator and crosslinker [63] (p. 28-29).

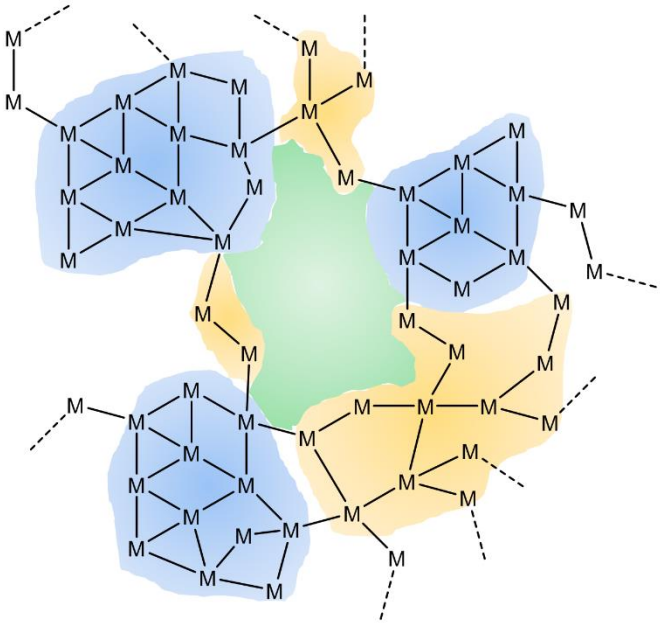

Figure 4: During polymerization the monomers are bound together with a different degree of crosslinking causing the formation of globules (blue area with a high degree of crosslinking) and polymer chains (yellow area with low degree of crosslinking). As a consequence of the globules and the polymer chains, pores (green area) are formed throughout the monolith.

The surface of the organic monoliths may be tailored towards an application by selecting monomers with the desired properties. Monomers may display different degrees of hydrophilicity and hydrophobicity. Acrylamide and 2-hydroxyethyl methacrylate are examples of hydrophilic monomers, while ethylene dimethacrylate (EDMA) is a hydrophilic crosslinking monomer. Monolithic columns have been used for separation of proteins and peptides by *e.g.* Premstaller *et al.* [64] using hydrophobic monomers styrene and divinylbenzene. The solid support intended for isolation of proteins should use monomers that display a high degree of hydrophilicity to prevent contribution of non-specific hydrophobic interactions with the proteins and peptides present (*i.e.* secondary interactions) besides the protein target [57].

The common structure of the monomers shown in **Figure 5** is a CH_2=CR group which is susceptible for rearrangement if activated by free radicals or an ionic initiator. This is due to the reactivity of the π-bond of the double bond between two carbon atoms [65] (p. 57). These type of monomers with CH_2=CR groups form polymers by chain reactions classified as addition polymers. Another type of polymers is called condensation polymers, as these are formed by elimination of a small molecule for each step of the monomer reactions [65] (p. 29).

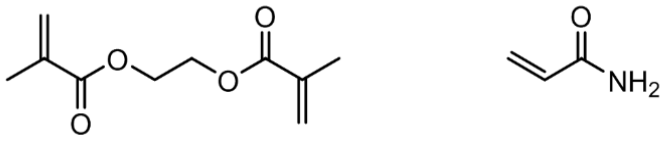

Figure 5: The structure of: (Left) a crosslinking monomer, EDMA and (Right) a hydrophilic monomer, acrylamide.

The initial choice of monomers may also affect the possibility of post-modification of the surface. By selecting reactive monomers such as glycidyl methacrylate (GMA) and 2-vinyl-4,4-dimethylazlactone (VDM), not only do they have the CH_2=CR group, but also contain an epoxide and an azlactone ring, respectively, that may be used for immobilization of additional molecules. Zacharis *et al.* [66] used GMA-co-EDMA monoliths to study drug-protein interaction of naproxen and bovine serum albumin (BSA), by immobilization of BSA to the epoxide group of GMA. The ring-opening reaction between VDM and functional groups (*i.e.* amino, hydroxyl and thiol groups) has been exploited for a multitude of biomolecule reactors. By reaction with amino groups *e.g.* pepsin, trypsin, and LysC have been immobilized by VDM [58, 67]. The ring-opening reaction between amino groups and VDM, shown in **Figure 6** is active under pH conditions from pH 4 to 9 [37].

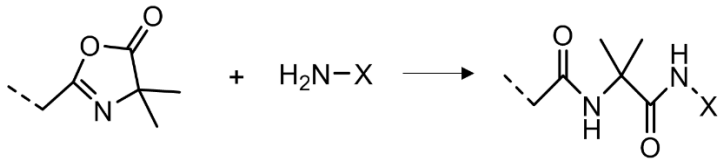

Figure 6: Immobilization of a molecule X (*e.g.* trypsin) through a ring-opening reaction between VDM and an amino group on the molecule. The dashed lines indicate where the VDM monomer is bound in the polymer chain of the monolith.

Another reactive monomer that is an integral part of organic monoliths is 3-(trimethoxysilyl)propyl methacrylate (γ-MAPS). The γ-MAPS monomer consists of the reactive carbon-carbon double bond and a silane coupling group (*i.e.* -$Si(OR)_3$ group). The monomer is attached to the capillary wall by a reaction between the -$Si(OR)_3$ group of the monomer and the free silanol groups on the inner wall of the fused silica capillaries shown in **Figure 7**. The CH_2=CR group is free to react with the polymer formed during polymerization to attach the polymer to the wall of the capillary [68, 69].

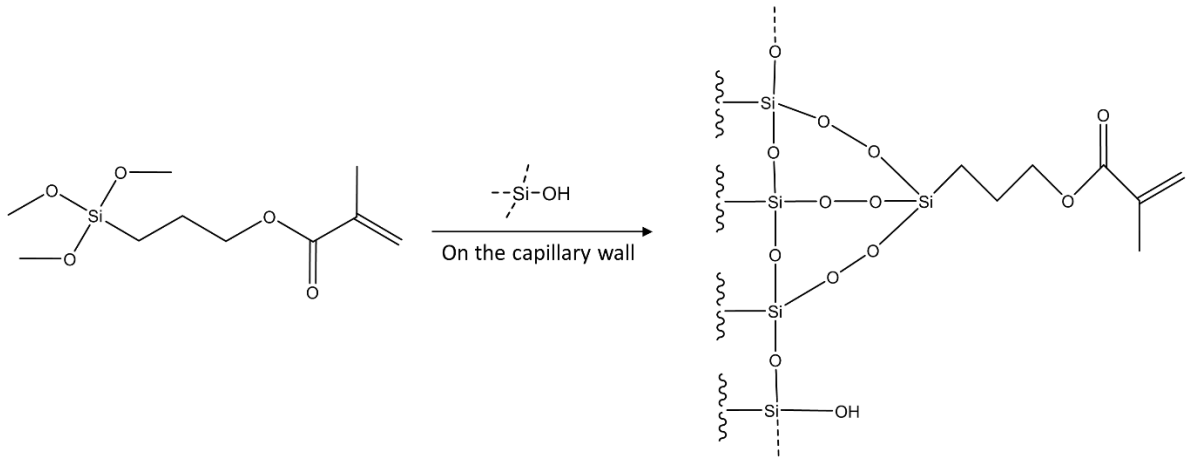

Figure 7: Attachment of γ-MAPS to the capillary wall of the fused silica capillary by reaction with the free silanol groups on the capillary wall.

1.4.3 Addition polymerization

The initiator of addition polymerizations may be either free radical, cationic or anionic. The best fitted initiator depends on the R group of the CH_2=CR bond, whether it is an electron-donating or an electron-withdrawing substituent. With electron-donating groups the nucleophilicity of the double bond is increased, and reaction with cationic species is favorable. With electron-withdrawing groups, the electron density is reduced, and encourages reaction with anionic species. However, with free radicals, a less selective group of species is able of resonance stabilization of the effect from radical interactions. An ionic initiator leads to complex polymerizations due to rapid reactions rate and high molar mass of the polymer, which also are difficult to reproduce. Use of free radical initiator is easier to control as the mechanism behind the polymerization is better understood [65] (p.57-60, 99).

A commonly used initiator is α,α‘-azobisisobutyronitrile (AIBN) which may be decomposed by either heat or UV radiation at 360 nm to form two free radicals that initiates the polymerization shown in **Figure 8** [58, 65, 70] ([64] p. 59). For polymerization in capillaries, thermally initiated free radical polymerization can fill the entire closed cavity, while photoinitiated polymerization is more suited for applications which requires specific areas to be polymerized [71].

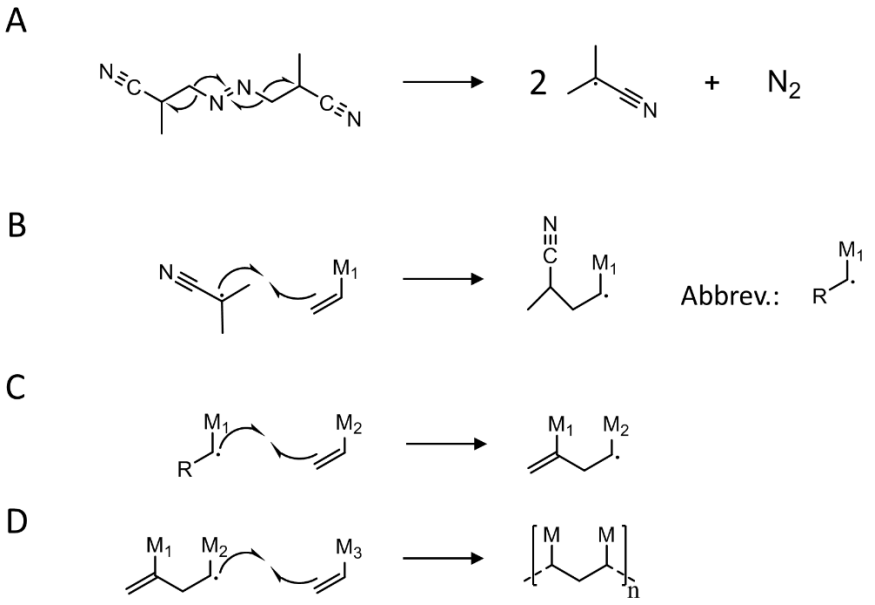

Figure 8: General scheme of free-radical addition polymerization utilizing AIBN as initiator. (A) Decomposition of initiator AIBN subsequently followed by (B) radical attack on monomer 1 (M_1) to form a chain carrier. (C) Propagation of the chain by radical attack on another monomer 2 (M_2) and eventually (D) a polymer chain consisting of a total of 2n monomers are formed. Adapted from [72].

1.5 Proteins and how to measure their presence

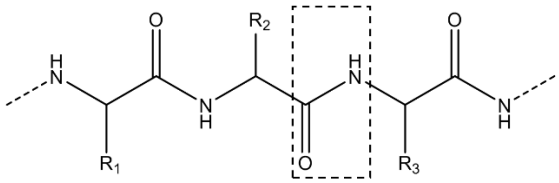

Figure 9: The protein backbone in the primary structure of proteins shown with three side chains (R_1, R_2 and R_3) of the amino acids. A peptide bond is marked with the dashed square.

Proteins are long chains of amino acids connected by peptide bonds, a bonding between a carboxyl group of one amino acid and an amino group of another amino acid. The polypeptide chain is shown in **Figure 9**, the peptide bond marked with a dashed square is planar in nature and favors a *trans* conformation of the side chains of the amino acids [1] (p. 17-24). Hydrogen bonds forming between the peptide bonds leads to the typical secondary conformations found in proteins: the α-helix (hydrogen bonds form along the axis of coiled peptide chains), the β-pleated sheet (hydrogen bonds formed between antiparallel sequences) and the β-turn (stabilized by hydrogen bond between peptide bonds 1 and 3 in the turn) [73].

In native state, as a consequence of intramolecular bonds, the entire peptide backbone will fold in a three-dimensional shape, also called the tertiary structure. Intramolecular bonds are the same type of interactions occurring in intermolecular bonds (more details in **Introduction 1.1**), but these are now present within the same molecule. In addition, cysteine residues are capable

of forming covalent bonds between each other due to thiol groups (*i.e.* disulfide bonds) [74]. Some proteins also display a quaternary structure as a consequence of protein-protein interactions[75], and may form large networks consisting of many protein molecules [76].

1.5.1 Methods for detection of proteins

Proteins, and especially proteins with a low abundance in cells, may be detected with immunoassays, *e.g.* enzyme-linked immunosorbent assay (ELISA) and western blot (WB), which utilizes specific antibodies for detection of the desired protein. The recent advances in mass spectrometry, and bioinformatics for identification and quantification of proteins has enhanced the sensitivity of protein detection by LS-MS [77]. A combination of protein analysis by LC-MS and WB is a powerful way of detecting and identifying proteins.

1.5.2 Antibodies

The immune system of the human body recognizes foreign cells due to a molecular signature (epitope) on the proteins (antigens) gathered on the outer surface of the cell and produces antibodies that binds to that specific antigen sending a signal for the immune system to destroy that cell [1] (p. 149-151). Concerning pharmaceutical development, antibody conjugated with drugs have been used for drug delivery to specific targets [78], and monoclonal antibodies has been developed to act as drugs [79]. Antibodies, also known as immunoglobulins, are large Y-shaped proteins shown in **Figure 10**. The antibodies are built up of two light and two heavy peptide chains, connected by disulfide bonds [80]. At the N-terminal end the antibodies have variable regions that are adjusted for binding of a singular specific epitope of the target antigen.

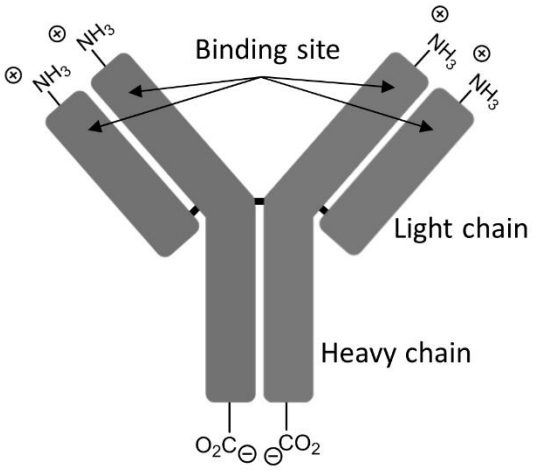

Figure 10: Antibody structure with the binding site of the epitope indicated by the arrows, and disulfide bonds indicated by black connections.

1.5.3 Western blot

Western blot is a targeted technique that utilizes the separation of proteins by gel electrophoresis and the specificity of antibodies for identification of the presence of a single protein or protein family. The process that is referred to as "western blotting" is the electrophoretic transfer (or blotting) of proteins from polyacrylamide gels to membranes [81, 82]. This process is beneficial as the separated proteins are immobilized making them available for interactions with antibodies [83] (p.150-151).

Gel electrophoresis

Gel electrophoresis is a separation technique that separates macromolecules (*e.g.* DNA, RNA and proteins) based on their size and/or charge. A gel based on agarose or polyacrylamide has small pores where macromolecules can move when exposed to a driving force. In gel electrophoresis the macromolecules are affected by a force exerted by an applied electric field. A general description of movement by charged units in an electric field, is that positively charged units will migrate towards the negatively charged end. In the opposite case, negatively charged units will migrate towards the positively charged end.

The most common gel electrophoresis is run in negative mode, where the samples are applied in wells on the gel near the negative electrode, while the other end is applied a positive charge. This is due to the fact that this technique is commonly used for DNA and RNA, which are naturally negatively charged. Proteins on the other hand, is less charged in their native state [1] (p. 17-29). By treatment with a denaturant (*e.g.* treatment with sodium dodecyl sulfate (SDS)) the proteins to unfold into a linear structure and SDS also complexes with the proteins resulting in negative charges on the linear structure shown in **Figure 11** [84]. SDS wraps around the polypeptide backbone of the proteins with 1.4 grams of SDS to 1 gram of protein, resulting in an identical net charge density of the proteins present in the sample [85]. The electrophoretic mobility of these proteins is then proportional to only the molecular size. Proteins with disulfide bonds may be denatured to a larger extent by adding 2-mercaptoethanol or dithiothreitol (DTT), which disrupts the disulfide bonds [86]. If a polyacrylamide gel is used, the technique is called SDS polyacrylamide gel electrophoresis (SDS-PAGE), which has been used in several methods for western blot and mass spectrometry [86], and for purification of protein [34, 87].

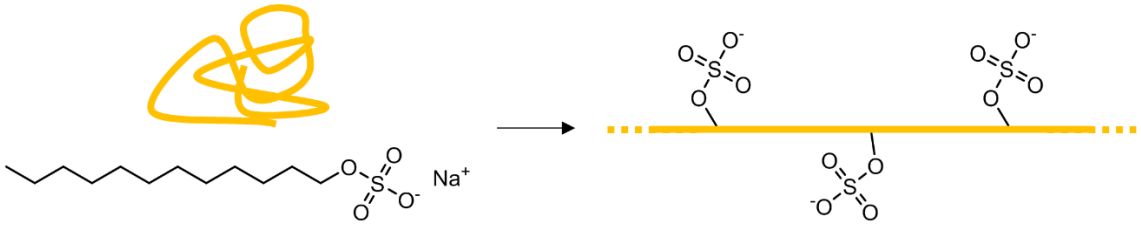

Figure 11: Denaturation of a protein by complexing with SDS forms a linear structure with a net uniformly distributed negative charge.

To achieve high resolution separation, a discontinuous electrophoresis system utilizing both a stacking gel and a running gel is used. The samples are loaded in individual wells in part of the stacking gel, while the separation occurs in the running gel. The stacking gel has a lower pH and percentage of acrylamide for the purpose of gathering (or stacking) the proteins in the narrowest bands possible, making the proteins in the samples entering the running gel at the same time. Running the electrophoresis at a low voltage during the protein migration in the stacking gel also reduces the width of the protein band. The narrower band heading into the running gel, the higher degree of resolution (degree of separation between compounds of similar molecular size) is achieved [88-90].

Western blotting

An incredible contribution to biochemistry was the development of a method that allowed transfer of proteins from polyacrylamide gels to adsorbent membranes, *e.g.* nitrocellulose, nylon or polyvinylidene difluoride (PVDF) membranes [91]. The transfer is done using an electric field in the same manner as during the gel electrophoresis. The difference is that the field is directed perpendicular to the gel surface, and not along the length of the gel. Therefore, the negatively charged proteins migrate from the gel and onto the membrane that binds the proteins.

To avoid drying of the membranes during electrophoretic transfer, a "transfer sandwich" is built in the following order: Filter paper, membrane, gel, and filter paper. The transfer may occur in either wet or semi-dry conditions. In wet conditions as described by Towbin *et al.* [81], the transfer sandwich is placed in a vertical position between two platinum wire electrodes, and the container is filled with a transfer buffer. Kyhse-Andersen [92], designed a simpler set-up where the transfer sandwich is placed between two plate electrodes in a horizontal manner, and the filter paper has been soaked in transfer buffer, set-up is shown in **Figure 12**. The horizontal blotting reduces the consumption of organic solvents, and utilizes less expensive electrodes and

power sources [93]. Large proteins (>$2 \cdot 10^5$g/mol) [94], prefer wet conditions, and due to the more extensive supply of buffer the membrane is better protected towards drying [90].

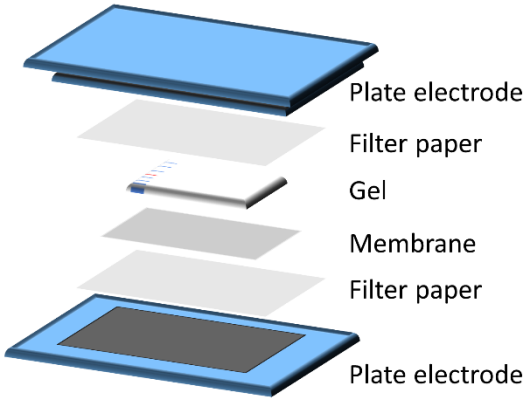

Figure 12: The transfer sandwich consisting of filter paper, gel, membrane and another filter paper is placed between to plate electrodes, where the electrode on the top works as a cathode and the one on the bottom as an anode.

After protein transfer, the membrane will have areas unoccupied by proteins. These must be blocked, or quenched, too avoid nonspecific binding of antibodies that are used for immunodetection of the immobilized proteins. Proteins from non-fat milk or BSA have been successfully applied for this purpose [90].

Visualization

The binding between antigen and antibody is utilized in immunodetection and in WB the preferred detection system utilizes enzyme-linked antibodies [83] (p.150-151). Indirect immunodetection in WB is based on the membrane being treated with primary antibody targeting the antigen (in WB the protein of interest), and then a secondary antibody targeting the primary antibody. The secondary antibody is linked to an enzyme that in reaction with a chemiluminescent reagent produces light visualizing protein bands, if the targeted protein is present. The intensity of the bands depends on the amount of protein present and the amount of successfully bound antibodies. In direct immunodetection the primary antibody is linked to the enzyme rendering the secondary antibody redundant. The process of antibody attachment to the protein present on a membrane is shown in **Figure 13**. The sensitivity of WB analysis depends on the specificity of the antibodies used for detection. The specificity of the antibody does not only depend on production of the antibody and characterization of the antibodies non-specific bonding of proteins, but it has been discussed that storage reduces activity and that immobilization of the antigen may sterically hinder the antibody from reaching the epitope [80].

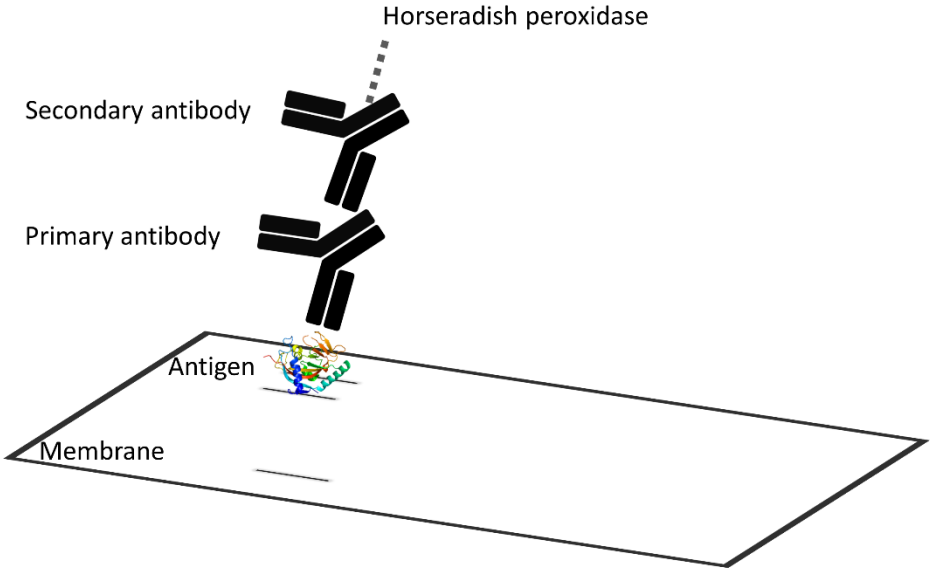

Figure 13: Visualization of proteins in WB by bound primary antibody and secondary antibody linked with the enzyme horseradish peroxidase.

1.5.4 Protein measurement by liquid chromatography mass spectrometry

While WB is a targeted technique, LC-MS may be both comprehensive (*i.e.* trying to identify as many proteins as possible) and targeted, depending on the mass spectrometric method. The favored method for detection of proteins is identification via peptides, a so called bottom-up analysis, where the proteins are digested by a protease prior to separation and identification by LC-MS.

For bottom-up analysis, the protease must cleave at known positions in the protein sequence to make it possible to compare the masses of the digested peptides to that of the theoretical peptides from the native sequence in the proteins without the fear of false positive matches. Trypsin is one such protease that offers high specificity for cleavage of peptide bonds after lysine and arginine residues in the polypeptide backbone, except when proline is next in the amino acid sequence, shown in **Figure 14** [95]. As complex proteins samples become even more intricate after digestion, an aid for the MS comes in form of separation of these peptides by LC prior to MS. It is worth noting, that trypsination traditionally took place in-solution, but the procedure has been automated and incorporated online with the LC-MS instrumentation by application of monoliths with immobilized trypsin, so called immobilized monolithic enzyme reactors (IMERs) [52, 67].

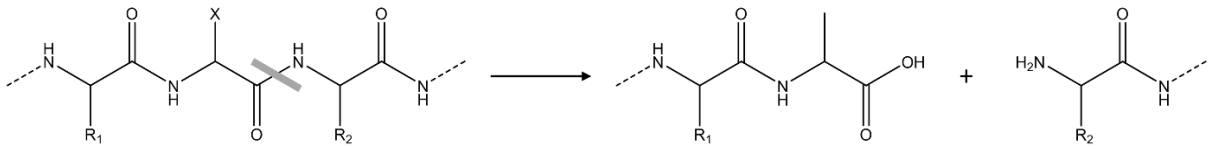

Figure 14: Digestion of proteins by trypsin will cleave the amino acid sequence at the carboxyl side of lysine or arginine residues except when proline is next in the sequence (R_2). The placement of the side chains of lysine and arginine on the protein backbone is marked by X, and the gray cut in the sequence marks the point where the peptide chain is broken.

Liquid chromatography separates the compounds with use of an analytical column, the most common formats are described in **Introduction 1.4**. Compared to affinity chromatography which seeks to trap the interacting compounds, liquid chromatography usually seeks to separate compounds by distribution between the stationary phase (*i.e.* functional group on the solid material in the analytical column) and the mobile phase. The principle of separation depends on the type of stationary phase and how the compounds interacts with it.

The most frequently used principle of separation is reversed phase (RP) chromatography which uses a non-polar hydrophobic hydrocarbon chain stationary phase (SP) and an aqueous mobile phase with pH-control mixed with a miscible organic solvent. The separation occurs based on degree of hydrophobicity, the more hydrophobic peptides will be retained more by the SP than the less hydrophobic peptides. For elution of peptides with similar hydrophobicity, isocratic elution (*i.e.* a constant composition of the mobile phase) is used and for samples containing peptides with larger variations in hydrophobicity, gradient elution (*i.e.* the mobile phase composition is changed during measurements) is utilized. Common mobile phase composition is a mixture of water and acetonitrile (ACN) with formic acid (FA) for pH-control. Gradient elution is achieved by increasing the amount of organic solvent (ACN) as this counter affects the affinity to the SP.

When coupling LC with MS, the ions need to be transferred from an atmospheric pressure liquid phase to high vacuum gas phase. This is usually done by an ion source, and the most commonly used LC-MS interface for samples containing peptides is electrospray ionization (ESI) [96]. As a voltage is applied on the capillary (*i.e.* the emitter), the ions will move and form a Taylor cone at the capillary outlet. Droplets containing the ions are sprayed out of the Taylor cone, with a high charge on the droplet surface. As a consequence of solvent evaporation, the droplets will decrease in size, and repulsive forces (*i.e.* coulomb fission) will cause the droplets to split. A combination of solvent evaporation and repulsive forces will eventually transfer the ions from the solution into gas phase. Reduced flow and more narrow inner diameters of the emitters will

give more efficient droplet formation and increased efficient solvent evaporation [97]. ESI have therefore been further developed using emitters that allow flow rates in the $nLmin^{-1}$ range, this is referred to as nanospray [46] (p.86-88).

Due to the coupling with ESI-MS, a downscaling of the chromatographic system utilizing the traditional 4.6 mm ID columns to <50 µm ID columns has been important. As a sample is injected into equivalent efficient columns where the only difference is the ID, the sample eluted from a narrower column will have a higher concentration than the sample eluted from the wider column. This process of radial dilution is shown in **Figure 15**, the sample band in the 0.05 mm ID column is diluted in a significantly reduced amount of solvent compared to the 4.6 mm ID column. The importance of downscaling the LC-ESI set up, is that while MS is a mass sensitive detector, the combination of ESI-MS is concentration sensitive.

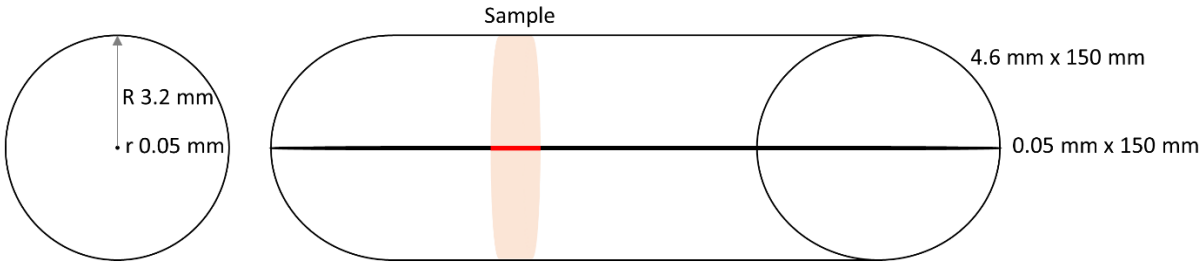

Figure 15: Comparison of dilution of sample in equivalent efficient columns with a different inner radius, where the sample has been introduced with same initial concentration and experiences the equal band broadening. Scaled for a traditional 4.6 mm ID and a miniaturized 50 µm ID column. Color intensity of the sample band is representative of the sample concentration in the diluted sample on both columns.

As mentioned, the MS measures ions in a high vacuum environment. For measurements of proteins it is easier to monitor peptides than intact proteins, and a high mass resolution of the MS is needed to separate the closely related *m/z* values resulting from the multitude of peptides present in digested protein samples. A high resolution MS is the quadrupole-Orbitrap MS, described in [98], consisting of a higher-energy collision dissociation (HCD) cell and both a quadruple mass filter [99] and a Orbitrap mass analyzer [100]. By operating the MS in MS/MS mode the digested peptides with be fragmented further in the HCD cell forming different possible fragments ions associated with amino acid residues, shown in **Figure 16**.

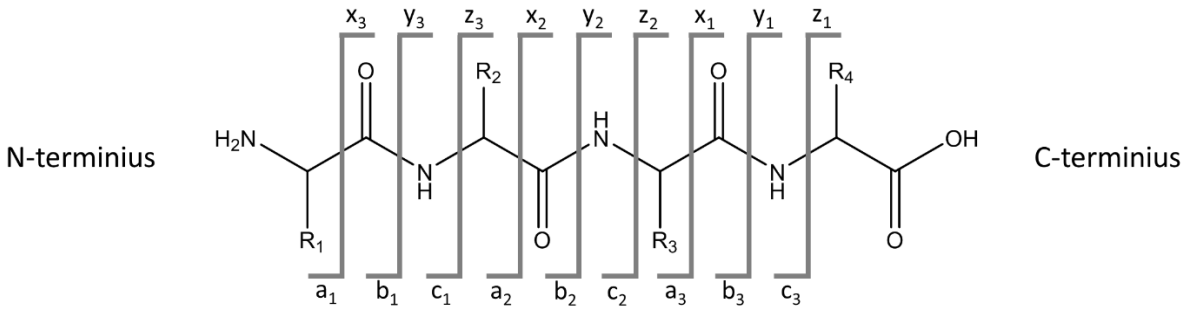

Figure 16: Peptide fragmentation, where the A, B and C fragments are named from N-terminus and Z, Y and X fragments are named from C-terminus. The R_1 to R_4 represent amino acid side chains, and the index number on the peptide fragments represent the number of amino acid side chains present in the fragment. [REPLACE small letters]

By computational methods, these fragments obtained by MS/MS is processed to identify the precursor amino acid sequence of the peptides and as a consequence of multiple identified peptides, the precursor protein can be identified. A processing tool is the SEQUEST algorithm. A SEQUEST algorithm measures the closeness between experimental MS/MS mass spectra and theoretically predicted MS/MS mass spectra from a peptide sequence, and reports a correlation score along with a percentage of sequence coverage [101].

1.6 Choice of model system for developing new method for drug discovery

To explore the possibility of using monoliths with immobilized drug for drug discovery, a known drug-target system was needed. A signaling pathway that is often connected to human disease and especially cancer is the Wnt-signaling pathway [102]. The Wnt-signaling pathway is crucial for maintenance of tissue due to the control over the protein β-catenin that is part of regulation and coordination of cell adhesion (*i.e.* a process where cells interact and connect with neighboring cells) and transcription of proteins [103].

An inactive Wnt-signaling pathway leads to formation of a destruction complex (formed by the proteins axin, glycogen synthase kinase 3 (GSK) and adenomatous polyposis coli (APC)) where β-catenin is destroyed, and as a consequence cell adhesion and transcription of proteins will not occur in the cell [104]. An active Wnt-signaling pathway is a consequence of a Wnt associated protein binding to a receptor that stabilizes axin, and as a consequence axin is not available to form a destruction complex leaving β-catenin free to activate cell adhesion and transcription of proteins. An inactive Wnt-signaling pathway is desired in cancer cells, as these defect cells are inhibited from interacting with neighboring cells. An active Wnt-signaling pathway has been

viewed as the source of many cancers, making a Wnt-inhibitor an attractive drug for cancer treatment [105].

Protein targets that have been reported in a multitude of cancers are tankyrase 1 and tankyrase 2 (TNKS1/2) [8]. TNKS1/2 are involved in Wnt-signaling through regulation of axin. By inhibition of TNKS1/2, levels of axin would be increased in the cells, and as a consequence of increased levels of axin the destruction complex would be formed, and the Wnt-signaling pathway would be inhibited.

TNKS1/2 are low abundant drug targets that are difficult to extract from cells in their native shape and in a magnitude making it possible for quantitative and qualitative measurements by LC-MS [106]. However, both Voronkov *et al.* [87] and Huang *et al.* [34] have been able to extract and purify TNKS1/2 from cells for examination of possible Wnt-inhibitors targeting TNKS1/2.

TNKS1/2 belongs to the ADP-ribosyltransferase (ARTD) enzyme family, also known as poly(ADP-ribose)polymerase (PARP). TNKS1/2 are distinguishable from the family due to a unique sterile alpha motif (SAM) structure and several ankyrin repeat cluster (ARC). TNKS1 and TNKS2 are distinguishable due to the Histidine-Serine-Proline rich domain (HPS) present in TNKS1, but not in TNKS2, shown in **Figure 17**. The ankyrin groups in TNKS1/2 causes protein-protein interactions with over 100 possible protein binding partners [107]. The SAM domain in TNKS1/2 makes it possible for self-oligomerization and TNKS1/2 may form complexes consisting of over 30 molecules [108].

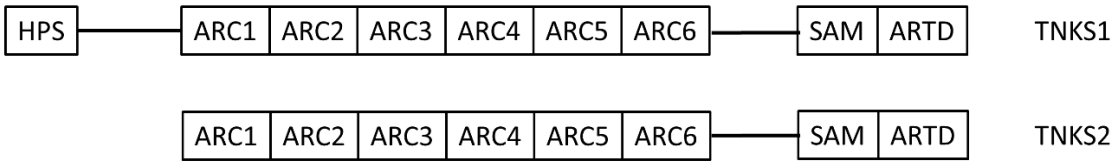

Figure 17: Structural organization of domains in TNKS1/2. Adapted from [8].

Wnt-signaling pathway inhibitors targets two different subsites on the enzymes in the ARTD family: The nicotinamide subsite and the adenosine subsite [8]. Wnt-inhibitors targeting the adenosine subsite offers high selectivity towards TNKS1/2 (*e.g.* Wnt-inhibitor 161 [87]), while targeting the nicotinamide subsite binds additional enzymes from the ARTDs family (*e.g.* Wnt-inhibitor XAV939 [34]).

1.7 Aim of study

The aim of this study was to immobilize a drug onto a monolithic support displaying low secondary interactions for selective purification of the protein target of the drug.

A hypothesis was that this tool, suitable for incorporation online an LC-MS method, would allow identification of low abundant targets from cell lysate as a consequence of reduced handling time, contaminations, and loss of sample.

As proof-of-concept, a 180 µm ID or 250 µm ID EDMA-co-VDM monolith immobilized with Wnt-inhibitor 161 would attempt to selectively trap a low abundant target protein, tankyrase 2.

2 Experimental

2.1 Reagents and standards

For the synthesis of the Wnt-signaling pathway inhibitor LDW639, the following reagents were purchased from Fluorochem (Hadfield, United Kingdom): methyl-4-oxotetrahydro-2H-thiopyran-3-carboxylate (beta-keto ester, 95%), 4-boc-aminomethylbenzamidine (boc-benzamidine, 97%) and 2,2-dimethyl-4-oxo-3,8,11-trioxa-5-azatridecan-13-oic acid (97%). In addition, potassium carbonate (anhydrous, Redi-Dri™, ≥ 99%), magnesium sulfate (anhydrous, ReagentPlus, ≥ 99.5%) and N,N-dimethylformamide (DMF, anhydrous, 99.8%) were acquired from Sigma Aldrich (St. Louis, MO, USA). Methanol (MeOH, 100%), ethyl acetate (99.9%) and diethyl ether were purchased from VWR (Radnor, PA, USA). Trifluoroacetic acid (TFA), 4-methylmorpholine (NMM) and 2-(7-aza-1H-benzotriazole-1-yl)-1,1,3,3-tetramethyluronium hexafluorophosphate (HATU) were obtained from Fluorochem. Dichloromethane (DCM, 99.9%) was acquired from Honeywell (Morris Plains, NJ, USA). Acetyl chloride (98%) was obtained through Acros Organics (Geel, Belgium) now a part of Thermo Fisher Scientific (Waltham, MA, USA).

The reagents needed to produce the monolithic supports; ethylene dimethacrylate (EDMA, 98%), 2,2-diphenyl-1-picrylhydrazyl (DPPH), DMF (99.8%), 3-(trimethoxysilyl)propyl methacrylate (γ-MAPS, 98%), α-α'-azoisobutyronitrile (AIBN, ≥ 98.0%), 1-propanol (99.7%), 1,4-butanediol (ReagentPlus®, ≥ 99%), ethanolamine hydrochloride (≥ 99.0%), and monobasic sodium phosphate (BioXtra, ≥ 99.0%) were all from Sigma Aldrich. 4,4-Dimethyl-2-vinyl-2-oxazolin-5-one (Vinyl azlactone, VDM, ≥ 95%) was purchased from Polyscience Inc. (Warrington, PA, USA). Acetone (GPR rectapure) and acetonitrile (ACN, HPLC grade) were obtained from VWR. Sodium hydroxide pellets (pro analysis, 99.0%) and ammonium acetate (extra pure, ≥ 96%) were acquired from Merck (Darmstadt, Germany).

Chemicals used for cell lysis and protein digestion: DL-dithiothreitol (DTT, Bioextra, ≥ 99.0%), imidazole (ACS reagent, ≥ 99%), iodoacetamide (IAM, BioUltra, ≥ 99%), glyserol (≥ 99%), urea (98%), ammonium bicarbonate (ABC, ReagentPlus®, ≥ 99.0%), SigmaFast™ protease inhibitor (general use), formic acid (FA, reagent grade, ≥ 95%), and trypsin from bovine pancreas were purchased from Sigma Aldrich. Sodium chloride (ACS reagent, ≥ 99.5%) was

obtained from Merck. Tris buffer (1M, pH 8.0) was acquired from the Department of Microbiology at Oslo University Hospital.

Reagents used at Unit of Cell Signaling at Oslo University Hospital; Tris-HCl (pH6.8), sodium dodecyl sulfate (SDS), glycerol (100%), β-mercaptoethanol (99%), ethylenediaminetetraacetic acid (EDTA), bromophenol blue, trizma® base (≥ 99%) and glycine (≥ 99%) were all from Sigma Aldrich. PageRuler™ Prestained protein ladder was from Thermo Fisher. Tris buffered saline with Tween™ (TBS-T) tablets was purchased from Medicago AB (Uppsala, Sweden). Nonfat dried milk powder was acquired from PanReac AppliChem ITW reagent (Dramstadt, Germany). Technical methanol was acquired from VWR, and radioimmunoprecipitation assay (RIPA) lysis and extraction buffer were obtained from Thermo Fisher Scientific. Amersham™ enhanced chemiluminescence (ECL™)-prime was acquired from GE Healthcare Life Science (Chicago, IL, USA).

The water used in the project was either HPLC grade water from VWR or type 1 water acquired from a Milli-Q® Integral water purification system equipped with a Q-POD dispenser (0.22 µm filter) from Merck Millipore (Billercia, MA, USA). Unless otherwise stated, type 1 water will be referred to as water. Calibration buffers TVS Titrinorm buffer solution pH 7 and pH 4 were obtained from VWR chemicals.

A solution of Wnt-signaling pathway inhibitor "161" dissolved in 0.5 mL dimethyl sulfoxide (DMSO) was obtained from Steven R. Wilson.

Proteins and antibodies

Myoglobin from equine heart (≥ 90%), human serum albumin (HSA, ≥ 99%), cytochrome C from bovine heart (≥ 95%), recombinant active human tankyrase 2 (amino acids: 667-1166) expressed in baculovirus infected *Sf*9 cells were purchased from Sigma Aldrich.

Primary mouse monoclonal antibody for tankyrase-1/2 (E-10, lot# F0711, cat: sc-365897), horseradish peroxidase (HPR) conjugated polyclonal secondary donkey anti-mouse antibody (cat: sc-2314), HPR conjugated polyclonal secondary donkey anti-rabbit antibody (cat: sc-2313) were acquired from Santa Crus Biotechnology (Dallas, TX, USA). Primary rabbit polyclonal antibody for actin (A2066, lot#018M4753V) was purchased from Sigma Aldrich.

2.2 Solutions and preparation equipment

The following tubes and bottles were used for preparation of samples and solution storage. For sample preparation involving proteins 1.5 mL Protein LoBind tubes were used, while for samples not containing proteins 1.5 mL Safe-lock tubes were used, both types from Eppendorf (Hamburg, Germany). Autosampler vials (0.3 mL) were from VWR. Solutions were stored in either centrifuge tubes in the sizes 15 mL and 50 mL, and 100 mL Borosilicate bottles from VWR. Mobile phase reservoirs on the LC-systems was 25 mL PYREX® bottles from Corning (Corning, New York, USA).

Pipettes in the range from 20 µL to 10 mL and 5µL to 40 µL were respectively Finnpipette®F2 and Finnpipette® campus, respectively, were from Thermo Scientific. An Eppendorf Research pipette was used for a range from 0.5 to 10 µL. Finntip® pipette tips for these volumes were also from Thermo Scientific. For gel electrophoresis and western blotting pipettes were used in the range from 1 µL to 1000 µL and both the pipettes and tips were from VWR.

Weighing were done using a Mettler AT200 analytical balance from Mettler Toledo (Columbus, OH, USA). Sonication was done in an ultrasonic bath from either ATU ultrasonidos (Valencia, Spain); model ATM40-0.7LC Digital Ultrasonic Cleaner, or from Branson (Danbury, CT, USA); model 5510.

For centrifugation an Eppendorf centrifuge 5424R was used, while concentration under vacuum was done using an Eppendorf Concentrator plus with an high vacuum pump from Edwards (Burgess Hill, England). Smaller equipment used were an incubator (model: PSC-20) from Grant instruments (Cambridge, England), a microspin (model: Mini Star silverline) from VWR and a whirlmixer (model: MS2 minishaker) from IKA® (Staufen, Germany).

Saturated solution for synthesis

Saturated potassium carbonate solution was prepared by dissolving 120 g of potassium carbonate per 100 mL of water and allowing the solution to cool to room temperature.

Solutions for preparation of monoliths

For pretreatment, a 0.1 M NaOH solution was made by dissolving 1.6 g of NaOH pellets in 40 mL water. An approximately 1 mL solution of DPPH, DMF, and ɣ-MAPS *(0.5/66.08/31.32,*

w/w/w) was used for silanization. The polymerization solution (approximately 0.5 mL) consisted of AIBN, VDM, EDMA, 1-propanol and 1,4-butanediol *(1/23/16/34/26, w/w/w/w/w)*.

Buffers

A 50 mM phosphate buffer was made by dissolving 0.5999 g of $NaHPO_4$ in 100 mL water, while a 50 mM ammonium solution was prepared by dissolving 0.384 g of ammonium acetate in 100 mL water. Both buffers were pH adjusted to pH 7.2 by adding 0.1 M NaOH and monitoring by a Thermo Orion 720Aplus pH-meter equipped with a glass pH-electrode BlueLine 11 pH from Schott AG (Mainz, Germany) a part of the Carl Zeiss foundation (Heidenheim an der Brenz, Germany). Ammonium solutions pH-adjusted to pH 7.2 will be referred to as AmAc solutions.

Immobilization solutions

A freshly prepared stock immobilization solution was made by dissolving 2.5 mg synthesized drug in 1 mL 50 mM phosphate buffer, yielding a 2.5 mg/mL solution. Before use the stock was further diluted ten times by adding 100 µL stock to 900 µL phosphate buffer. A solution consisting of 1 M monoethanolamine (MEA) was made by dissolving 2.73 g ethanolamine hydrochloride in 28 mL water.

Protein solutions

A TNKS2 solution of 0.028 µg/µL was made by diluting 10 µL of 0.28 µg/µL recombinant TNKS2 to 100 µL with 50 mM AmAc, while a TNKS2 solution of 0.035 µg/µL was made by diluting 12 µL recombinant TNKS2 to 96 µL with HPLC-grade water or 50 mM AmAc. A 0.28 µg/µL cytochrome C solution was made by dissolving 2.8 mg of cytochrome C in 10 mL 50 mM AmAc. An equal solution of 0.28 µg/µL of myoglobin was made in the same manner. An HSA solution of 1 µg/µL was made by dissolving 1.3 mg of HSA in 1.3 mL of 50 mM AmAc.

A protein mixture consisting of 0.035 µg/µL TNKS2, 0.035 µg/µL myoglobin and 0.035 µg/µL cytochrome C was made by mixing 12 µL of 0.28 µg/µL TNKS2 (diluted in 50 mM AmAc), 12 µL of 0.28 µg/µL cytochrome C and 12 µL of 0.28 µg/µL myoglobin, and diluting this mixture to 96 µL with 50 mM AmAc.

Solutions for elution

Solutions of 10%, 20%, 30%, 40%, 50% ACN in water (called 10% ACN etc.) made by mixing respectively 100, 200, 300, 400 and 500 µL ACN with 500, 400, 300, 200, 100 µL water. Solution consisting of 0.3 M NaOH was made by dissolving 240 mg NaOH pellets in 20 mL water, while 30% ACN in 0.1 M NaOH was made by dissolving 80 mg NaOH pellets in 6 mL ACN and 14 mL water. Mixture of (4/96, v/v) isopropanol/ 50 mM AmAc was made by mixing 0.5 mL isopropanol with 12 mL 50 mM AmAc.

A solution consisting of 2% FA in HPLC-grade water (v/v) was made by mixing 2 µL concentrated FA and 98 µL HPLC-grade water, while 2% SDS in 60 mM tris buffer (w/v) was made by mixing 200 mg SDS and 0.6 mL of 1M tris-buffer (pH 8.0), and diluting to a total of 10 mL with water (referred to as 2% SDS).

An 1 M AmAc solution was made by dissolving 3.84 g of ammonium acetate in 100 mL water. The solutions was pH-adjusted to 7.2 with 0.1 M NaOH. The solution was diluted to 200 and 500 mM, respectively, with water and both of these solutions were pH-adjusted to 7.2 in the same manner.

Solutions for cell lysis

A 10x protease inhibitor solution was prepared by dissolving a single tablet in 10 mL water and a 40x protease inhibitor solution was prepared by dissolving a single tablet in 2.5 mL water. Aliquots of 1 mL of each of the protease inhibitor solutions were stored at -20 °C.

Cell samples disrupted by ultrasonication were diluted to 100 µL with either water or 13.8 M urea in 230 mM ABC. This solution was prepared by dissolving 207 mg urea and 18 mg ABC in 1 mL water.

For cell lysis with buffer, a non-denaturing lysis buffer based on Voronkov *et al.* [87] was made by mixing 4.0 mL glycerol, 4 mL 10x protease inhibitor, 700 mg sodium chloride, 28 mg imidazole, 3 mg DTT and 1.2 mL 1 M tris buffer (pH 8.0), diluted with water to 40 mL.

Gel electrophoresis solutions

Both an in-house and a commercial loading buffer were used for preparing samples prior to gel electrophoresis. The commercial loading buffer was a Novex™ 4X Bolt™ lithium dodecyl

sulfate (LDS) sample buffer from Invitrogen™ (Carlsbad, CA, USA) a part of Thermo Fisher Scientific. The in-house loading buffer (4x) was pre made by Shoshy Mahmuda at the Unit of Cell Signaling, Oslo University Hospital. The in-house loading buffer (4x) consisted of 2.0 mL 1 M tris-HCl (pH 6.8), 0.8 g SDS, 4.0 ml glycerol, 0.4 mL 14.7 M β-mercaptoethanol, 1.0 mL 0.5 M EDTA and 8 mg bromophenol blue.

The 1x running buffers for the gel electrophoresis was prepared by 25 mL of either 3-morpholinopropane-1-sulfonic acid (MOPS) SDS NOVEX® (20x) or tris-acetate SDS NOVEX® (20x) diluted to 500 mL with tap water, and both running buffers were from Thermo Fisher Scientific.

Western blot solutions and antibodies

A 10x transfer buffer was pre made by Shoshy Mahmuda by mixing 30.3 g Trizma® base and 144.0 g glycine, and diluting to 1000 mL with water. The 1x transfer buffer was made by mixing 100 mL of the 10x buffer with 200 mL technical methanol and 700 mL water. A TBS-T solution was made by dissolving 10 TBS-T tablets in 5 L water. These solutions were stored at room temperature (RT).

Milk solution was made by dissolving 10 g nonfat dried milk powder in 200 mL TBS-T, yielding a 5% milk in TBS-T (w/v). The antibodies were diluted as follows in 40 mL tubes, 1:250 mouse anti-tankyrase1/2 (v/v), 1:5000 donkey anti-mouse (v/v), 1:1000 rabbit anti-actin (v/v) and 1:5000 donkey anti-rabbit (v/v) in 5 mL 5% milk in TBS-T.

Positive controls for TNKS1/2 for WB was pre made by Dr. Nina Therese Solberg at the Unit of Cell Signaling, Oslo University Hospital. The controls consisted of cell lysate of HEK293 cells treated with DMSO and Wnt-inhibitor 007-LK, and had a concentration of 1.07 µg protein/µL.

In-solution digestion and desalting of proteins

Solutions consisting of 0.5 M DTT, 0.5 M IAM and 10 mg/mL trypsin respectively were pre-made by PhD candidate Henriette Engen Berg. Prior to use of the trypsin solution this was further diluted to 30 µg/mL by diluting 3 µL of 10 mg/mL trypsin to 1000 µL with water. A 50 mM tris buffer was made by diluting 1.5 mL 1 M tris buffer to 30 mL with water. Formic acid solutions were made in both HPLC-grade water and type 1 water, 0.1% FA was made by

diluting 1 µL in 1 mL water, while 1% FA was made by diluting 10 µL in 1 mL water. A solution consisting of 1% FA/ACN (1+2, *v*+*v*), were made by mixing 100 µL of 1% FA and 200 µL of ACN. A pre-digested 1µg/µL HSA sample was also pre-made by PhD candidate Henriette Engen Berg.

2.3 Procedure dependent equipment

In the following sections equipment used for the specific procedures: Gel electrophoresis, western blotting, synthesis and production of monoliths, are presented.

2.3.1 Equipment for gel electrophoresis and western blotting

The different equipment and consumables used during gel electrophoresis and western blotting is presented. A heating block was from Grant instruments. Gel electrophoresis was completed in a mini Cell electrophoresis chamber from Thermo Fisher. Power supplies were from Bio-Rad (Hercules, CA, USA). The 1 mm thick gels with 10 wells used for electrophoresis were Invitrogen NuPAGE™ with 4-12 % 2-bis (2-hydroxyethyl) amino-2-(hydroxymethyl) propane-1,3-diol (Bis-tris) or 3-8% Tris-acetate from Thermo Fisher Scientific. Samples and protein ladder were loaded using microcapillary pipette tips from VWR. Protein transfer onto 45 µm nitrocellulose membranes from Thermo Scientific, was done in a Trans-Blot® SD semi-dry transfer cell from Bio-Rad. A roller from Stuart (Stone Straffordshire, UK) and a mixing plate from Edmund Bühler GmbH (Bodelshausen, Germany) were used. Other consumables were extra thick Blot Filter papir from Bio-Rad and Nobo transparency film obtained from ACCO Brands (Lake Zurich, IL, US). The protein bands were developed with Chemidoc touch imaging system from Bio-Rad, the raw files were treated using Image Lab version 6.0.1 also from Bio-Rad.

2.3.2 Labware utilized for synthesis

All the steps involved in the synthesis of the Wnt-signaling pathway inhibitor were completed in either 25 mL, 50 mL, 100 mL, 250 mL or 500 mL round-bottomed flasks or a 250 mL three-neck flask when a reagent needed to be added dropwise. All reactions were protected from the surrounding air by closing the flask necks with glass stoppers. For addition of acetyl chloride, a 20 mL cylindrical addition funnel was utilized. Suction filtration of the synthesis product was

completed using a Büchner funnel and a 500 mL Büchner flask. All extractions were completed using a 500 mL separatory funnel and extracts were collected in 250 mL Erlenmeyer flasks. For reflux reactions, a condenser flushed with tap water and an oil bath were applied. Reduction and expansion adapters were used to attach the different sizes of glass flasks to the rotary evaporator (rotavapor). Prior to use, all glassware was washed with water and acetone, and dried in an oven at 50 °C. All of the above mentioned glassware was from by VWR.

Thin layer chromatography (TLC) analysis was performed in a tall form beaker with a watch glass as a lid. The plates were TLC Silica gel 60 F_{254}, or TLC Aluminium oxide 60 F_{254} (neutral) on aluminium sheets from Merck. A 1600 W heat gun from Steinel (Herzebrock-Clarholz, Germany) was used for drying of the TLC-plates. The TLC-plates were manually checked at 254 nm ultraviolet light on a fluorescence analysis cabinet, Spectroline® model CM-10, from Spectronics Corporation (Westbury, NY, USA). All reagents were weighed on an Adventurer™Pro weight from Ohaus (Parisippany, NJ, USA). The TLC system is described in **Figure 18**.

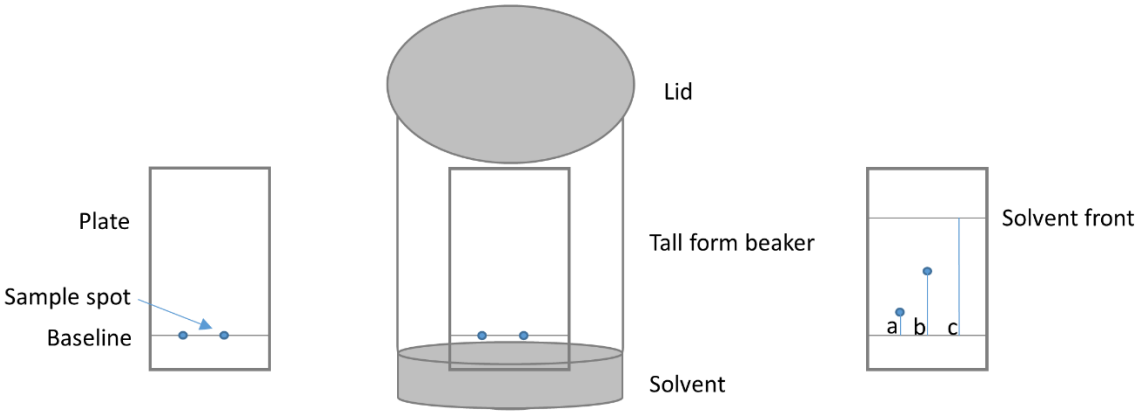

Figure 18: The set-up for TLC analysis of samples. A baseline is drawn with a pencil on the plate, and the samples are spotted onto this line using long glass pipette. The plate is placed in a tall form beaker filled with solvent to cover the bottom, and a lid is placed on top. When the plate is removed the length of the migration of the solvent is marked with a pencil. The length of the migration of the two sample spots and the solvent are marked with a, b and c respectively.

Rotary evaporator

A Hei-Vap™ value rotavapor from Heidolph (Schwabach, Germany) with heated water bath was applied to evaporate the solvents from the reaction mixtures for the synthesis of the Wnt-signaling pathway inhibitor. It was equipped with a PC 3001 VARIO^{pro} vacuum pump and a CVC 3000 vacuum controller from Vacuubrand (Wertheim, Germany).

2.3.3 Equipment for monolithic polymer preparation and evaluation

The monoliths were prepared in polyimide-coated fused silica tubing with an inner diameter (ID) 180 ± 6 µm or 250 ± 6 µm, both with an outer diameter (OD) 360 ± 6 µm, from Polymicro Technologies (Phoenix, AZ, USA). The solutions were made in 1.5 mL Chromatography Autosampler Vials from VWR. The capillaries were attached with 1/16", 0.3 mm ID Valcon polyimide fused silica adapters (ferrules) from Vici Valco (Houston, TX, USA) and 1/16" top nuts. The inner diameter of the ferrules were drilled to 0.37 mm by Inge Mikalsen. The capillaries were filled using a pressure bomb system described in **Figure 19**.

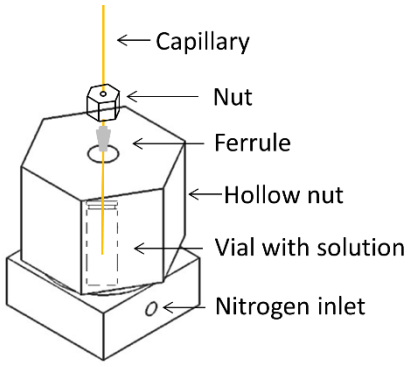

Figure 19: In-house pressure bomb system for filling of capillaries [109, 110]. A capillary is fastened to the hollow nut by a ferrule and a top nut. A vial filled with the desired solution is placed in the cavity of the platform, and the nut with the capillary is screwed airtight onto the platform. When nitrogen gas is turned on, it pressurizes the cavity inside the bomb, and the filling-solution is pushed into the capillary.

The nitrogen gas (99.99%) was purchased from Praxair (Oslo, Norway). After filling GC septa were used to seal both ends of the capillary. For reactions at elevated temperatures, a GC-17A oven from Shimadzu (Kyoto, Japan) was used. The pH was monitored using MColorpHast indicator stripes from Merck (Darmstadt, Germany).To oversee the filling of solutions and formation of monolithic structure a light microscope (W10x/20) from Motic (Xiamen, China) was utilized. Micrographs of the cross-section of the monoliths were captured with a Quanta 200 FEG-E scanning electron microscope (SEM) from FEI Company (Hillsboro, OR, USA) now a part of Thermo Fisher Scientific. For coupling in nanoLC systems fused silica tubing with the specifics of 30 ± 1 µm ID, 360 ± 6 µm OD were used, also from Polymicro Technologies.

2.4 In-situ formation of monolithic polymer

The support for entrapment of TNKS was in this study a monolithic polymer formed *in-situ* by co-polymerization of EDMA and VDM. The pressure bomb in **Figure 19** (previous section) was used to fill, flush and dry the capillaries in the following steps.

2.4.1 Pre-treatment

Appropriate length (2-3 meters) of fused silica capillaries were filled with 1 M NaOH and sealed in both ends by GC septa. The capillaries were left in room temperature (20-23 °C) overnight, 22 h ± 1 h. Residues of NaOH were washed out with water to pH below 7 before the capillaries were flushed with 1.5 mL ACN and dried with nitrogen gas for 20 minutes.

2.4.2 Silanisation

The pre-treated capillaries were filled with a silanisation solution consisting of DPPH, DMF and γ-MAPS. The solution was sonicated for 5 min before use. Both ends were sealed, and the capillary was placed in an oven at 110 °C for 6 hours. After cooling in room temperature for 3 minutes, they were flushed with 1.5 mL ACN and dried with nitrogen gas for 20 minutes. Both pre-treatment and silanisation were based on Hustoft *et al.* [111].

2.4.3 Polymerization

Prior to polymerization the capillaries were cut to 17 cm long pieces and filled with polymerization solution individually. The solution was sonicated for 5 minutes before use. The capillaries were sealed with GC septa and placed in an oven at 70 °C for 24 hours. During polymerization the capillaries were kept close to horizontal in a straight shape, not bent (shown in **Appendix 7.1**, **Figure 52**). Following 3 minutes cooling at room temperature, the capillaries were flushed with 1.5 mL acetone for 20 minutes and dried with nitrogen gas for 20 minutes. The polymerization step was based on the procedure by Geiser *et al.* [58].

2.5 Evaluation of the monoliths and chemicals used

Backpressure over the monoliths was measured using a Proxeon EASY nLC pump from Bruker now Thermo Fisher Scientific. Both mobile phase reservoirs A and B contained 100% ACN, but the isocratic flow was run with 100% B. The pressure monitored over pump B then equaled the pressure exerted on the tubing and monolith. The difference between pressure over tubing with monolith and only the tubing equaled the backpressure of the monolith. Backpressure was measured for the following flow rates: 0.2, 0.4, 0.5, 0.6, 0.8 and 1.0 µL/min.

The cross-section of the monolith was examined by SEM after drying with N_2. From the dry EDMA-co-VDM monolith 1 cm was cut off and glued in an upright position to a sample holder with carbon tape. The sample holder was placed in the sample chamber before the chamber was pumped to low vacuum. A large field detector at 15.0 kV, 12 mm distance for the sample and with a 4.0 spot size was used to capture the micrographs.

The liquid chemicals (*i.e.* DMF, γ-MAPS, VDM, EDMA, 1-propanol and 1,4-butanediol) were replaced during the study and both the new and old chemicals were analysed by Senior engineer Dirk Petterson by standard methods in proton nuclear magnetic resonance (^{1}H-NMR). The spectra were recorded on an AVII400 NMR instrument (400 MHz) with a BACS-120 automatic sample changer both from Bruker (Billerica, MA, USA) and the chemicals were dissolved 1+9 in deuterated dimethyl sulfoxide (DMSO-D^6) from Cambridge Isotope Laboratories (Tewksbury, MA, USA).

2.6 Synthesis of Wnt-signaling pathway inhibitor

The synthesis was completed with the coaching and guidance from Dr. Christian Schnaars and Professor Pål Rongved. The different steps of the synthesis were executed several times and always with a small test scale before a larger scale. In the following description of the reactions, a large-scale example is given. ^{1}H-NMR acquisitions of the crude material and cleaned product were recorded by Christian Schnaars. DMSO-D^6 from Euriso-top (Saint Aubin, France) was used as solvent and the spectra were recorded on DPX200 (200 MHz), DPX300 (300 MHz) or AVII400 (400 MHz) NMR instrument from Bruker depending on availability. Standard methods from Bruker were used for recording. The labware and TLC set-up used during synthesis is described in **Experimental 2.3.2**. Engineer Osamu Sekiguchi at the laboratory for mass spectrometry at the Department of Chemistry executed composition analysis for confirmation on the molecular formula, described in **Appendix 7.4**.

2.6.1 Formation of *tert*-butyloxycarbonyl protected LDW639

The first step of the synthesis, **Figure 20**, was performed at room temperature by mixing 2.0 g (11.48 mmol, 1.0 equiv.) of the beta-keto ester with 3.005 g (12.05 mmol, 1.05 equiv.) BOC-benzamidine in 60 mL of MeOH. To this 3.173 g (22.96 mmol, 2 equiv.) of K_2CO_3 was added with magnetic stirring. The reaction mixture was left on stirring overnight (~18 to 20 hours) in

a closed vessel. The mixture was filtered and washed twice with 3.5 mL MeOH before evaporating the solvents using a rotavapor (60 °C, 300 → 0 mbar).

The dried material was dissolved in 500 mL water and pH adjusted to pH 5 by adding 1 M HCl dropwise. The precipitated material was separated from the solution by suction filtration and washed with 75 mL cold water/MeOH *(1/1, v/v)* and 75 mL cold diethyl ether. The material was dried further using the rotavapor (60 °C, 300 → 0 mbar).

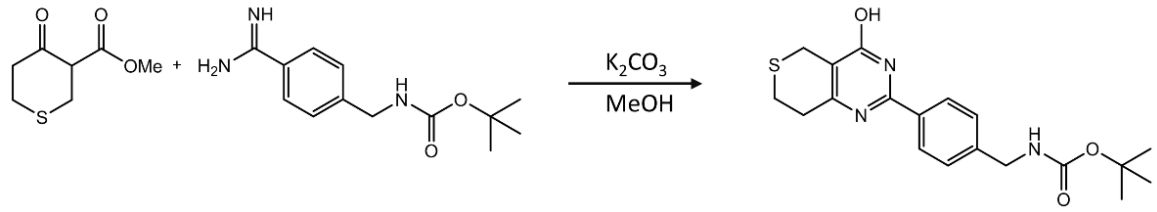

Figure 20: First step in the synthesis of the linked LDW639.

2.6.2 Deprotection of *tert*-butyloxycarbonyl protected LDW639

The crude material (2.93 g, 7.85 mmol, 1.0 equiv.) dissolved in 300 mL MeOH was cooled to 0 °C by half submerging the reaction vessel in a cold bath (50/50 tap water and ice). The compound was then deprotected by dropwise adding 11.2 mL (157.01 mmol, 20.0 equiv.) acetyl chloride over a period of 15-min. The mixture remained on stirring overnight (~18 to 20 hours) while increasing the temperature from 0 °C to room temperature in an airtight three-neck flask. The solvents were evaporated using the rotavapor (60 °C, 600 → 0 mbar). The step is summarized in **Figure 21**.

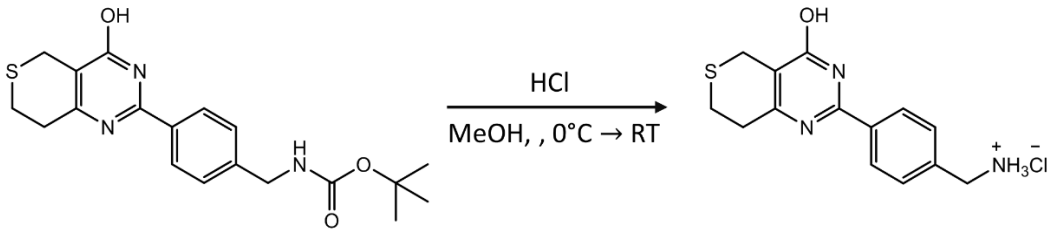

Figure 21: Second step in the synthesis of the linked LDW639.

2.6.3 Adding *tert*-butyloxycarbonyl protected linker through a peptide coupling

The LDW639 (2.05 g, 6.65 mmol, 1.0 equiv.) in form of a chloride salt was dissolved in 65 mL DMF on magnetic stirring and cold bath. To the mixture 1.84 g (6.98 mmol, 1.05 equiv.) 2,2-

dimethyl-4-oxo-3,8,11-trioxa-5-azatridecan-13-oic acid (*i.e.* the linker used in this study) and 2.78 g (7.32 mmol, 1.1 equiv.) HATU was added. NMM (1.8 mL, 16.63 mmol, 2.5 equiv.) was added dropwise over a 10-minute period. The reaction remained on stirring and in a cold bath overnight (~18 to 20 hours) increasing the temperature of the mixture from 0 °C to room temperature slowly. The synthesis step is summarized in **Figure 22**.

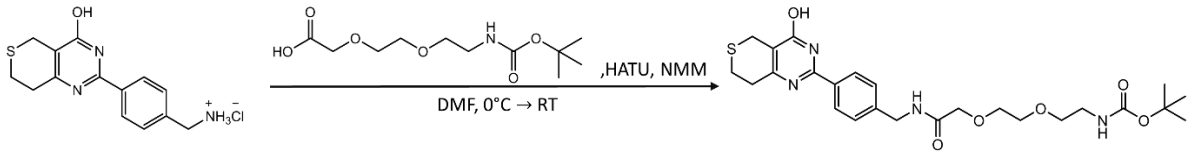

Figure 22: Third step in the synthesis of the linked LDW639.

The solvents were then removed on the rotavapor (60 °C, 450 → 0 mbar), before dissolving the residue in 100 mL water and adding 100 mL saturated K_2CO_3 solution. The mixture was extracted three times with 150 mL ethyl acetate. The three fractions of the organic phase were mixed and dried by adding a $MgSO_4$ powder for 60 min. The mixture was then filtered and evaporated on the rotavapor (60 °C, 450 → 0 mbar).

The dried powder was added to 100 mL ethyl acetate for recrystallization. By heating under reflux on an oil bath at 70 °C, the powder was dissolved giving a saturated solution. A filtration of the hot solution was completed to remove insoluble impurities before slowly cooling to room temperature for 45 min and cooled further at 4 °C in the fridge for 15 min. An additional 50 mL ethyl acetate was used to wash the reaction vessel and the filter before and after hot filtration. The precipitate was gathered by suction filtration and concentrated to dryness using the rotavapor (60 °C, 600 → 0 mbar).

The last step of the synthesis was an identical deprotection of the linker with acetyl chloride as described in **Experimental 2.6.2** and shown in **Figure 23**.

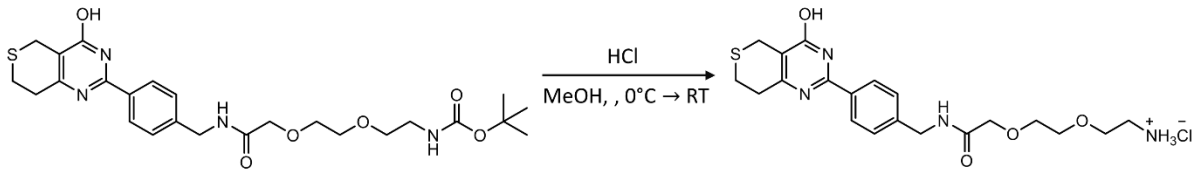

Figure 23: Last step in the synthesis of the linked LDW639.

2.6.4 Determination of Wnt-activity

To establish if the synthesized drug did affect Wnt-signaling, a SuperTOPFlash-luciferase assay (STF-Luc) for Wnt-activity was executed by technician Eric Maximilian Lycke at the Unit of Cell Signaling, Oslo University Hospital. The STF-Luc assay was performed as described by Voronkov *et al.* [87]. The synthesis product was tested in the following concentration range: 0.12, 0.37, 1.1, 3.3, 10 and 25 µM, and incubated for 24 hours. The activity of both luciferase and *Renilla* was measured. In addition to the synthesis product, HCl controls were analysed in the same concentration range.

2.7 Immobilization of drug on monolith

Prior to immobilization of the linked LDW639, the monoliths were flushed with 50 mM phosphate buffer (pH 7.2) for 5 minutes using the pressure bomb system. Subsequently the monoliths were flushed with either a 0.25 mg/mL or 5 mg/mL drug dissolved in 50 mM phosphate buffer (pH 7.2) for 3 hours (approx. 0.5 mL). The solution flushed through the monolith was collected in a tube and marked as "Flush". The monolith was then washed with 50 mM phosphate buffer.

The monoliths with drugs immobilized will be referred to as a *capti remedium ad monolitus* reactor, CRAM reactor. The CRAM reactors were filled with 50 mM phosphate buffer, sealed with GC septa and stored at 4 °C in the fridge. A reference monolith was made by flushing 1 M MEA for 3 hours in the same way as the solution consisting of drug, and was stored in the same manner as the CRAM reactors.

For the collected solutions and the remaining immobilization solution the UV-Vis absorbance were measured. For measuring either a SpectraSystem UV2000 with an on-column capillary cell (model 9550-0155), both from Thermo separation products now Thermo Fisher Scientific, or a NanoDrop2000 spectrophotometer with pedestal from Thermo Scientific were used.

2.7.1 Ultraviolet detection using a capillary CZE cell

A Hot-Strip™ thermal wire stripper equipped with wolfram filament from Ungar Electric Tools, a part of Eldon Industries (Compton, CA, USA) was used to burn off a detection window (~3 mm) on empty 17 cm, 250 µm ID fused silica tubing. The residue of the burnt coating was

washed off with water and MeOH. The baseline was set with an empty capillary, and a capillary filled with 50 mM phosphate buffer was used as a blank sample. The samples collected during the immobilization procedure were filled in capillaries using the pressure bomb system. Absorbance of the samples was measured at 254 nm.

2.7.2 Ultraviolet-visible absorbance measured by nanodrop

A NanoDrop2000 spectrophotometer with pedestal was also used for measuring of the ultraviolet-visible (UV-Vis) absorbance of the collected solutions from the immobilization procedure. For each sample, 2.5 µL was applied to the pedestal, and 50 mM phosphate buffer was used as blank sample. An absorbance spectrum was recorded in the range 190 nm to 840 nm.

2.8 Human embryonic kidney 293 cells

The cells used in this project were received from the unit of Cell Signaling, Oslo University Hospital after cell cultivation by Petter Angell Olsen. The cell lines human embryonic kidney 293 cells (HEK293) were purchased from American Type Culture Collection (ATCC, Manassas, VA, USA), and maintained according to the ATCC guidelines. The stable reporter cell line Super-Topflash (STF) HEK293 was obtained from Vladimir Korinek and transfected with linearized Renilla (REN) plasmid to yield STF/REN HEK293.

Samples containing 18 million cells of a human cell line HEK293 – STF/REN and 18 million cells of a HEK293 cell line transfected with an enhanced green fluorescence protein for overexpression of tankyrase 1 (HEK293-EGFP-TNKS1) were received. The cells were dissolved in 1000 mL water and redistributed to new tubes with ~1 million cells (56 µL) in each. Prior to freezing at -80 °C, 1 µL of 40x protease inhibitor was added. Prior to sample preparation the cell samples were thawed on ice and kept on ice during preparations.

2.8.1 Cell lysis by ultrasonication

Prior to ultrasonication the samples were added either 43 µL of 13.8 M urea in 230 mM ABC or 43 µL water. The samples were vortexed by pipetting up and down before being placed in an ultrasonic bath for 30 min at 40 kHz. The ultrasonic bath was filled with a mixture of water and ice to hold a temperature of 8 °C. Subsequently the samples were centrifuged for 5 min at

4 °C at 9391 relative centrifugal force (rcf). The supernatant was pipetted into new tubes, and stored at -20 °C.

2.8.2 Cell lysis with buffer

For cell lysis with a non-denaturing buffer the procedure was based on Voronkov *et al.* [87]. The cell samples were added 200 µL of the buffer and vortexed by pipetting up and down a minimum of 10 times. During the incubation time of 30 min on ice, the samples were ultrasonicated at 40 kHz prior to incubation and after 15 min. After incubation the samples were centrifuged for 15 min at 14000 rcf, and the supernatant was pipetted into new tubes and stored at -20 °C. The procedure for cell lysis with RIPA buffer was done as described for the non-denaturing buffer.

2.8.3 Protein concentration determined with bicinchoninic acid assay

The concentration of protein present in the cell lysates samples was determined by bicinchoninic acid assay (BCA assay) using a BCA™ protein assay kit from Thermo Scientific. Reagent A and reagent B were mixed 50:1, and 40 µL of this solution was distributed in a 96-microwell plate from VWR. The accompanying BSA calibration standard was distributed to 6 wells giving the following amount of protein 0, 2, 4, 6, 8 and 10 µg. Three replicates of the calibration standards were made. Triplicates of 2.5 µL of cell lysate samples were analysed. The total volume in the wells were after dilution with water 45 µL. Both the standards and samples were vortexed by pipetting up and down. The 96-well plate was placed in a Shimadzu GC-oven for 30 min at 37 °C. Subsequently the absorbance at 562 nm was measured with a NanoDrop2000 spectrophotometer. An example of the calculation of the amount of proteins in the samples are given in **Appendix 7.9**.

2.9 Experimental set-up for manual application of protein standards on a CRAM reactor

Initially a simple manual technique was used to apply solutions onto the monolith. A 25 µL glass syringe from SGE Analytical Science a part of Tarjan Scientific and Medical (Melbourne, Australia) was coupled to an empty fused silica for filling of the syringe, and coupled to a

CRAM reactor for applying the solution onto the reactor, shown in **Figure 24**. The coupling consisted of a 1/16" stainless steel union, nuts and ferrules.

This set-up was used twice, once for a tankyrase solution consisting of 0.028 mg/mL recombinant TNKS2, and once for a protein mix consisting of recombinant TNKS2, myoglobin and cytochrome C all in a concentration of 0.035 mg/mL.

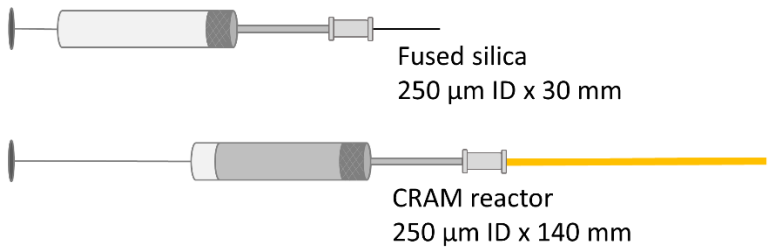

Figure 24: Manual application equipment for CRAM reactor.

The CRAM reactor was first rinsed twice with 25 µL of 50 mM AmAc. Then over a 25 min time period, 20 µL of tankyrase solution (or protein mix) was added stepwise, pushing in 3 µL and wait for 5 min, repeated 5 times. The solution coming out of the reactor was collected and marked as "Flush". Following injection of tankyrase the syringe was washed with 25 µL AmAc, 75 µL MeOH and 25 µL AmAc. In the next step, the CRAM reactor was rinsed twice with 20 µL AmAc, and solution pushed through was collected and marked as "Wash1" and "Wash2". Following this step, 20 µL of an elution solvent was pushed through the reactor, collected and marked "Elution X", where X was the name of the elution solution used for that collection, the solutions are given in **Table 1**. After use the CRAM reactor was washed and filled with 50 mM phosphate buffer for storage at 4°C. The procedure was the same for monoliths without immobilized drugs.

Table 1: Overview of the elution solutions.

#1	10% ACN	**#4**	40% ACN	**#7**	30% ACN in 0.1M NaOH
#2	20% ACN	**#5**	50% ACN	**#8**	0.3M NaOH
#3	30% ACN	**#6**	0.1M NaOH	**#9**	isopropanol/AmAc (4/96, v/v)

2.10 Semi-automated experimental set-up for application of lysed cells on a CRAM reactor

The manual system in the previous section replaced by a Proxeon EASY nLC pump with both mobile phase reservoirs A and B contained 100% HPLC-grade water, and was run with 35% B having an equal pressure distribution on both pumps. Injection was performed using an external 6-port two-position valve from Vici Valco with an attached 20 µL Proxeon polyetheretherketone (PEEK) sample loop and a 250 µL glass syringe from SGE Analytical Science. Attachments to the 6-port valve was done using 1/16" ferrules and nuts. The CRAM reactor was attached to the external port as shown in **Figure 25**, and the pump was set at 1 $\mu Lmin^{-1}$ flow rate.

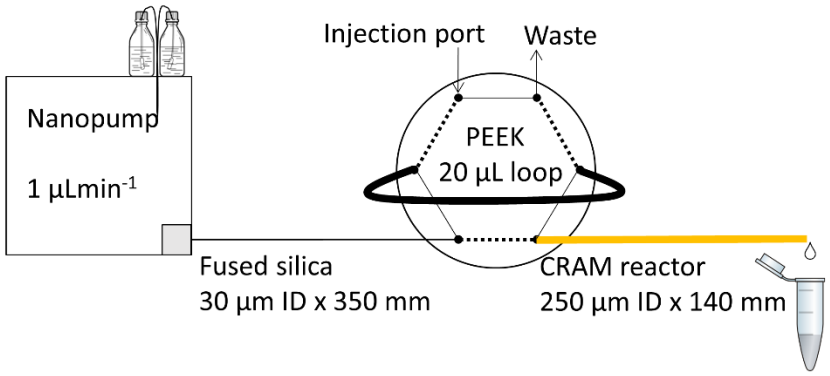

Figure 25: Scheme of a semi-automatic instrumentation using a nanoLC pump connected to an external 6-port valve with a 20 µL PEEK sample loop for application of solutions onto CRAM reactors. The external valve is depicted in "inject" position, by switching to "loading" position the injection port would be connected to the loop and waste, while the pump would be connected directly to the CRAM reactor.

The CRAM reactor was first rinsed for 30 min with the mobile phase with the valve in loading position, while cell lysate was filled into the sample loop. The valve was switched and the cell lysate passed through the CRAM reactor and the eluate was for the following 30 min collected in a tube marked "Flush". In the next 30 min another fraction was collected and marked "Wash1", this was repeated once, this fraction marked "Wash2". During the last collection the sample loop was washed and filled with an elution solution. The elution solution was passed through the CRAM reactor for 30 min, collected and marked "Elution Y", where Y was the name of the elution solution used for that collection, the solutions are given in **Table 2**. After use the CRAM reactor was washed and filled with 50 mM phosphate buffer for storage at 4°C. The procedure was the same for monoliths without immobilized drugs.

Table 2: Overview of the elution solutions.

#a	isopropanol/AmAc (4/96,v/v)	**#e**	1 M AmAc (pH 7.2)
#b	50 mM AmAc (pH 7.2)	**#f**	2% FA
#c	200 mM AmAc (pH 7.2)	**#g**	2% SDS
#d	500 mM AmAc (pH 7.2)		

2.11 Western Blot

In this section the final procedure used for analysis of samples by WB is presented. The first experiment was carried out with the help of PhD candidate Frøydis Sved Skottvoll, as a way to learn the mechanics of running a WB analysis.

Prior to application of sample on the gel, in-house loading buffer was mixed 1+3 (*v+v)* with sample diluting it to a 1x loading buffer and heating the samples at 70 °C for 10 min on a heating block.

Gel electrophoresis

For gel electrophoresis, a 3-8% Tris-acetate gel was washed gently with tap water and inserted in the electrophoresis chamber. The chamber between the two gels (if only one gel was run, a dummy gel was used in the second position) was filled with 25 mL SDS tris-acetate (20X) running buffer diluted to 500 mL with tap water. For each type of sample 10 µL of protein ladder were distributed to a well on the gel. 20 µL of each sample was distributed to the wells.

The gel was applied 75 V (200 mA) for 1 hour before the voltage was increased to 110 V (200 mA) for another hour allowing the horizontal bromophenol blue lane to reach the end of the gel. After turning off the voltage, the gels were removed from the covers using a spatula. The gels were cut at the bromophenol blue line, and the wells were cut away. The gels were rinsed and incubated with transfer buffer (1x) for 15 min.

Immunoblotting

A 45 µm nitrocellulose membrane was cut to match the size of the gels for protein transfer. The membrane was washed in transfer buffer (1x) for 15 min. Protein transfer from gel to membrane was done building a “transfer sandwich” in the following order in the cell: filter paper,

membrane, gel and filter paper. The filter paper was partly soaked in transfer buffer (1x). Each layer was rolled with a 10 mL pipette to remove air bubbles and kept semi-dry by adding transfer buffer (1x). The chamber was left overnight at 4 °C with 1 W applied.

On the following day, the membranes were cut according to the size of the gels. The membranes were blocked for 1 hour in 5% nonfat-milk in TBS-T on a mixing plate. To 5 mL of 5 % nonfat-milk in TBS-T in a 50 mL tube, 20 µL of primary antibody for tankyrase-1/2 (host animal mouse) was added (1:250 dilution). The membranes were transferred to the tubes with primary antibody and incubated at 4 °C on a roller overnight.

Before incubation with secondary antibody (donkey-antimouse, diluted 1:5000 in 5 % nonfat-milk in TBS-T), the membranes were rinsed and washed in TBS-T on a mixing plate for 20 min. Transferring the membrane to tubes containing secondary antibodies in a solution, the membranes were incubated with secondary antibodies for 2 hours on a roller at RT.

Visualization

The membranes were twice rinsed and washed with TBS-T for 20 min on a mixing plate. Enhanced chemilumiscence prime (ECL-prime) was made by mixing the two components 1+1 *v+v* giving 500 µL per membrane. The ECL-prime was pipetted back and forth over the membranes for 3 min. Finally, the membranes were placed between two sheets of transparency film and covered with additional ECL-prime. Bubbles were removed by stroking filter paper over the film surface. The protein bands were developed with Chemidoc touch imaging system from Bio-Rad.

Loading control

After visualization the membranes were twice rinsed and washed with TBS-T for 20 min on a mixing plate, before primary (rabbit-antiactin, dilution 1:1000 in 5% nonfat-milk in TBS-T) and secondary (donkey-antirabbit, dilution 1:5000 in 5% nonfat-milk in TBS-T) antibodies for actin were applied in the same manner as described above and the membranes were visualized again for actin.

2.12 Liquid chromatography mass spectrometry

In this section the experiments conducted using LC-MS will be described. The final synthesis product, a linked LWD639, and a known Wnt-inhibitor 161 were introduced into the MS by direct injection. Samples from protein standards applied on monoliths with immobilized through linker on LDW639 were measured by adopting an LC-MS method made for measuring HSA by PhD candidate Henriette Engen Berg.

2.12.1 Confirmation of monoisotopic mass by mass spectrometry

Wnt-inhibitor 161

The Wnt-inhibitor 161 was analysed by direct injection on a triple quadrupole MS after being diluted 1:10000 in 0.1% FA in HPLC-grade water. The mass spectrometer was a TSQ Quantiva^{TM} Triple Quadrupole Mass Spectrometer from Thermo Fisher Scientific. By using a syringe pump (model Fusion101) from Chemyx Inc. (Stafford, TX, USA), the inhibitor was introduced into the nanospray interface with a flow rate of 2 µL/min. The syringe pump was coupled to the nanospray needle using a 50 µm ID polyimide-coated fused silica capillary. The nanospray interface was operated in positive mode with + 2.2 kV applied onto the needle and the ion transfer tube into the MS was held at 310°C. The MS was operated in full scan mode, scanning over *m/z* range 100 to 1100, while searching for the monoisotopic mass of inhibitor 161, 578.09 Da. The MS was operated with a scan rate of 1000 amu/s and a resolution of 0.7 at the first quadrupole mass filter.

Synthesis product; Linked LDW639

The analysis of the linked LWD639 was done on a Q-Exactive Mass Spectrometer from Thermo Fisher Scientific with a heated electrospray ionization (HESI) ion source. The sample of LDW630 was made in the concentration 5µg/µL by dissolving 3.8 mg in 0.76 ml 0.1% FA and further diluted to 0.1 µg/µL (10 µL of 5µg/µL in a total of 500 µL) prior to injection with a syringe pump (model pump 11 elite) from Harvard Apparatus (Holliston, MA, USA) at a flow of 5 µL/min. The syringe was coupled to the ion source using a 130 µm ID PEEK capillary. The HESI interface was operated in positive mode with +4.0 kV applied onto the needle and the transfer capillary temperature was 350°C. The MS was operated in full scan mode, scanning over *m/z* range 50 to 600 with no fragmentation while searching for the monoisotopic mass of

the linked LDW639, 419.1748 Da. The MS was operated with a working resolution of 70000, a target $1x10^6$ automatic gain control (AGC), and a maximum injection time of 30 s.

2.12.2 Sample preparation prior to analysis by liquid chromatography mass spectrometry

Prior to introducing the samples to the LC-MS, the samples were in-solution digested with trypsin and desalted by Zip-tip. All steps were completed in 1.5 mL Protein LoBind tubes. The Zip-tip used was a PerfectPure C-18 from Eppendorf.

In-solution digestion of proteins

For in-solution digestion the samples were first concentrated to dryness using an Eppendorf concentrator and resolved in 100 µL 50m M tris-buffer (pH 8.0) and whirlmixed at max speed for 10 s. Then 2 µL of 0.5 M DTT was added to the tubes by pipetting up and down ten times. The samples were then heated at 37°C on an incubator for 45 min, before cooling down to room temperature. Subsequently 6 µL of 0.5 M IAM was added to the tubes by pipetting up and down ten times. The samples were placed in the dark at room temperature for 20 min. Following this 5 µL of 30 µg/mL trypsin was added, and the samples were incubated at 37°C on a shaker with 1000 rpm. After 20 hours, 3 µL of 1% FA in HPLC-grade water was added. The samples were concentrated to dryness using an Eppendorf concentrator and resolved in 10 µL 0.1 % FA in HPLC-grade water and whirlmixed at max speed for 1 min.

Desalting of peptide sample

For each sample that is to be desalted, 10 µL of 1% FA in ACN (1+2, *v*+*v*) were distributed to new tubes. The following steps were repeated for each sample: First the Zip-tip was washed by pipetting 10 µL of 1% FA in ACN (1+2, *v*+*v*) three times to waste, followed by 10 µL of 1% FA twice. The sample was then loaded on the Zip-tip by pipetting up and down 4 times. The Zip-tip was then washed twice with 10 µL HPLC-grade water, before the sample was eluted in the prefilled tubes by pipetting the solution of 1% FA in ACN (1+2, *v*+*v*) up and down three times.

After desalting the samples were concentrated to dryness on an Eppendorf concentrator, resolved in 15 µL 0.1% FA in HPLC-grade water, and transferred to 0.3 mL autosampler vials.

All samples were desalted using the same Zip-tip, and the Zip-tip was stored in MeOH after use.

2.12.3 Adopting a human albumin serum method for measurement of tankyrase

The method described in this section was developed by PhD candidate Henriette Engen Berg. The analysis of the peptide samples was done on an Easy-nLC1000 pump with auto sampler and a 20 µL NanoViper PEEK sample loop, in combination with a Q-Exactive MS with a Nanospray Flex ion source, all from Thermo Fischer Scientific. The emitter was a 20 µm ID x 40 mm (length) stainless steel nanobore emitter also from Thermo Fisher Scientific. The 50 µm ID x 30 mm pre-column and 50 µm ID x 150 mm analytical column were particle packed columns, and the packing material was 2.6 µm particles with pore size 150 Å (15 nm) Accucore C-18, a type of core-shell particles. Both columns were prepared by PhD candidate Henriette Engen Berg. The instrument set-up is shown in **Figure 26**. All of the couplings consisted of 20 µm ID fused silica capillaries, stainless steel unions, ferrules, nuts, and a T-piece from Vici Valco.

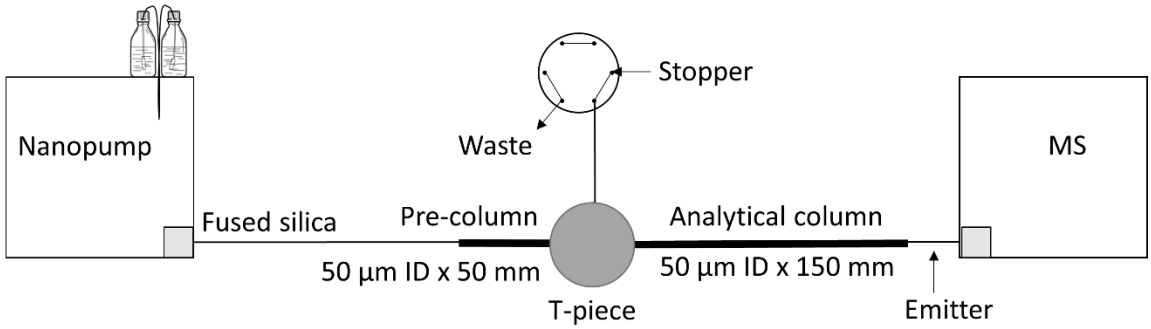

Figure 26: Scheme of the instrumentation and coupling of the pre- and analytical column to the emitter for introducing samples to the MS.

The chromatographic method

The mobile phase reservoirs contained: (A) 0.1% FA in HPLC-grade water (*v/v*), and (B) 0.1% FA in 90%/10% ACN/HPLC-grade water (*v/v/v*). Prior to each run the pre-column and the analytical column were equilibrated respectively with 2 µL and 4 µL of mobile phase A, with the flow restricted at 400 bar. Sample loading of 5 µL was executed from the auto sampler and the flow was restricted at 300 bar. The gradient used for elution is shown in **Figure 27**, and the flow rate was 150 $nLmin^{-1}$.

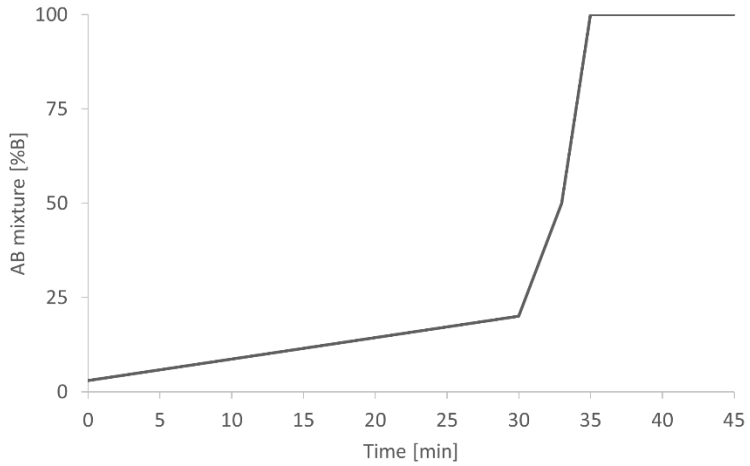

Figure 27: Gradient used in the method presented by the percentage of mobile phase B at a given time during the runs.

Mass spectrometry settings

The MS was operated in positive polarity and +1.8 kV applied onto the emitter and the transfer capillary temperature was at 275°C. The MS was operated in full scan mode with a working resolution of 70000, a target $1x10^6$ AGC, and a maximum injection time of 120 s. The MS scanned over a *m/z* range 350 to 1850 m/z. In data dependant (dd)-MS/MS mode, the working resolution was 17500, with a AGC target of $1x10^5$, and a maximum injection time of 60 ms. The following charges were excluded: 1, 7, 8 and >8, and dynamic exclusion was 40 s. The HCD cell had a normalized collision energy set at 28.

Data processing

Data processing of mass spectra was completed using Xcalibur™ software, while identification of peptides was done with Proteome Discoverer™ 1.4 software, both from Thermo Fischer Scientific. The peptide searches were completed using a SEQUEST algorithm. For identification of HSA, TNKS2, cytochrome C and myoglobin, their respective FASTA-files (*i.e.* peptide sequence) were downloaded from UniProt. The file of TNKS2 was manually adjusted to only contain the amino acids 667 to 1166. The search criteria were restricted by 2 missed cleavages, precursor mass tolerance 10.0 ppm and fragment mass tolerance 0.6 ppm. The allowed modification of the peptides were oxidation of methionine side chains, carbamidomethylation of cysteine side chains, and acetylation of N-terminus.

3 Results and discussion

The objective of the present study was to develop a method for drug discovery utilizing monolithic polymers for immobilization of a drug (named a CRAM reactor by the author), and examine if the protein target of the drug could be selectively trapped. For evaluation of this method, an EDMA-co-VDM monolith was immobilized with a linked Wnt-signaling pathway inhibitor, and the CRAM reactor was evaluated for the potential of selectively trapping the protein target TNKS1/2. TNKS1/2 was selected as the model drug target due to it being a low abundant protein, displays protein-protein interactions, and may self-oligomerization to form large TNKS1/2 complexes consisting over 30 molecules [107, 108].

If successful, the method would offer more information and a securer target identification from cell lysate for drugs with unknown targets, compared to the biased traditional screens used to assess selectivity and off-targets liabilities [38].

The project is presented in three parts with the outline described in **Figure 28**. The first two parts discusses the production of the individual parts of the CRAM reactors: the monolithic support (**Chapter 3.1** and **3.2**) and the Wnt-inhibitor drug (**Chapter 3.3** and **3.4**). The last part shows the examination of immobilization of the drug onto the monolith (**Chapter 3.5**) and the performance of the CRAM reactor (**Chapter 3.6**).

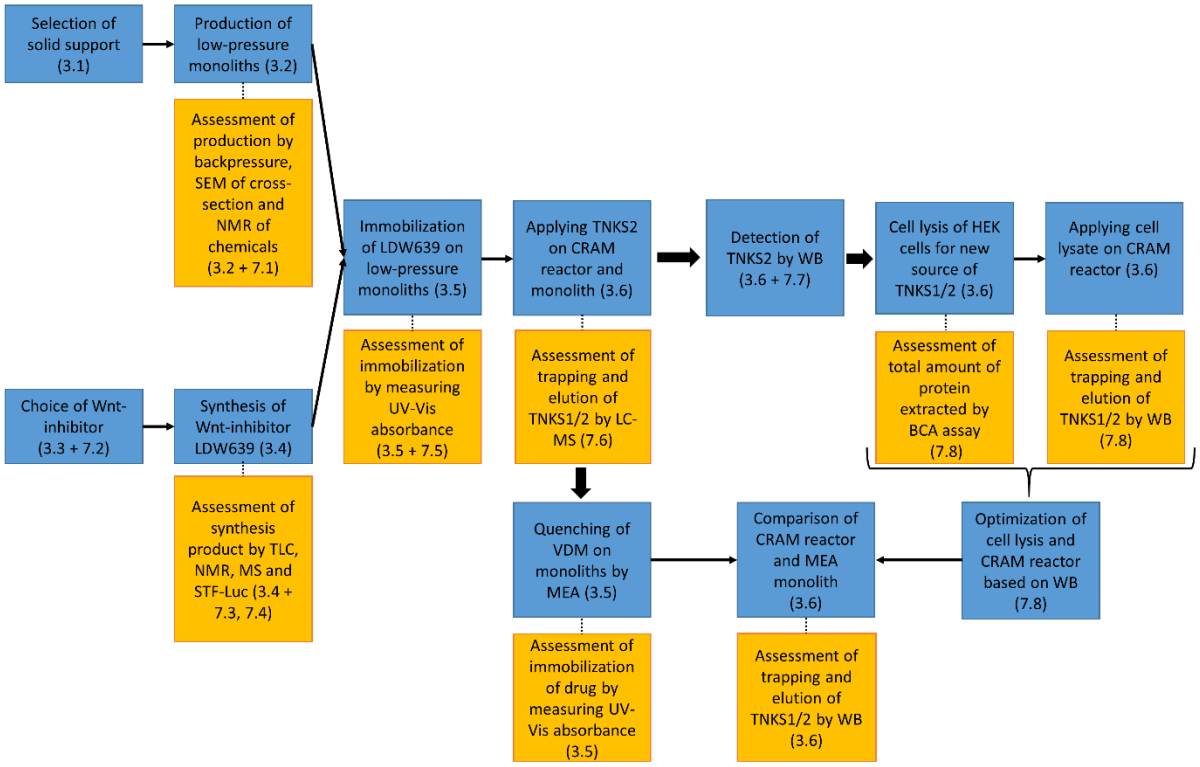

Figure 28: Outline of the presentation of the results and discussion section, the numbers represent the chapter presenting the content in the box. The large black arrows indicate major changes (*e.g.* changing detection method from LC-MS to WB).

3.1 Selection of solid support for immobilization

Organic monoliths were selected as solid support for immobilization of drugs, due to their low backpressure (*i.e.* allows faster loading of samples), the reported easy attachment of additional molecules after polymerization and the accessibility of these molecules [52]. The EDMA-co-VDM monolith was selected based on low secondary interactions and the functionality of VDM [112]. Organic molecules and biomolecules with nucleophiles, *e.g.* amines, thiols and alcohols, may be covalently bound with VDM by a ring-opening reaction [113-115]. This process is still active after a co-polymerization with a different monomer to form both beads and monoliths. Protein A was immobilized on methylene-bis-acrylamide (MBA)-co-VDM beads by Coleman *et al.* [37], and the EDMA-co-VDM monolith has been used for immobilization of pepsin by Geiser *et al.* [58]. Additionally, the author of this study has previously immobilized trypsin on the EDMA-co-VDM monolith [116].

3.2 Production of 250 µm inner diameter monoliths

The author had previously successfully prepared 180 µm ID EDMA-co-VDM monoliths [116], but a large surface area of the monoliths are important in this study as the monolith is immobilized with drug after preparation. A monolith with a larger surface area would have a larger number of sites with drugs attached compared to monoliths with a smaller surface area. A larger ID of the capillary used for preparation of the monoliths would give a large surface area. A 250 µm ID capillary with the same outer diameter was available and selected for preparation. The monoliths prepared in 180 µm ID and 250 µm ID capillaries should be assessed by backpressure and the structure of the monolith. The monoliths were polymerized individually in capillaries shorter than 20 cm as the formation of polymer was not repeatable in capillaries longer than 20 cm [116].

Initially the EDMA-co-VDM monoliths were prepared in both 180 µm ID and 250 µm ID capillaries, but during pressure testing of the monoliths disturbingly large variations were discovered for the 180 µm ID monoliths as shown in **Appendix 7.1**, **Table 8**. The background for this deviation was revealed by SEM micrographs, examples are given in **Figure 29** and **Figure 30**. The monoliths prepared in 180 µm ID had issues with both attachment to the capillary wall, and formation of large through-pores breaking the desired monolithic structure. No problems were discovered by SEM for the 14 EDMA-co-VDM monoliths prepared in 250 µm ID capillaries. The problems with the 180 µm ID monoliths persisted even as the same silanisation solution and polymerization solution was used to prepare 180 µm ID and 250 µm ID monoliths. The 180 µm ID monolith and the 250 µm ID monolith in **Figure 29**, were prepared with the same silanisation solution and polymerization solution. Only the 250 µm ID monolith had the desired uniform structure. Based on these findings 250 µm ID EDMA-co-VDM monolith were used for testing as CRAM reactors.

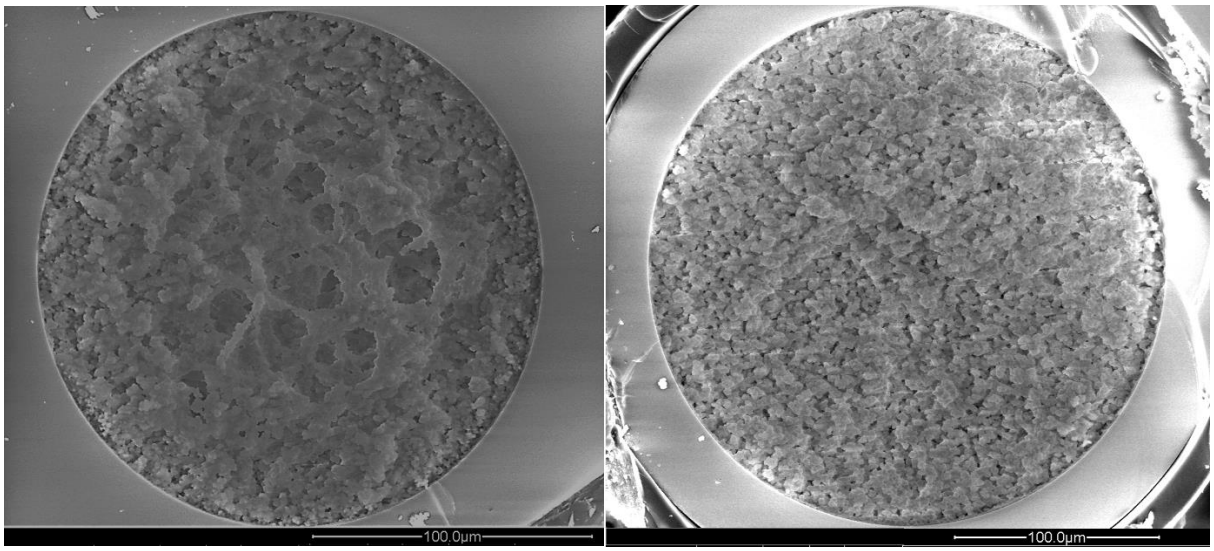

Figure 29: SEM micrographs of the cross-section of two EDMA-co-VDM monoliths prepared with the same batch of silanisation solution and polymerization solution: (left) 180 µm ID capillary and (right) 250 µm ID capillary.

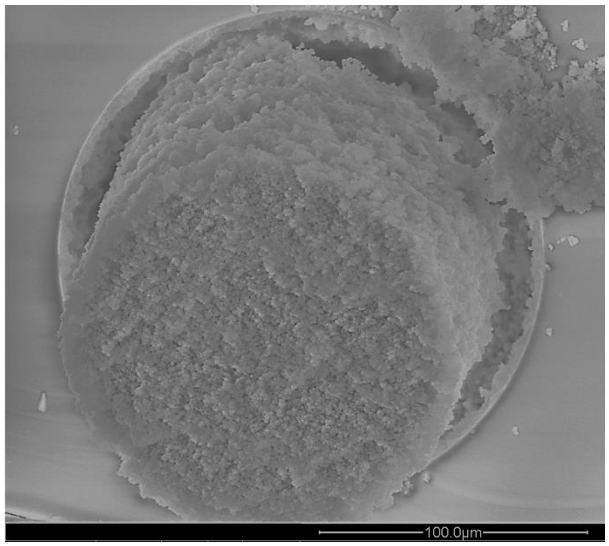

Figure 30: SEM micrograph of the cross-section of a 180 µm ID EDMA-co-VDM monolith where the monolith has not successfully covalently attached to the capillary wall.

Compared to the recipe the EDMA-co-VDM monolith was based on (Geiser *et al.* [58]), the percentage of AIBN was increased from 0.4% to 1% serendipitously. The increased concentration of initiator should give a faster reaction mechanism, which in theory should give smaller globules and pores. Comparison of the micrographs of the EDMA-co-VDM monolith reported in Geiser *et al.* [58] and the one presented in this study is shown in **Figure 31**. The size of the globules and pores appears to be large in the 100 µm ID EDMA-co-VDM monolith prepared by Geiser *et al.* compared to the 250 µm ID EDMA-co-VDM monolith prepared in this study. The reduction of the globules and the pores gives a larger surface area available for

immobilization, and as mentioned at the beginning of this section, a large surface area was desired in this study.

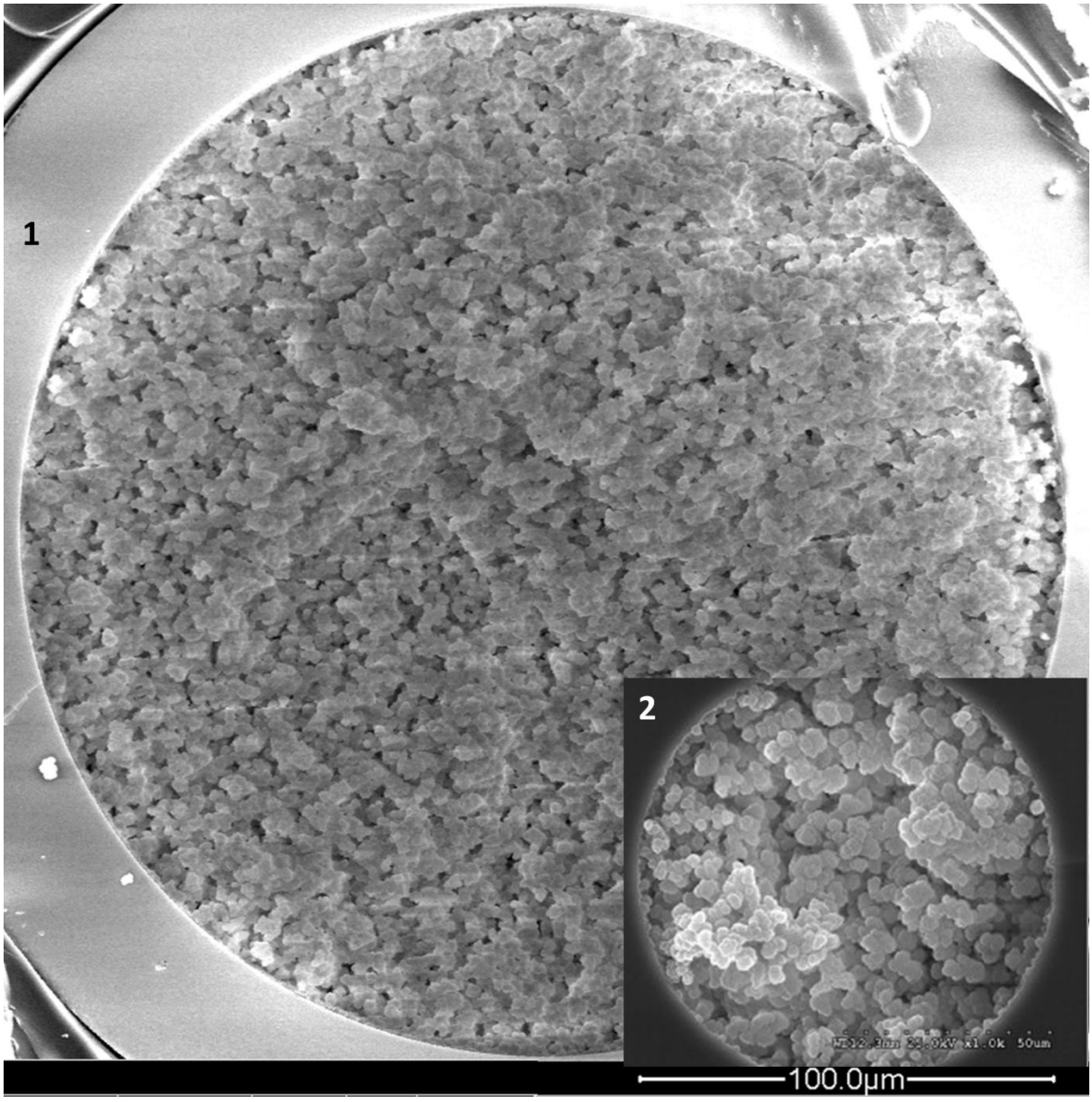

Figure 31: SEM micrographs of the cross-section of EDMA-co-VDM monoliths: (1) prepared in 250 µm ID capillary in the present study and (2) prepared in 100 µm ID capillary by Geiser *et al.* [58]. SEM micrograph of the monolith marked as number 2 was adapted from Geiser *et al.* [58]. The micrographs are presented with the same scale.

Replacement of chemicals used for monolith preparation

During the study the supply of VDM ran out, and as a consequence of the problems discovered with the 180 µm ID monoliths, the other liquids used for preparation of the EDMA-co-VDM monolith were also replaced. To be certain that the exchange of liquid did not disturb the production of the monoliths, both old and new chemicals were examined by ^{1}H-NMR to see if

any degradation or contaminations were present. Also, a comparison of backpressure on monoliths prepared with old and new chemicals was carried out for the 250 µm ID monoliths. Due to time constraint, it was not prioritized to produce 180 µm ID monoliths with the new chemicals.

The ^{1}H-NMR spectra of the chemicals are given in **Appendix 7.1.1**, and no degradation of the old chemicals was found that could explain why the production in 180 µm ID capillaries did not work, while the production in 250 µm ID capillaries did work. Also, by running a statistical ANOVA test on monoliths prepared in 250 µm ID capillaries with old and new chemicals, based on backpressure measured at 6 different flow rates, the monoliths were not found to be significantly different using new and old chemicals. Based on the backpressure not being significantly different for monoliths prepared with new and old chemicals, it is expected that the structure of the monoliths would be similar and it was not prioritized to capture micrographs of the 250 µm ID monoliths produced with new chemicals.

The backpressure of the 250 µm ID EDMA-co-VDM monoliths at a flow rate of 1 $\mu Lmin^{-1}$ was found to be 36 $barm^{-1}$ and 25 $barm^{-1}$ for the monoliths prepared with old and new chemicals, respectively. This low backpressure allows for fast loading of samples at flow rates in $\mu Lmin^{-1}$ range instead of $nLmin^{-1}$ range.

An observation that was done when the new chemicals replaced the old ones in the production, was that the viscosity of 1,4-butanediol was experienced differently. The old chemical seemed less viscous than the new replacement. A determination of the actual viscosity was attempted, but due to difficulties of the pipettes to deliver an equal volume of viscous liquid this was aborted. It could be possible to measure this viscosity by using graded Eppendorf tubes. However, even if a difference in viscosity is determined, it is difficult to be certain that the reduced viscosity is the reason for production failure of monoliths in the narrower 180 µm ID capillaries compared to 250 µm ID capillaries.

Low backpressure EDMA-co-VDM monoliths were successfully prepared in 250 µm ID capillaries with increased surface area compared to the original recipe of the EDMA-co-VDM monolith described by Geiser et al. [58]. Replacing the old chemicals with new chemicals did not give a negative effect on the production of the EDMA-co-VDM monolith.

3.3 Choice of Wnt-signaling pathway inhibitor

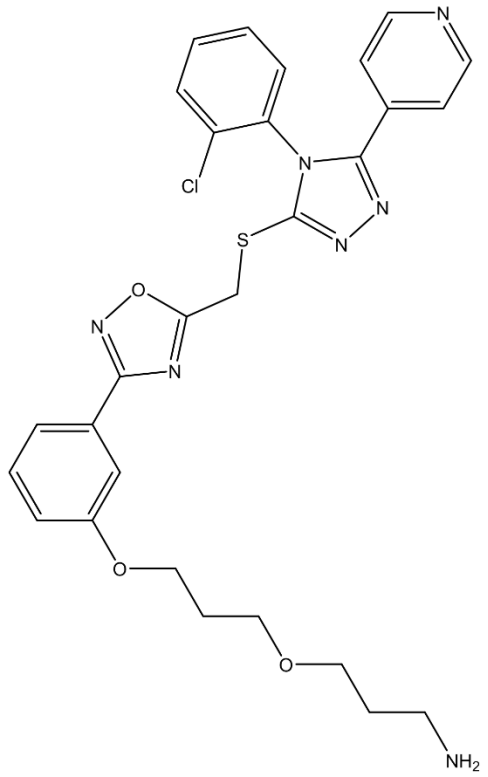

Figure 32: Structure for WNT-inhibitor "161", the pharmacophore of the molecule is the three rings attached to the sulfur atom, while the linker is placed on the opposite end of the molecule to prevent steric hindrance.

Initially, the known Wnt-signaling pathway inhibitor 161, **Figure 32**, was selected to be immobilized on the monolith support. This inhibitor binds to the adenosine binding site, offering high selectivity towards tankyrase 1 and 2, and the IC_{50} value determined by STF-Luc was 3.9 µM [8, 87]. STF-luc assays are commonly used to determine IC_{50} values of Wnt-inhibitors [34, 117].

An unknown amount of inhibitor 161 was received dissolved in approx. 0.5 mL DMSO. For immobilization of the inhibitor, approx. 0.5 mL solution was expected to be used per reactor, even though Geiser *et al.* [58] used a flow rate of 250 $nLmin^{-1}$ needing only 45 µL of a 5 mg/mL pepsin solution to successfully immobilize pepsin.

From previous experience with the in-house pressurized filling system, it is very difficult to achieve a constant flow rate of 250 $nLmin^{-1}$ over a long time period, and much more than 45 µL solution would be needed per reactor.

To determine if the amount of inhibitor was sufficient for the planned testing, the inhibitor solution was analysed by MS. Due to the inhibitor being dissolved in DMSO, a solvent that is not compatible with MS, the inhibitor was introduced diluted 1:10000 in 0.1% FA. The mass spectrum of inhibitor 161 is given in **Figure 33**, showing the presence of other compounds than inhibitor 161. The pattern of peaks cannot be explained by common molecular ions observed in ESI mass spectra [118]. This observation makes it probable that 161 has degraded since production, or that the solution contains large amounts of contaminants. The UV-Vis absorbance of the inhibitor solution was also measured by nanodrop, but as shown in **Appendix 7.2**, **Figure 65**, the spectrum is not consistent with the presence of inhibitor 161.

A possibility of attaining a purer inhibitor 161 is by synthesis. From the description of the synthesis of inhibitor 007-LK by Voronkov *et al.* [87], an structural analogue of inhibitor 161, the synthesis of 161 would consist of over 10 different steps.

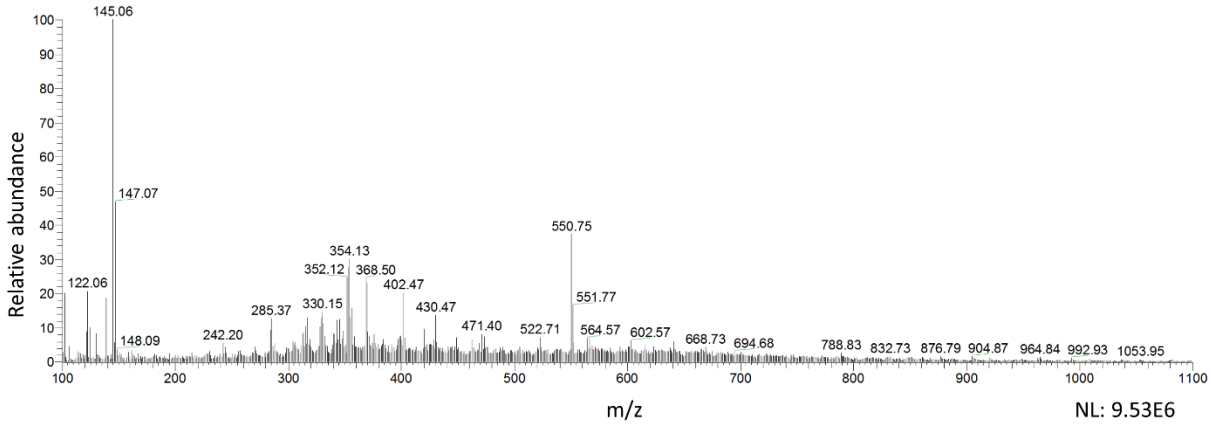

Figure 33: Mass spectrum of a Wnt-inhibitor 161 diluted 1:10000 in 0.1% FA. Monoisotopic weight of the inhibitor is 577.166 g/mol. The normalized level (NL) gives the intensity of the peak with the highest intensity in the mass spectrum set at 100% (the base peak).

With only 0.5 mL of the inhibitor available and a questionable presence of the desired structure of inhibitor 161, it was decided that the amount was insufficient for the planned immobilization of several monoliths. An external synthesis of the inhibitor would cost 150 000 NOK, exceeding the budget for this master thesis. Due to the extensiveness of the synthesis of 161, successful synthesis would not be possible for the author of this study within the time frame of the project, therefore a another inhibitor was needed.

3.4 Selection of a different Wnt-inhibitor; LDW639

Another known Wnt-signaling pathway inhibitor that targets TNKS1/2 is XAV939 [34]. Two structural analogues along with XAV939 from Huang *et al.* [34] are presented in **Figure 34**. The importance of the structure for the bioactivity of the drug is revealed from the inactivity of LDW643, as a consequence of the sulfur atom being replace by a nitrogen atom with an attached acyl group, while LDW639 remains bioactive with a primary amino group in place of the trifluoromethyl. XAV939 is a more potent inhibitor than LDW639, but due to the trifluoromethyl on XAV939, it is not suited for attachment of a linker via organic synthesis.

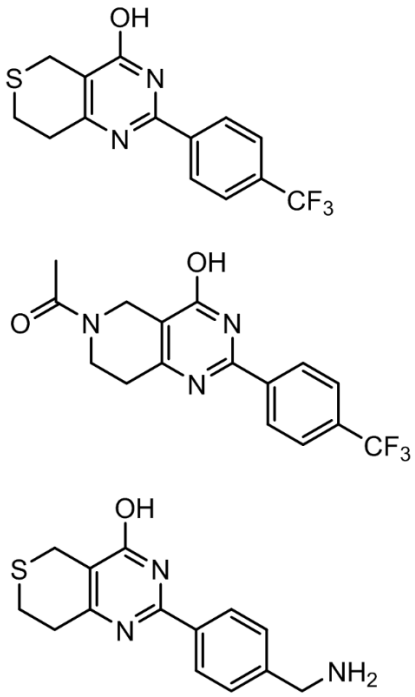

Figure 34: Wnt-inhibitor XAV939 (upper), structural analogues LDW643 (middle) and LDW639 (lower).

Trifluorometyl also makes it difficult to immobilize XAV939 on the monolithic support as VDM does not bond with trifluoromethyl. This stability of trifluoromethyl is due to fluorine being the most electronegative element, additionally it is strongly oxidizing. These characteristics of trifluoromethyl makes the C-F bond one of the strongest in organic chemistry, generally difficult to work with [119, 120]. The bioactive analogue LDW639 with a primary amino group makes it possible to attach a linker by a peptide coupling, or immobilize LDW639 directly on the monolithic support via VDM ring-opening reaction [115, 121]. In addition, the synthesis path (see following section, **Figure 35**) is much shorter and more manageable than a synthesis of the large inhibitor 161.

As LDW639 remained biologically active after replacement of the trifluoromethyl group, LDW639 was selected for synthesis and testing of the CRAM reactors in this study. This was based on the assumption that an addition of a linker on the amino group, that replaced the trifluoromethyl, would not cause biological inactivity.

3.4.1 The final linear synthesis path for LDW639 with linker

The linear synthesis path for LDW639 with a linker is given in **Figure 35**. The first two steps in the synthesis were based on the supporting material to Huang *et al.* [37]. Originally, the deprotection in step 2 [37] was completed with TFA in DCM, but these were exchanged with HCl in MeOH, as this is less expensive and offers reduced hazards compared to TFA [121]. The procedure on *in-situ* formation of HCl in MeOH was described by Nudelman et al. [122]. This procedure allows for a controlled concentration of HCl to be formed under exothermic conditions from acetyl chloride.

TLC was used during synthesis to monitor the conversion from reagents to product, additionally the synthesis products were evaluated by ^{1}H-NMR. Concerning the ^{1}H-NMR spectra presented in this section, the spectra were not intended for quantitative purposes, but for qualitative

detection of the molecular structure and gross purity issues. In addition to TLC and ^{1}H-NMR, selected synthesis products were examined with MS to confirm the molecular composition.

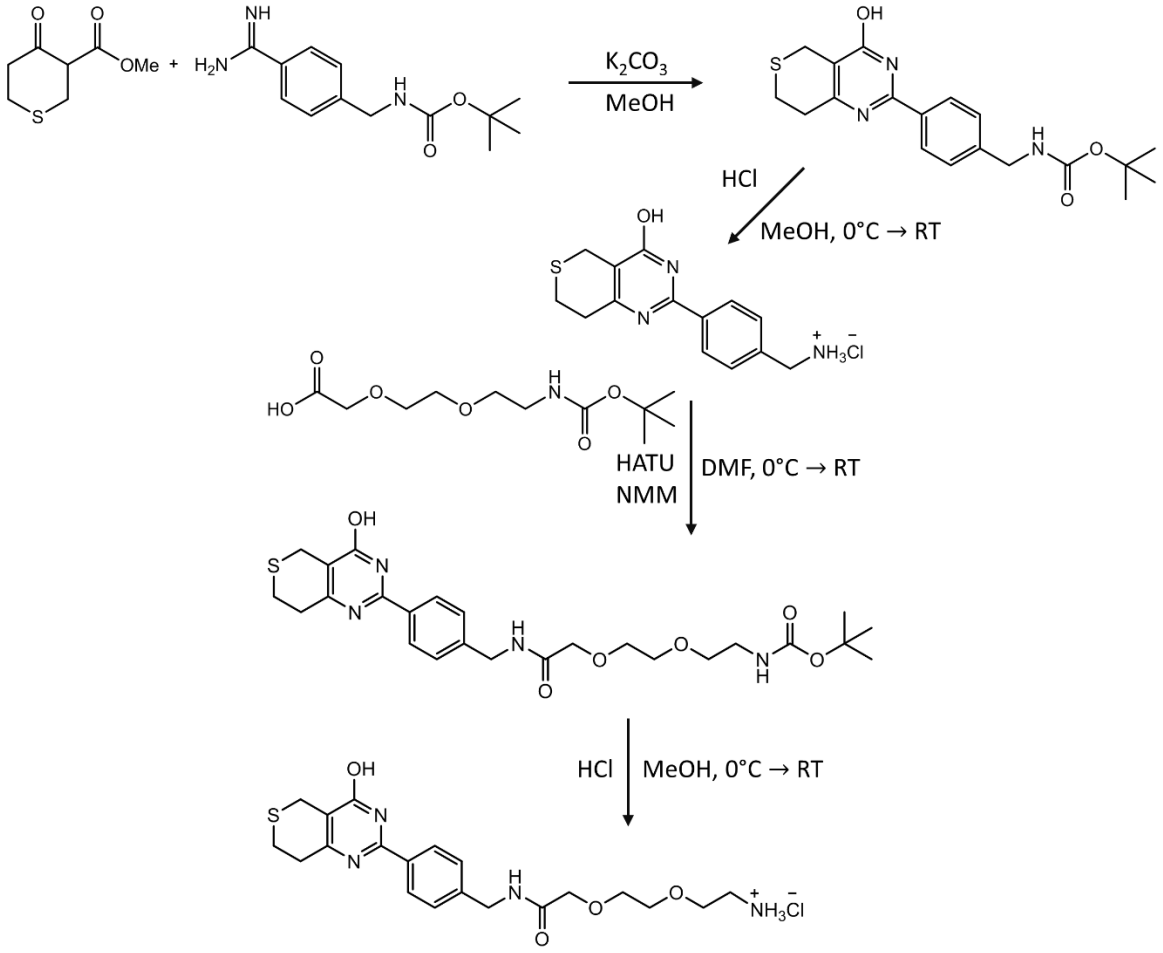

Figure 35: The linear synthesis path for LDW639 with linker attached by peptide coupling.

3.4.2 Thin layer chromatography used for monitoring of the product during synthesis reactions and extractions

TLC plates made of Silica gel 60 F_{254} or Aluminium oxide 60 F_{254}, will under UV light at 254 nm fluoresce green, as a consequence of zinc sulfide in the adsorbent [122] (p.162-169). Compounds will be visualized as dark spots, as they block the UV-light from the zinc sulfide. Using these types of TLC plates along with aromatic solvents, it important to dry the plate before visualization, as residues of solvent may conceal any products present.

By optimization of solvent mixtures and TLC plates, the following TLC systems were found to be appropriate for product control. A TLC system with a fluorescent aluminum oxide plate with a solvent mixture of 2.5% MeOH in DCM was successful at separating the product in the first

step from the reagent BOC-benzamidine, which remained at baseline. For the third step, a fluorescent silica plate with 5% MeOH in DCM eluted the reaction mixture in two spots, with a retardation factor of 0.15 and 0.26, respectively. The TLC system using 5 % MeOH in DCM with a silica plate was also suited for an automatic flash chromatography system with silica particles using an Armen Flashmaster to purify the BOC protected linked LWD639, see **Appendix 7.3.1**.

The fluorescent plates also made it possible to monitor the product during liquid-liquid extractions, by spotting both the organic and water phase, and then conclude which phase contained the product based on the dark spot(s) occurring during visualization. In step 3 of the synthesis, the peptide coupling reagent HATU was separated from the product and remained on the baseline. By spotting both the water phase and the organic phase from the liquid-liquid extraction, the water phase showed a spot at baseline, while the product was extracted to the organic phase and migrated from the baseline.

3.4.3 Successful synthesis of LDW639 with linker

Step 1 of the synthesis of linked LDW639

During the first step of the synthesis, the reaction mixture changed form a milky white solution to a clear orange-brown solution. After acidification, suction filtration and drying, an off-white powder was collected and evaluated by ^{1}H-NMR. The proton spectrum, **Figure 36**, shows the characteristic singlet peak of the *tert*-butyloxycarbonyl (*t*-BOC) group at 1.4 ppm of 9 hydrogens. The other peaks in the spectrum are consistent to the ^{1}H-NMR data by the supporting material to Huang *et al.* [34]. In this paper by Huang *et al.*, the limiting agent of this reaction was the beta-keto ester, while the BOC-benzamidine was in excess. However, the reaction would be easier to follow by TLC with excess of the beta-keto ester, as the BOC-benzamidine is UV-absorbing while the beta-keto ester is not. During formation of the product, the BOC-benzamidine as the limiting factor would be exhausted as the reaction ran to 100% completion, and TLC would show only the product spot. For the three times this reaction were repeated, the beta-keto ester was the limiting factor the first two times. The yield of the unpurified and dried material *in vacou* these three times was 53%, 82% and 98%, respectively. A combination of being able to check by TLC that the reaction had run to 100% completion with BOC-benzamidine as the limiting factor, and the author gaining experience led to a higher

yield in the last attempt. Note that the yield of products is overestimated in this step as the crude material has not been purified, and drying in a rotavapor does not guarantee 100% removal of solvents.

Step 2 of the synthesis of linked LDW639

The deprotection in step 2 of the synthesis was completed once with TFA and three times with HCl. Using TFA for deprotection was done as described with HCl in **Experimental 2.6.2** with the following differences: DCM was used as solvent instead of MeOH and 42 equivalents of TFA for one equivalent of *t*-BOC-LDW639, whereas the reaction with HCl used 20 equivalents of acetyl chloride. As a consequence of TFA being more hazardous to work with, the solvent also needed to be removed by a rotavapor in a fume hood.

The white powder collected at the end of this reaction was analysed by ^{1}H-NMR, and the proton spectrum is given in **Figure 37**. The characteristic signal of the t-BOC group at 1.4 is not present, indicating that the deprotection was successful and the product exists as a hydrochloride salt. The broad singlet at 12.7 is missing compared to the spectra of the previous product, **Figure 36**, making it possible that the pyrimidine ring (hetrocyclic aromatic ring with nitrogen in position 1 and 3) has been protonated and that the hydroxyl group is present as a carbonyl group. It may be that this process gives rise to the broad singlet at 6.45 ppm. The amount of product exceeded the theoretical maximum for the small scale for the first time with both TFA and HCl, this is a consequence of the crude material not being purified and the drying being insufficient. For the following two repetitions of this step, HCl in MeOH was selected for deprotection as the procedure is less hazardous than with TFA and as hydrochloric salts are easier to work with. The yield in last two repetitions was found to be approx. 89%, but this is still an overestimation of the actual yield.

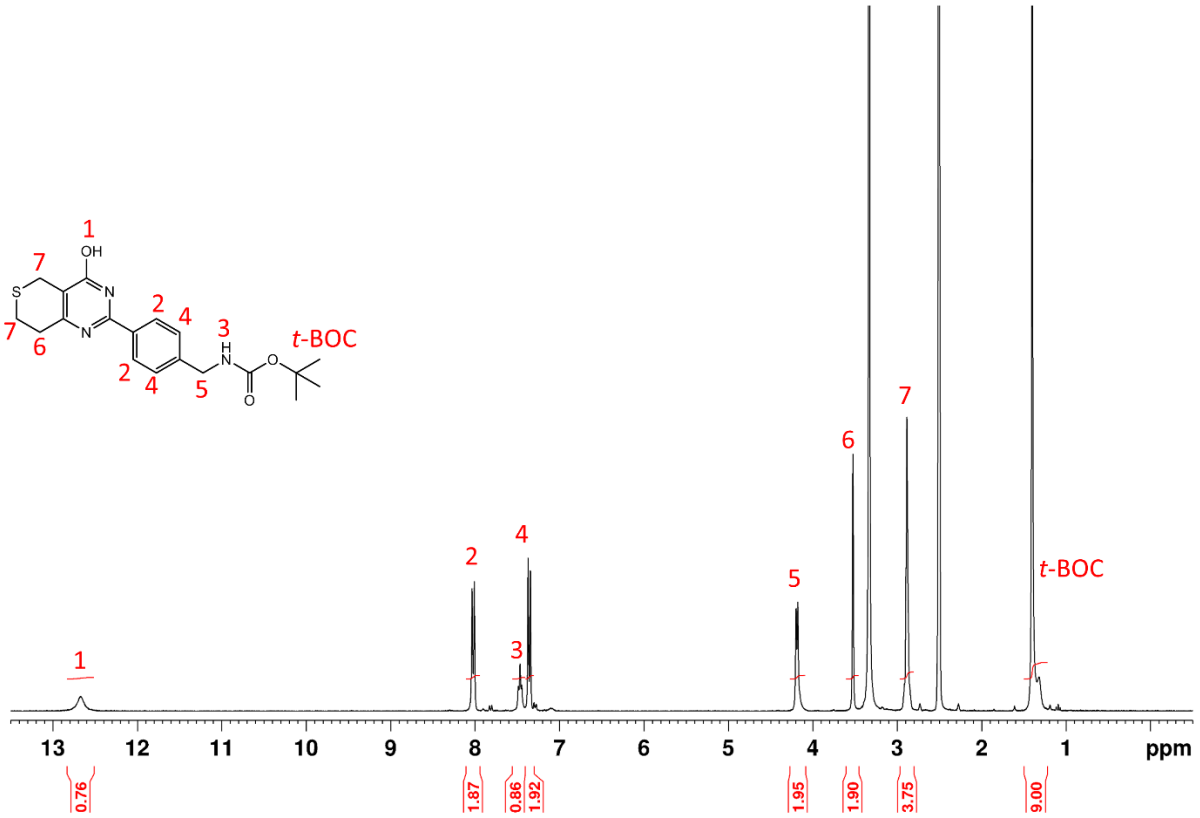

Figure 36: ^{1}H-NMR spectrum of *t*-BOC protected LDW639 dissolved in DMSO-D^{6}, 16 scans on DPX300 (300 MHz).

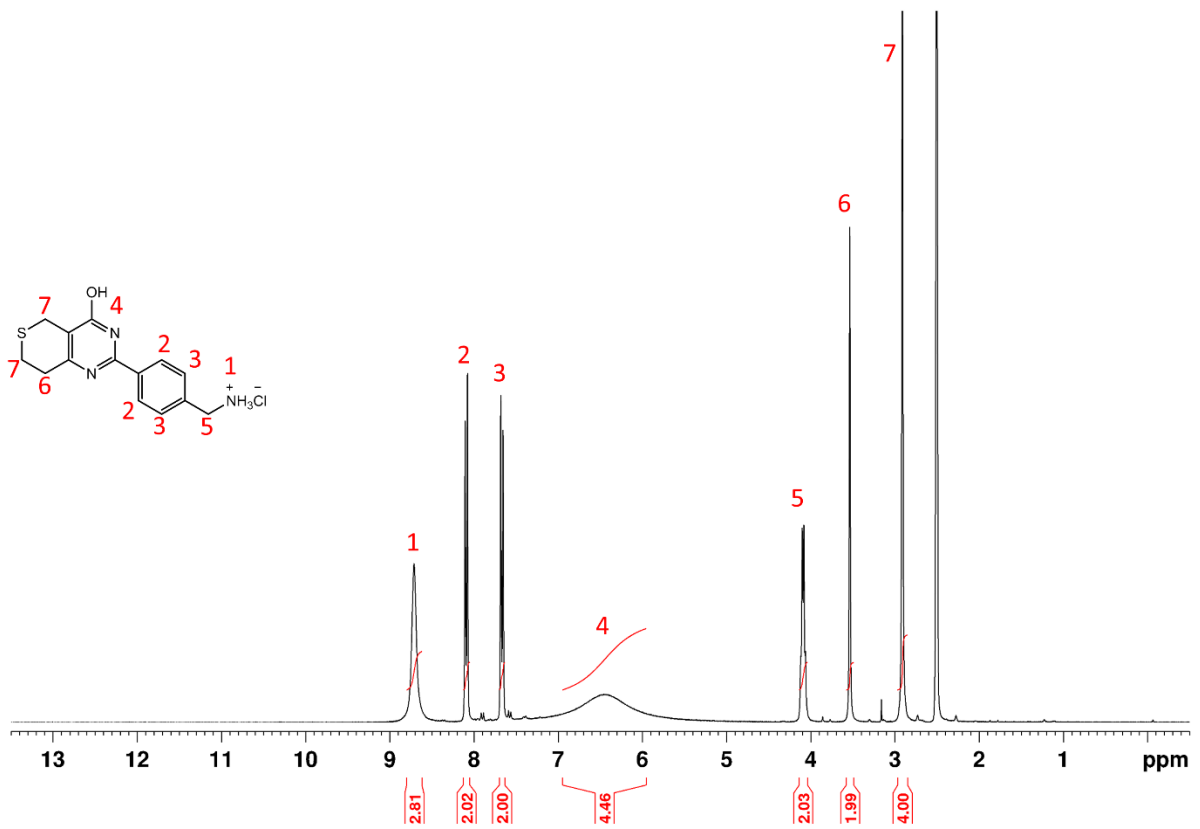

Figure 37: ^{1}H-NMR spectrum of hydrochloric LDW639 salt dissolved in DMSO-D^{6}, 16 scans on DPX300 (300 MHz).

Step 3 of the synthesis of linked LDW639

Dr. Christian Schnaars selected the coupling reagents for the peptide coupling of the hydrochloride salt of LDW639 with 2,2-dimethyl-4-oxo-3,8,11-trioxa-5-azatridecan-13-oic acid. The selected reagents were NMM and HATU. The coupling that happens using HATU has been reviewed and compared to other reagents in great detail [123, 124]. HATU offers a quick formation of the amide bond in mild conditions that usually provide high yields [125]. The peptide coupling obtained using the coupling reagents is presented in a general form in **Figure 38**. When HATU is dissolved with a tertiary amine such as NMM, the solution should become transparent yellow. If a precipitate is formed, more solvent (in this case DMF) is needed for the reaction to proceed as desired.

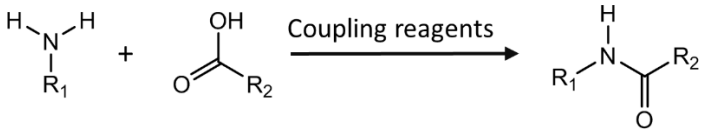

Figure 38: Scheme of the peptide bond formed during coupling of a primary amine and carboxylic acid.

The third step in the synthesis of linked LDW639 was a peptide coupling subsequently followed by a purification by an automatic flash chromatography system (**Appendix 67.3.1**) or by recrystallization, the yields of the crude material and purified material is given in **Table 3**. Recrystallization was selected as the preferred purification method as it on average gave two times the amount of purified material.

Table 3: Yield of the crude material and purified material in step 3 in the synthesis of linked LDW639 performing purification by automatic flash chromatography or recrystallization.

Purification method	Yield of crude material	Yield of purified material
Automatic flash chromatography	78%	22.5%
Recrystallization	> 100%	47%
	> 100%	37%

The recrystallization that yielded 47% had a smaller ratio of solvent to crude material (150 mL to 6.35 g), than the second recrystallization, which had (200 mL to 3.9 g). In the second recrystallization, the amount of solvent was increased as the crude material did not dissolve in 100 mL solvent, and therefore another 50 mL of solvent was added. The last 50 mL of solvent, in both cases, came from washing out residues from the glassware during hot filtration. The reduced saturation of the pure product in the second recrystallization led to less precipitate. A

possibility to enhance the yield would have been to increase the temperature of the oil bath used for heating, instead of increasing the amount of solvent. Also, the process of recrystallization could have been attempted a second time on the collected solution from suction filtration, as this solution would contain the remaining crude material.

The spectra for the crude material of the BOC protected linked LDW639 (**Figure 66**) and the purified product (**Figure 67**) using the automatic flash system in **Appendix 7.3.1** show that the product contains less contaminations and residues from reagents after purification. The proton spectrum of the BOC protected linked LDW639 purified by recrystallization is given in **Figure 39**. For the purification by recrystallization, the proton spectrum is consistent with the peaks found in the flash purified product concerning both chemical shift and multiplicity. The characteristic signal of the *t*-BOC group is present at 1.4 ppm, confirming that the linker was attached. The molecular formula, $C_{25}H_{34}N_4O_6S$, of the product was confirmed by composition analysis presented in **Appendix 7.4**. The molecule was detected as a sodium adduct, and the elemental components were confirmed with 0.0 ppm deviation from the monoisotopic mass.

The last step of the synthesis of linked LDW639

The final step of the synthesis was the deprotection of the *t*-BOC group present on the linker. This was done in the same manner as the first deprotection, and resulted in a white powder that was evaluated by ^{1}H-NMR, the spectrum is given in **Figure 40**. The step was completed three times with yields exceeding 100 % of the crude material. From the second batch it was attempted to extract the free amine instead of the hydrochloric salt shown in **Appendix 7.3.2**. The yield of the free amine was only 18 %, and with expected reduced storage capacity of the free amine, the extraction was not a part of the final synthesis.

Concerning the ^{1}H-NMR spectrum shown in **Figure 40**, the signal correlated to the *t*-BOC group at 1.4 ppm is not present, confirming that the deprotection had occurred. The signal at 12.7 ppm that arises from the phenol group on the pyrimidine ring is missing. This makes it difficult to determine if the structure present is with a protonated pyrimidine ring (upper structure in **Figure 40**) or with a phenol group (lower structure in **Figure 40**).

Nathubhai *et al.* [126] who studied the SAR of TNKS inhibitors have used XAV939, the analogue pharmacophore of the synthesized LDW639, with a protonated pyrimidine ring. Huang *et al.* [34] reported XAV939 with a phenol group on the pyrimidine ring. The reported

IC_{50} values of these two resonance structures of XAV939 are given in **Table 4**. Whether this small variation in reported IC_{50} values towards TNKS 2 and poly (ADP-ribose) polymerase (PARP) 1 is due to the structural difference or the sensitivity of the assay used for determination is difficult to assess, but the take home message is that the synthesized inhibitor should remain bioactive independent of the structure on the pyrimidine ring.

Table 4: The reported IC_{50} values of the variations of XAV939 for TNKS1/2 and PARP1/2

Variation of XAV939	TNKS 1	TNKS 2	PARP 1	PARP 2
Protonated pyrimidine ring [126]	10 ± 3 nM	17 ± 6 nM	1200 ± 23 nM	-
Phenol group[34]	11 nM	4 nM	2194 nM	114 nM

The molecular formula, $C_{20}H_{27}N_4O_4S$, of the product was confirmed by composition analysis presented in **Appendix 7.4**. The elemental components were confirmed with 0.0 ppm deviation from the monoisotopic mass, confirming the final structure of the inhibitor being successfully synthesized.

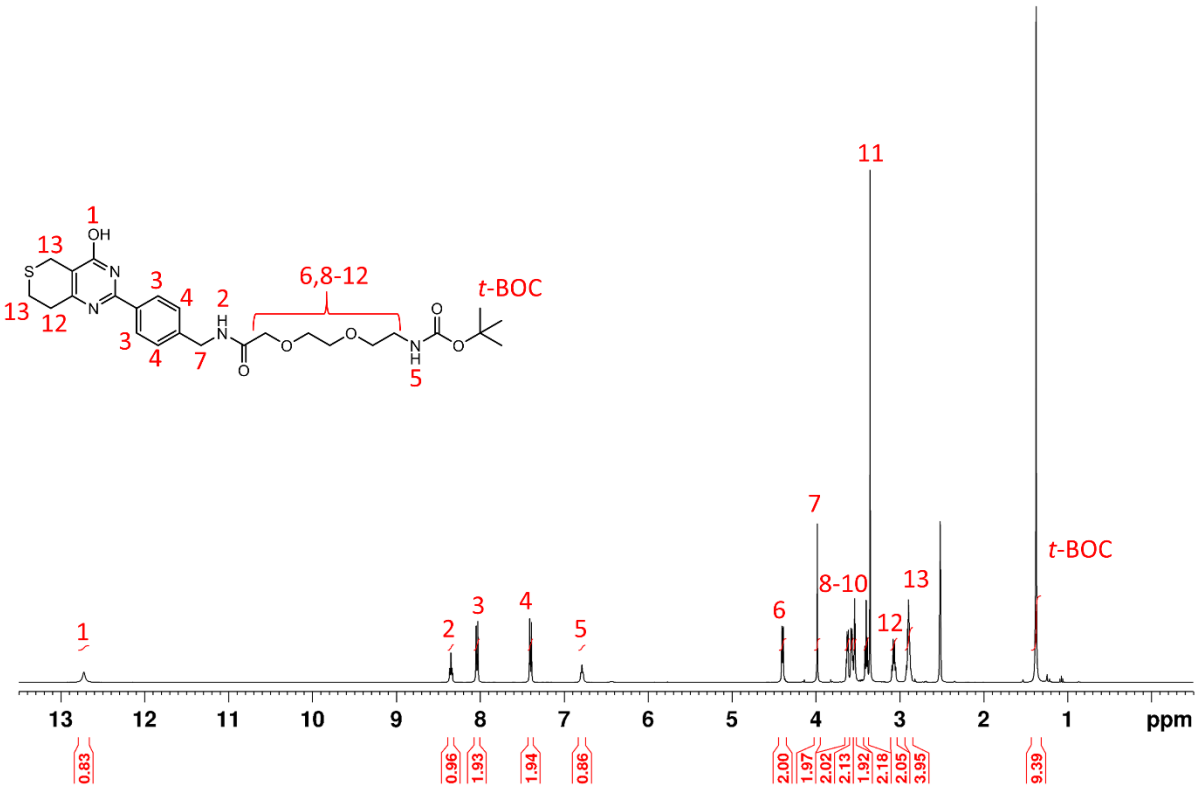

Figure 39: ^{1}H-NMR spectrum of *t*-BOC protected linked LDW639 dissolved in DMSO-D^{6}, 16 scans on DPX300 (300 MHz

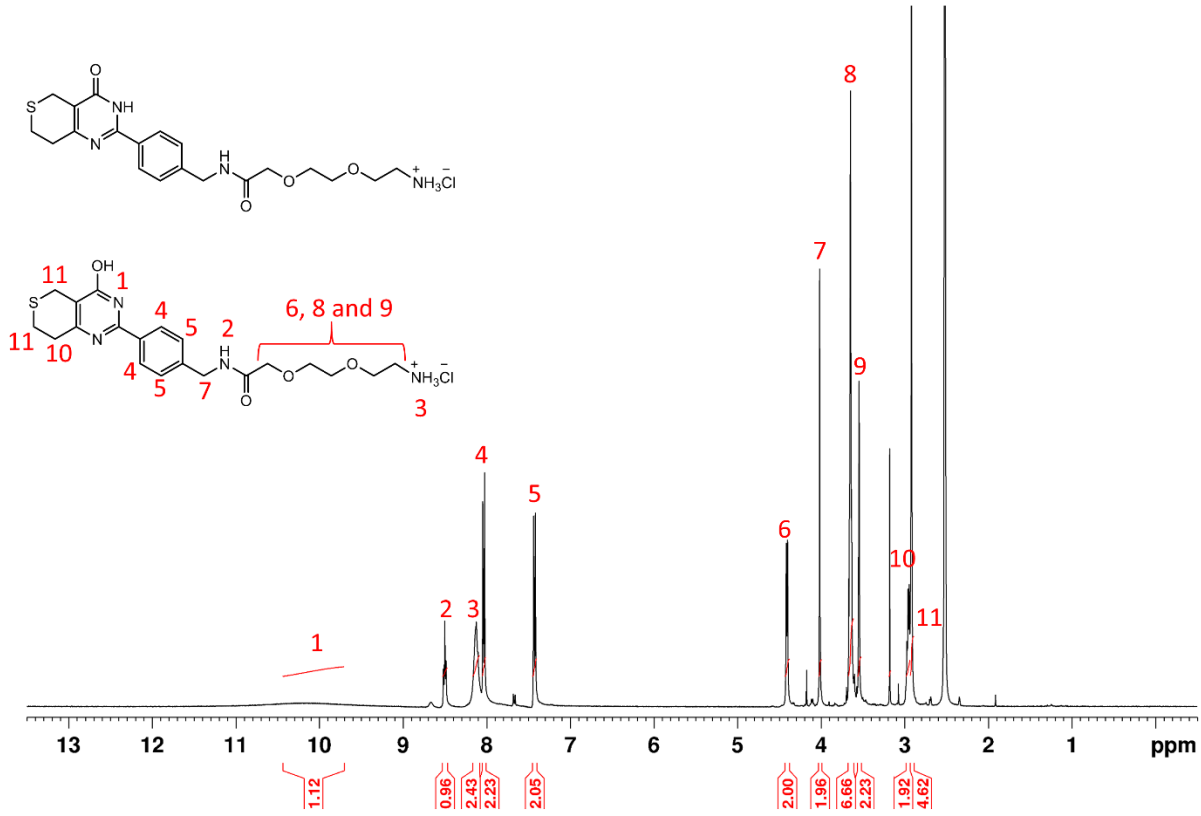

Figure 40: ^{1}H-NMR spectrum of linked LDW639 as hydrochloric salt dissolved in DMSO-D^{6}, 16 scans on AVII400 (400 MHz).

3.4.4 Excellent stability of the final synthesis product

After six months storage at 4 °C, and a multitude of heating to room temperature and cooling, the final synthesis product was introduced into the MS to see if the structure had degraded. The mass spectrum from direct injection MS is shown in **Figure 41**. The peak at *m/z* 419.174 matches the monoisotopic mass of the linked LDW639 from the hydrochloric salt, $(M+H)^+$. The peak at *m/z* 210.091 is consistent with $(M+2H)^{2+}$ for the linked LDW639. The presence of $(M+H)^+$ and $(M+2H)^{2+}$ confirms that the inhibitor has remained intact.

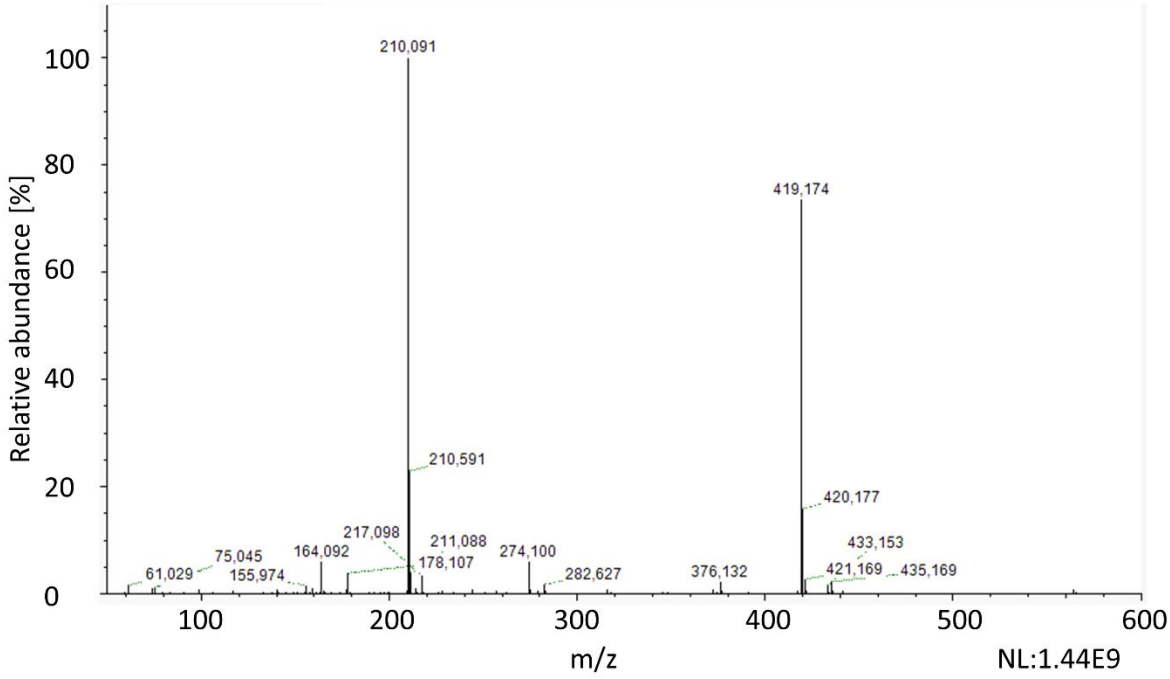

Figure 41: Mass spectrum of linked LDW639 introduced in the Q-Exactive MS at a concentration of 0.1 µg/µL diluted in 0.1% FA. Monoisotopic mass of the inhibitor is 419.1748 Da.

3.4.5 Synthesis product inhibits Wnt-signaling

If the linked LDW639 is found to inhibit Wnt-signaling in a STF-Luc assay [87], it means that the drug is active towards TNKS1/2, and possibly PARP1/2 as LDW639 targets the nicotinamide subsite.

The analysis was completed by Eric Maximillian Lycke at the Unit of Cell Signaling, Oslo University Hospital. The stable reporter cell line was conditioned with Wnt3a containing media (Wnt3a is a protein that is encoded by the WNT3a gene), and the activity of Wnt3a is reported as cells lose their capacity in expressing transfected genes during extensive culturing. The STF-Luc assay held a 70% Wnt3a activity and after incubation with the drug for 24 hours, no visual

detection of toxicity or crystal formation was observed. The activity of Wnt-signaling pathway is estimated from the activity of luciferase and *Renilla*. From the plot of % activity of Wnt-signaling pathway versus concentration of the synthesis product in **Figure 42**, the IC_{50} value of the linked LDW639 was found to be 10.96 µM after 24 hours incubation. The same plot for the blank control of HCl is given in **Figure 43** and shows that HCl did not affect the Wnt-activity. The data points were fitted as in Voronkov *et al.* [87], to the Langmuir Binding Isotherm.

The IC_{50} values of inhibitor 161 and a structural analogue G007-LK found by STF-Luc assay, TNKS1/2 and PARP1/2 are shown in **Table 5**. The G007-LK inhibitor had no effect on PARP1/2, making it a more selective TNKS inhibitor compared to XAV939 (see **Table 4** in **Section 3.4.3**).

Table 5: The reported IC_{50} values of the inhibitor 161, and a structural analogue 007-LK found for STF-Luc assay, TNKS1/2 and PARP1/2

Wnt-inhibitor	STF-Luc	TNKS 1	TNKS 2	PARP 1/2
161 [87]	3920 ± 299 nM	-	-	-
007-LK [87]	50 ± 20 nM	46 ± 1 nM	25 ± 6 nM	No effect

The inhibitor that has been synthesized is a less potent inhibitor of Wnt-signaling than XAV939, 161 and 007-LK, but it is bioactive and should succeed in trapping TNKS due to drug-protein interactions. As the main focus of the thesis was not the synthesis of the inhibitor, possible effect of a linker was not investigated. The synthesis product in step 2, the hydrochloric salt of LDW639, was not examined in the STF-Luc assay for comparison of IC_{50} values of LDW639 with and without linker.

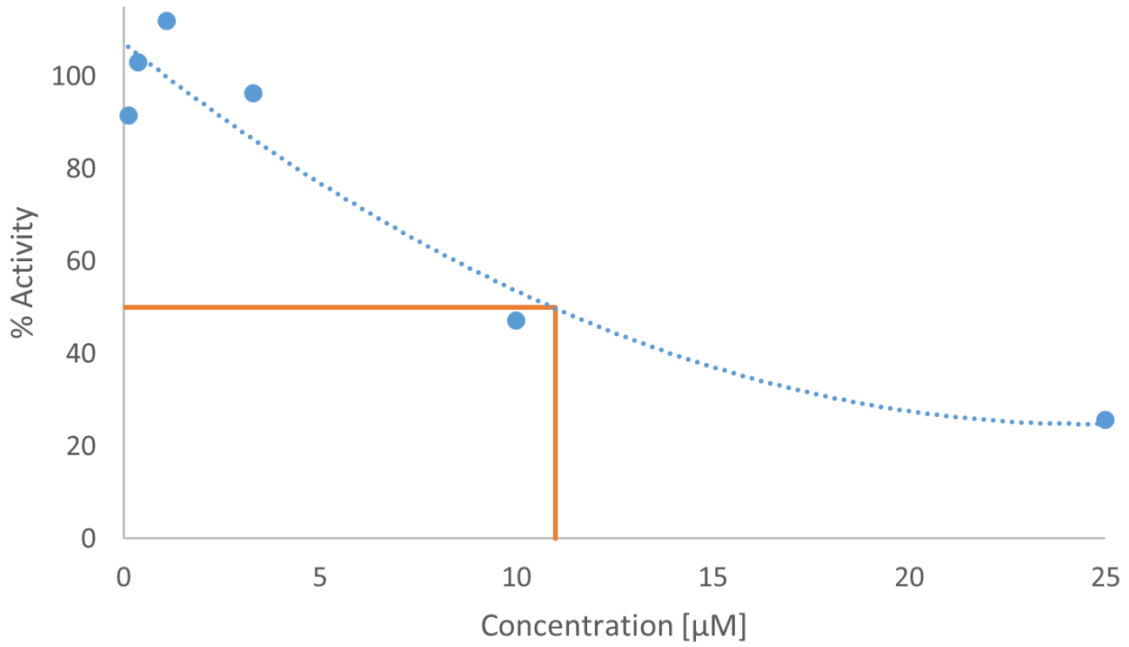

Figure 42: % activity of Wnt-signaling pathway vs. concentration of linked LDW639 showing the inhibition of the Wnt-signaling pathway after 24 hours incubation with linked LDW639. The IC_{50}-value of the linked LDW639 is estimated to be 10.96 µM.

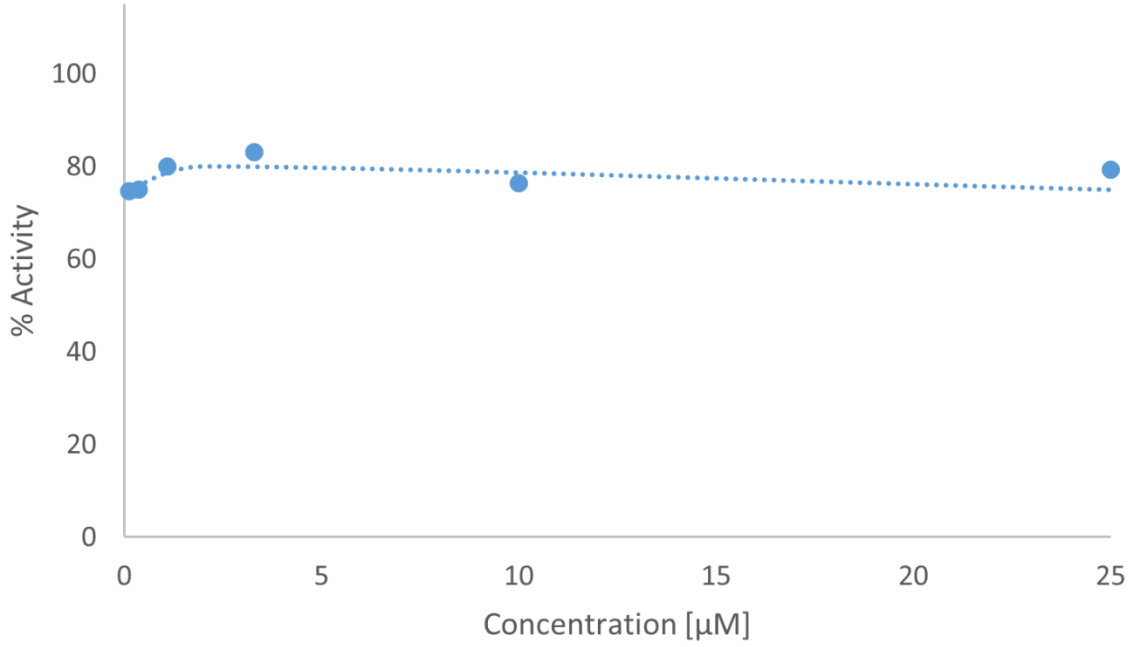

Figure 43: % activity of Wnt-signaling pathway vs. concentration of HCl showing the inhibition of the Wnt-signaling pathway after 24 hours incubation with HCl. HCl does not appear to inhibit Wnt-signaling pathway

The linked LDW639 was successfully synthesized and resisted degradation after six months storage. In addition, the linked LDW639 displayed inhibition of the Wnt-signaling pathway, and the IC_{50} value was found to be 11 µM.

3.5 Immobilization of drug onto the monolith

The immobilization of drug onto the monolith (**Chapter 3.5**) was conducted in parallel with the assessment of the CRAM reactors (**Chapter 3.6**). For the sake of clarity the discussion is separated in two chapters, as the assessment of immobilization of drug and the potential of the CRAM reactors was conducted with different methods.

It is a challenge to measure if the drug has been immobilized onto the solid support. Based on the experience of using the UV-absorptivity of the products during the synthesis, it was decided to measure possible difference in the UV-Vis absorbance of the monolith before and after immobilization of the drug. This was planned to be done by removing the polyimide coating of at least a 3 mm on the monolith detection window. However, the removal of the coating was not possible by direct flame or using a wire striper with a wolfram filament without destroying the monolith.

It was attempted to make the monoliths after the detection window was in place, but by removing the coating the capillaries became vulnerable to breaking. This would also make the production of monoliths a lot more tedious, and the planned tests after immobilization would become more difficult due to reduced mechanical strength.

Therefore measuring the UV-Vis absorbance of the drug immobilization solution before and after flushing through an EDMA-co-VDM monolith was attempted. Under the assumption that the possible difference in absorbance could be explained by loss of drug to the monolith.

3.5.1 Significant drop of ultraviolet-visible absorbance of immobilization solutions by flushing through monoliths

A preliminary experiment using a capillary cell to measure UV-Vis absorbance of immobilization solution before and after flushing a monolith was attempted. The measurements are presented in **Appendix 7.5.1**, and by ANOVA the UV-Vis absorbance for immobilization solution before and after flushing a monolith was found to be not significant. However, the relative standard deviations (%STD) was 52% and 75% for the measurements of the UV-Vis absorbance of the immobilization solutions before and after flushing of a monolith, respectively. To determine if this was a natural variance of the absorbance of the solutions, or

if the contribution to the variance originated from the measuring Unit, the experiments were repeated by measuring the UV-Vis absorbance on nanodrop.

By measuring the absorbance of 0.25 mg/mL drug dissolved in 50 mM phosphate buffer (*i.e.* immobilization solution) on nanodrop, the maximum absorbance of the molecule was found at 243 nm and a local maximum at 285 nm, as shown in **Figure 44**. An absorbance spectrum of the immobilization solution before and after flushing in a monolith is shown in **Figure 45**.

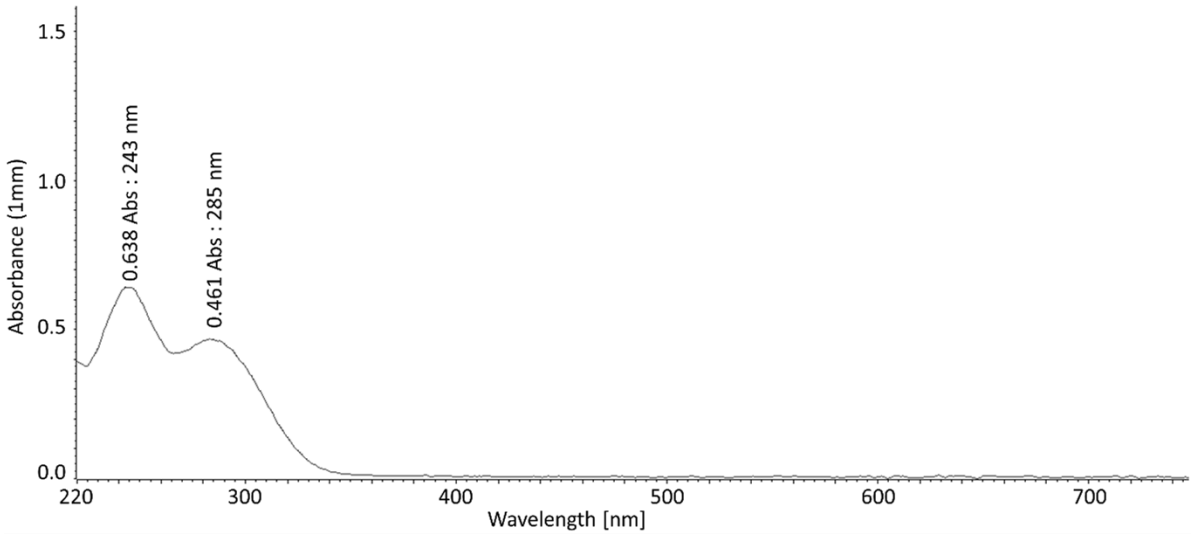

Figure 44: Absorbance spectrum of 0.25 mg/mL synthesized drug in 50 mM phosphate buffer, corrected for 50 mM phosphate buffer absorbance by a blank.

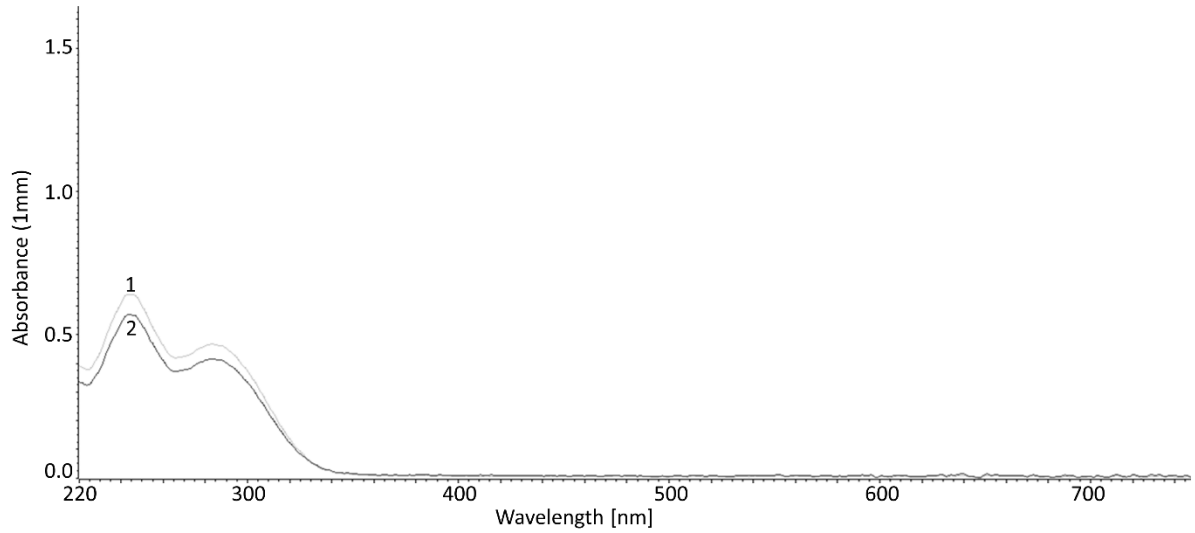

Figure 45: Absorbance spectrum of (1) 0.25 mg/mL synthesized drug in 50 mM phosphate buffer and (2) Same solution flushed through a 14 cm 250 µm ID EDMA-co-VDM monolith, corrected for 50 mM phosphate buffer absorbance by a blank.

The absorbance at 243 nm and 285 nm of the immobilization before and after flushing through a 14 cm, 250 µm ID EDMA-co-VDM monoliths are presented in **Figure 46**, for 5 replicates.

To determine if the absorbance from the immobilization solution before and after flushing of a monolith was significantly different, an ANOVA test was run in EXCEL given in **Appendix 7.5.2**, **Table 24** and **Table 26**. Both the data from 243 nm and 285 nm showed that the absorbance from immobilization before and after was significantly different, meaning that the amount of drug in the immobilization solution is reduced by flushing it through a monolith. However, whether the fraction lost, is only trapped on the monolith or undergone the intended binding with VDM is not possible to differentiate from this type of experiment.

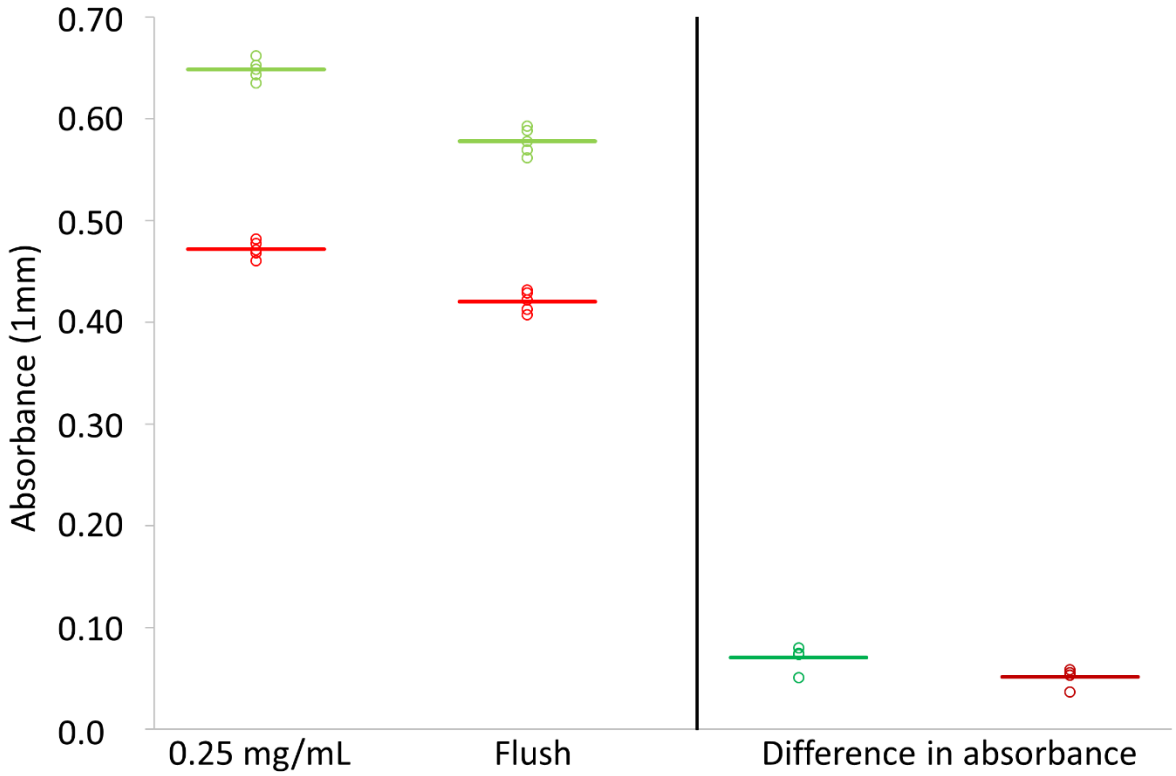

Figure 46: The absorbance at 243 nm (light green) and 285 nm (light red) of immobilization solution before and after flushing of a monolith, and the difference in absorbance at 243 nm (dark green) and 285 nm (dark red) is visualized. Five replicates of 14 cm 250 ID EDMA-co-VDM monoliths being flushed with 0.25 mg/mL drug dissolved in 50 mM phosphate buffer.

Another fraction that should have been measured for UV-Vis absorbance is the immobilization solution remaining inside the monolith after flushing. It was assumed that if no drugs had been immobilized, only trapped onto the monolith, several washing fraction after immobilization would show a considerable UV-Vis absorbance compared to the flushed immobilization solution, and that UV-Vis absorbance would slowly decline for each washing fraction.

To be able to remove this fraction of solution, the monoliths (or as drug is now immobilized, the CRAM reactors), need to be flushed with either nitrogen gas or storage solution (50 mM

phosphate buffer). It is most probable that flushing with nitrogen gas would give a more representative sample of the actual drug concentration in this fraction, but the drying of the CRAM reactor is usually avoided after immobilization as the effect on the drug is unknown. By flushing the remaining solution with storage solution, a dilution effect on the drug concentration would be unavoidable.

But as nanodrop allows a sample size of 2.5 µL, it was attempted in the following immobilizations to wash out the remaining immobilization solution by collecting at least the first fraction consisting of only the 2-4 drops first flushed out of the reactor.

Increased concentration of the immobilization solution after the first assessments of the CRAM reactors

The background for a change in initial concentration of immobilization solution was due to assessment of the first CRAM reactor by LC-MS and WB presented in **Results and Discussion 3.6** on the data given in **Appendix 7.6** and **Appendix 7.8**. Briefly explained, the initial CRAM reactor was compared to a monolith that had not been immobilized with drugs, and the monolith displayed a higher degree of retaining TNKS2. It is probable to assume that VDM in the monolith were able to react with amino groups, thiol groups and hydroxyl groups on the proteins, causing proteins to be trapped on the monolith. The decision of increasing the concentration of drug was based on a desire to have drug in excess during the reaction occurring with VDM inside the monolith, as this probably would increase the coverage of drug attached to VDM. An increased drug-VDM coverage would give reduce amount of VDM in the monolith free to react with the proteins injected on the CRAM reactor. By reducing the possibility of such secondary interactions, the CRAM reactors would hopefully show a higher selectivity of trapping the drug target TNKS1/2.

The assumption of washing fractions having a UV-Vis absorbance was to a degree hindered from evaluation as the initial concentration of the immobilization solutions was increased from 0.25 mg/mL to 5 mg/mL in the following immobilizations of monoliths. The absorbance spectra for a 2.5 mg/mL immobilization solution and a 5 mg/mL immobilization solution are shown in **Figure 47**, and it is clear that the measurements are above linear range. During the immobilization using 5 mg/mL, four fractions of washing solution was collected after collection of the flushed immobilization solution. The UV-Vis absorbance of the collected fractions, including the solution used for washing is given in **Table 6**. The immobilization solution and

the flushed immobilization solution is both above linear range. Wash 1 displays the same curve as the 0.25 mg/mL immobilization solution, but is still above linear range. However, the absorbance of Wash 2, Wash 3 and Wash 4 were within linear range and the absorbance was greatly reduced compared to 0.25 immobilization solution (approx. 5.5 times lower UV-Vis absorbance).

Based on Wash 2, Wash 3 and Wash 4 being within linear range and displaying a UV-absorbance 5.5 times lower that 0.25 mg/mL immobilization solution: Drugs are not continuously flushed out of the monolith with the washing solution, meaning drugs remaining on the monolith after flushing with immobilization solution can be presumed to be immobilized not only trapped.

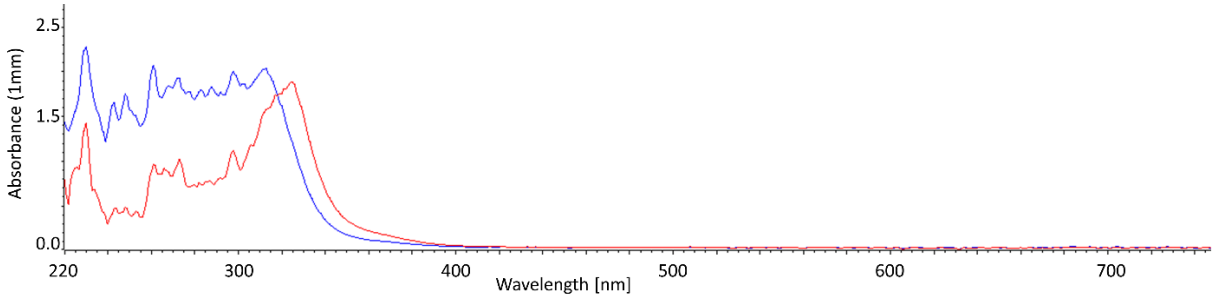

Figure 47: UV-Vis absorbance in spectral range 220 to 740 nm of immobilization solutions: (red) 5 mg/mL and (blue) 2.5 mg/mL.

Table 6: UV-Vis absorbance of 5 mg/mL immobilization solution, flushed immobilization solution, four collected washing fractions and 50 mM phosphate buffer, which was used for washing of the monolith. The UV-Vis absorbance of the 0.25 mg/mL immobilization solution is given for comparison. The UV-absorbance of each solution was measured three times.

Solution	Absorbance at 243 nm	Absorbance at 285 nm
5 mg/mL immobilization solution	0.457	0.799
Flushed immobilization solution	0.643	0.957
Wash 1	2.254	1.791
Wash 2	0.117	0.086
Wash 3	0.018	0.013
Wash 4	0.003	0.003
50 mM phosphate buffer	0.002	0.003
0.25 mg/mL immobilization solution	0.649	0.472

Based on the following observations: Significantly different UV-Vis absorbance of 0.25 mg/mL immobilization solution before and after flushing of a monolith, and that several washing fractions after flushing with a 5 mg/mL immobilization solution display 5.5 times lower UV-Vis

absorbance than 0.25 mg/mL immobilization solution. It is probable to presume that drug was immobilized onto the EDMA-co-VDM monolith using both 0.25 mg/mL and 5 mg/mL immobilization solutions.

3.5.2 Monolith resists immobilization of drug after quenching of vinyl azlacetone with monoethanolamine

As mentioned in the previous section, the initial assessment of the CRAM reactors presented in **Results and Discussion 3.6**, showed that a monolith without immobilized drugs retained TNKS2 to a larger extent than the CRAM reactors. It was also presumed that this was due to VDM reacting with proteins in the same manner as with the drug.

A way of reducing the amount of reactive VDM present on the monolith is flushing with a VDM-quenching reagent. One such reagent is MEA, structure shown in **Figure 48**, which quenches the VDM rings in the monolith by covalently binding to VDM in the same manner as the drug by a ring-opening reaction. MEA has been used for VDM quenching in both monoliths [127, 128] and in beads [37]. The remaining hydroxy groups (or amino groups) of MEA that does not react with VDM, is hydrophilic so it is expected that quenching VDM with MEA should not contribute to undesired secondary hydrophobic protein interactions.

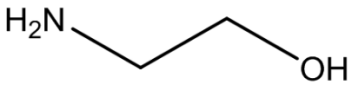

Figure 48: Structure of monoethanolamine.

If MEA could quench VDM reactivity, MEA could be used to produce monoliths that display no interactions with proteins. These monoliths flushed with MEA is referred to as MEA monoliths. To assess if such MEA monoliths did not interact with proteins, immobilization of drug was used for examination. Compared to evaluation of amount of proteins before and after flushing a MEA monolith, it is faster to evaluate the UV-Vis absorbance of the immobilization solution before and after flushing a MEA monolith. The immobilization of the MEA monolith would be carried out it the same manner as the immobilization of the monoliths, and the UV-Vis absorbance of the immobilization solutions could be compared between the two types of monolith.

To determine if MEA did quench the VDM reactivity, a monolith was flushed with 1 M MEA prior to immobilization. The absorbance spectra of the collected fractions from immobilization procedure is given in **Table 7** and shown in **Figure 49**. The absorbance of the 0.25 mg/mL immobilization solution and the fraction collected after flushing cannot be distinguished in **Figure 49**.

Table 7: UV-Vis absorbance of 0.25 mg/mL immobilization solution, flushed immobilization solution and a washing fraction collected from immobilization of a MEA monolith. The UV-absorbance of each solution was measured three times.

Solution	Absorbance at 243 nm	Absorbance at 285 nm
0.25 mg/mL immobilization solution	0.655	0.479
Flushed immobilization solution	0.640	0.468
Wash	0.011	0.008

The absorbance of both the immobilization solution and the flushed solution at 243 nm and 285 nm, lies within the ranges measured for the five immobilization solutions in the previous section. These ranges were [0.635, 0.662] at 243 nm and [0.461, 0,482] at 285 nm, meaning that the variation in absorbance between the immobilization before and after flushing a monolith treated with MEA cannot be caused by immobilization of drug on the monolith. Additionally, that the MEA monoliths resist immobilization confirms that MEA has been immobilized onto the monolith via VDM ring-opening reaction.

However, due to the difficulties of measuring absorbance of higher concentrations of immobilization solution, the experiment with MEA was only conducted once. The indication of MEA blocking immobilization of drugs needs to be confirmed by additional measurements of immobilization solutions flushed through a MEA monolith.

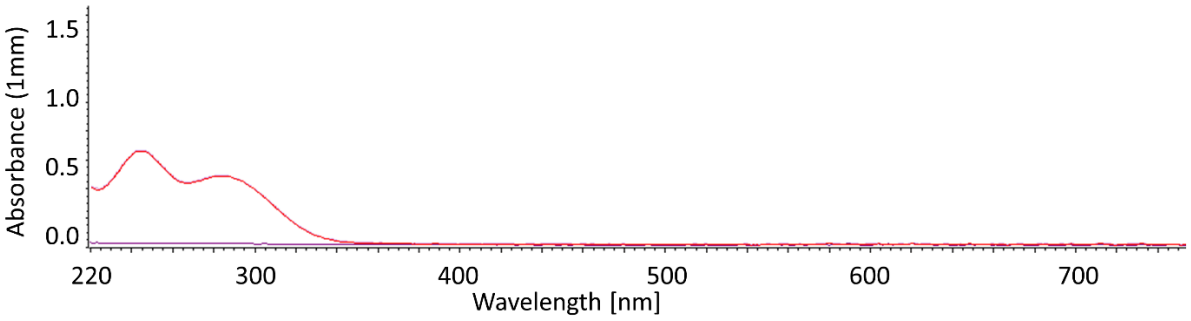

Figure 49: UV-Vis absorbance in spectral range 220 to 740 nm of solutions collected during immobilization of a 250 µm ID 14 cm EDMA-co-VDM monolith after flushing with 1 M MEA for 3 hours: (red) 0.25 mg/mL immobilization solution, (green) flush and (purple) 3 first drops of washing with storage solution).

It has been shown that MEA can quench VDM and produce MEA monoliths that resists immobilization of drugs. The MEA monoliths and the CRAM reactors may be used for comparison of trapping of TNKS1/2 and other proteins.

That the MEA monolith did not reduce the UV-Vis absorbance of the flushed immobilization, while the CRAM reactor did, increases the probability that drugs are being immobilized onto the EDMA-co-VDM monolith.

3.6 Assessment of the CRAM reactors potential of trapping and releasing tankyrases 1 and 2

At this point of the study, the drug (a linked LDW639) had been successfully synthesized and displayed inhibition of the Wnt-signaling pathway. In addition, a monolith (250 µm ID EDMA-co-VDM) had been produced and it has been shown that the monoliths were capable of immobilization of a linked LDW639.

To assess the TNKS trapping and elution potential of the CRAM reactors, a recombinant TNKS2 solution was applied onto a CRAM reactor and attempted eluted with different elution solutions. Subsequently, a comparison of the TNKS2 trapping potential of two CRAM reactors and a monolith was carried out. Initially, the collected fractions were measured by LC-MS, the measurements are described in **Appendix 7.6**. The adopted LC-MS method was successful at measuring and detecting recombinant TNKS2 in samples with a concentration below 0.028 mg/mL, an example of a fragment spectrum found for a peptide from TNKS2, EVPGVDFSITQFVR, is shown in **Figure 50**. However, the LC-MS analysis did not give any answers concerning the CRAM reactors potential for trapping of TNKS2 as the measurements had issues with carry over as a consequence of sample preparation. Additionally, secondary interactions towards proteins was revealed on the EDMA-co-VDM monolith. The cause of the secondary interactions was assumed to be interaction with VDM, as the samples were injected in the neutral pH range were VDM ring-opening reactions occur.

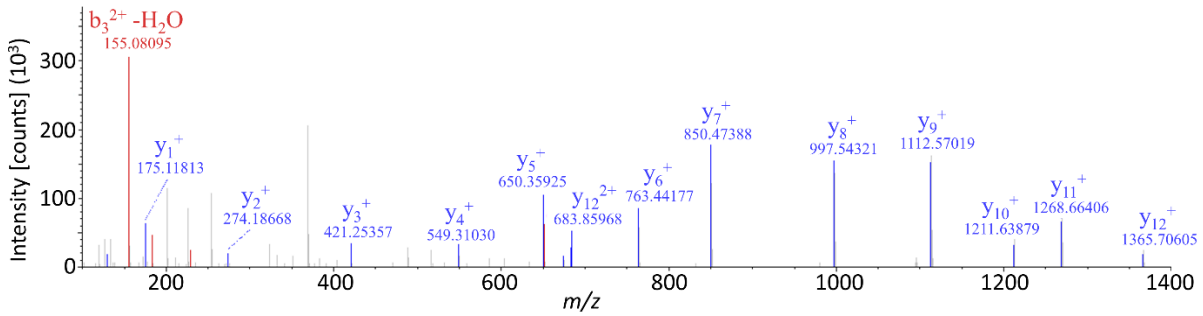

Figure 50: The fragment spectrum of EVPGVDFSITQFVR from the fraction Flush of protein mixture collected from CRAM reactor 1 (Appendix 7.6.2). The b-fragments are red, while the blue are y-fragments.

Due to technical issues with the Q-Exactive MS, WB replaced LC-MS for measuring of TNKS during the study. By repeating the comparison of applying recombinant TNKS2 on a CRAM reactor and an EDMA-co-VDM monolith not immobilized with drug, the fractions collected were analysed by WB, presented in **Appendix 7.7**. The experiment confirmed the presence of secondary interactions on the EDMA-co-VDM monolith. Additionally, the recombinant TNKS2 standard showed issues with purity due to degradation and dimer formation.

The initial assessment of the TNKS2 trapping potential of the CRAM reactor by LC-MS and WB revealed secondary interactions of proteins on the EDMA-co-VDM monolith and that the standard of TNKS2 was not suitable for assessment of the CRAM reactors.

To further assess the TNKS trapping potential of the CRAM reactors; TNKS needed to be extracted from cells by cell lysis and the WB procedure needed to be optimized towards full-length TNKS1 and TNKS2 from cell lysate. The optimization of the method for cell lysis and WB procedure is presented in **Appendix 7.8**. The final WB procedure, described in **Experimental 2.11,** was able to detect bands of TNKS1/2 in cell lysate (prepared by cell lysis with a non-denaturing buffer) from both cell lines HEK293 and HEK293-EGFP-TNKS1. However, the CRAM reactor with an increased concentration of linked LDW639 in the immobilization solution (5 mg/mL instead of 0.25 mg/mL) did not give bands of TNKS1/2 in any of the fractions that was collected. From assessing actin as a loading control it was shown that increasing the concentration of the immobilization solution did reduced secondary interactions towards proteins.

A final comparison of a CRAM reactor and a MEA monolith was carried out to assess whether or not immobilization of drug offered trapping potential of TNKS2 in a different manner than the MEA monolith. From the WB visualization of the fractions collected from the CRAM

reactor and the MEA monolith shown in **Figure 51**: the CRAM reactor and the MEA monolith showed actin in equivalent lanes, while TNKS2 was not found in any sample collected from the CRAM reactor or the MEA monolith. TNKS1/2 was present in the control of the cell lysate that was applied on the reactor and monolith.

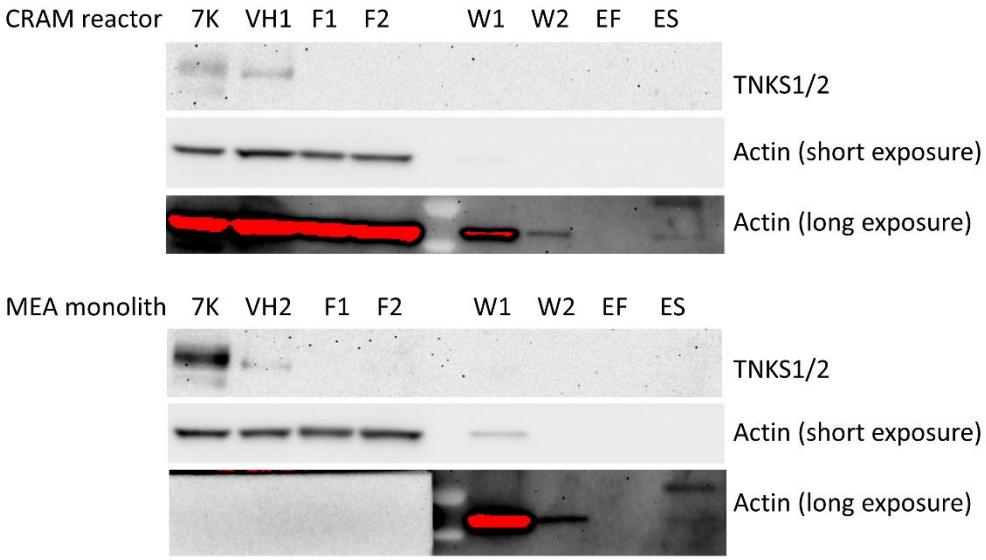

Figure 51: Western blot of: (7K) lane of 21 µg of protein from 007-LK control and (VH1) lane of 36.3 µg of protein from HEK293. Samples collected from the CRAM reactor (Upper) and MEA monolith (Lower) in the following lanes: (F1) Flush of 36.3 µg protein from HEK293, (F2) Flush of 36.3 µg protein from HEK293, (W1) Wash 1 with water, (W2) Wash 2 with water, (ES) eluted with 2% FA and (ES) eluted with 2% SDS. The raw files from WB is given in Appendix 7.10, Figure 88, Figure 89 and Figure 90. The exposure time was 7200 s for TNKS1/2 and 10 s (short exposure) and 2550 s (long exposure) for actin. During long exposure of the actin bands from the MEA monolith, the controls and the collected Flush fractions were covered with filter paper.

The CRAM reactor and the MEA monolith was not able to trap and elute TNKS1/2 in qualitative amount for WB, and no differences between the CRAM reactor and the MEA monolith was revealed based on detection of actin.

In a last attempt to explain the whereabouts of TNKS1/2, samples of cell lysate were collected from different parts of the application set-up described in **Experimental 2.10**. The experiment and measurements of the samples by BCA assay is presented in **Appendix 7.8.1,** showing that the concentration of protein in the cell lysate was reducing in samples transferred using a glass syringe compared to a pipette, also the PEEK sample loop did not affect the concentration of protein. The reduced concentration was assumed to be a consequence of dilution from residue solvent in the needle tip. WB analysis of the same samples, are needed to confirm that TNKS1/2 was not lost due to interaction with the glass syringe.

To find an explanation to why TNKS1/2 was not released in a detectable amount from the CRAM reactor and MEA monolith, more experiments need to be conducted. It is possible that TNKS1/2 are forming protein complexes with other proteins and other TNKS1/2 molecules, due to the ankyrin repeats and the SAM domain. It might also be that proteins with a larger mass compared to actin (42 kDa) are retained by the CRAM reactor and the MEA monolith, and only smaller proteins are eluted. This may be revealed by measuring proteins by LC-MS in samples prepared in the same manner as for the assessment by WB.

The issues with detection of TNKS1/2 may also be due to the monolith. Huang *et al.* [34] used LDW639 immobilized on Sepharose beads and were able to detect TNKS1/2 after bonding to the LDW639 beads. It is worth noting that LDW639 was used without an attached linker. An experiment using beads instead of the monolith may reveal whether or not the monolith is the reason behind the issues with detection of TNKS1/2.

Another possibility may be that the linked LDW639 is binding to other proteins in the ARTD superfamily, causing TNKS1/2 to be eluted of gradually and in amounts below the detection limit on WB. It was expected that the initial Wnt-inhibitor 161 would not show these issues with selectivity as it targets TNKS1/2 by the adenosine subsite offering higher selectivity for TNKS1/2. However, the method was developed to be utilized in target identification of new drugs, and to identify off-target effects, and therefore, to secure correct target identification be independent of the selectivity of the drug.

4 Conclusion

The aim of this study was to selectively trap drug targets on a monolithic support immobilized with drug to allow target identification. Several challenges were discovered during the study concerning both the EDMA-co-VDM monolith and the Wnt-inhibitor 161. First and foremost, another Wnt-inhibitor need to be selected as inhibitor 161 was deemed unsuitable for the planned experiments after examination by MS. This meant that a new inhibitor needed to be synthesized and characterized: The linked LDW639 was successfully synthesized and by determination by STF-Luc assay displayed inhibition of the Wnt-signaling pathway (IC_{50} value of 11 µM). A weakness of the develop method is the need to modify the drugs, between 50% and 80% of the crude material was lost during the synthesis step for attachment of the linker.

Additionally, the selected EDMA-co-VDM monolith displayed secondary interaction with proteins shown by reduced coverage of the TNKS2 by LC-MS on monoliths compared to CRAM reactors. This was confirmed by WB, where actin was not present in the Flush collected from CRAM reactors immobilized with 0.25 mg/mL linked LDW639, but actin was present in the Flush collected from the MEA monolith. Eventually, this was corrected by using MEA as a quencher of VDM present on the monolith and increasing the concentration of the immobilization solution to 5 mg/mL of linked LDW639.

The last major challenge discovered during the study was the elution of TNKS1/2 from the CRAM reactor. In all of the WB analysis of fractions collected from the CRAM reactors and the MEA monolith, no TNKS1/2 bands were present. The attempted elution solutions ranged from mild conditions 50 mM AmAc to a denaturing elution solution 2% SDS. The equipment used for application of TNKS was examined as the cause of the missing TNKS, but the measurements of protein concentration was inconclusive. WB analysis for TNKS of the same samples would be able to conclude whether or not TNKS was lost due to the equipment.

Concerning the hypothesis that the CRAM reactors would allow for identification of low abundant targets, the study showed that the reactors were not able to selectively trap and release TNKS1/2 in detectable amounts by WB. The reason why TNKS1/2 was not detected in any of the fractions collected from the CRAM reactors and the MEA monoliths was not solved during the study. The study shows that even with tailored materials, selective trapping of a targeted molecule from a complex matrix is a considerable challenge.

5 Further work

A comparison of the EDMA-co-VDM monolith and beads as solid support of the linked LDW639 may be carried out to reveal if the closed form of the monolith is reason for the difficulties experienced with trapping and eluting TNKS1/2. Also, measuring equivalent samples prepared for WB analysis by LC-MS may reveal how other proteins in the cell lysate interacts with the CRAM reactor and MEA monolith.

If the issues with trapping and elution are resolved on the CRAM reactor, the reactor may be combined online LC-MS with an immobilized enzyme reactor (IMER). The entire process from trapping of drug protein target(s), trypsination of the protein(s), separation and detection by LC-MS would then be possible to accomplish in a single work-flow. An automated system would then be possible for target identification of drugs, under the requirement that the drug is suitable for immobilization and attachment of a linker.

6 References

[1] G.L. Patrick, An introduction to medicinal chemistry, 5th ed. ed., Oxford University Press, Oxford, 2013.
[2] E.J. Corey, J.J. Li, Drug discovery : practices, processes, and perspectives, Wiley, Hoboken, N.J, 2013.
[3] C. Wermuth, C. Ganellin, P. Lindberg, L. Mitscher, Glossary of terms used in medicinal chemistry (IUPAC Recommendations 1998), Pure and Applied Chemistry, 70 (1998) 1129-1143.
[4] L.B. Kier, Molecular orbital theory in drug research, Academic Press, New York, 1971.
[5] M.S. Smyth, J.H. Martin, X ray crystallography, Molecular Pathology, 53 (2000) 8-14.
[6] R.M. Cooke, A.J.H. Brown, F.H. Marshall, J.S. Mason, Structures of G protein-coupled receptors reveal new opportunities for drug discovery, Drug Discovery Today, 20 (2015) 1355-1364.
[7] G.L. Card, L. Blasdel, B.P. England, C. Zhang, Y. Suzuki, S. Gillette, D. Fong, P.N. Ibrahim, D.R. Artis, G. Bollag, M.V. Milburn, S.-H. Kim, J. Schlessinger, K.Y.J. Zhang, A family of phosphodiesterase inhibitors discovered by cocrystallography and scaffold-based drug design, Nature Biotechnology, 23 (2005) 201.
[8] T. Haikarainen, S. Krauss, L. Lehtio, Tankyrases: structure, function and therapeutic implications in cancer, Current Pharmaceutical Design, 20 (2014) 6472-6488.
[9] A.R. Ortiz, M.T. Pisabarro, F. Gago, R.C. Wade, Prediction of drug binding affinities by comparative binding energy analysis, Journal of Medicinal Chemistry, 38 (1995) 2681-2691.
[10] G. Sliwoski, S. Kothiwale, J. Meiler, E.W. Lowe, Computational Methods in Drug Discovery, Pharmacological Reviews, 66 (2014) 334-395.
[11] L. Ferreira, R. dos Santos, G. Oliva, A. Andricopulo, Molecular Docking and Structure-Based Drug Design Strategies, Molecules, 20 (2015) 13384.
[12] J.K. Dhanjal, S. Sharma, A. Grover, A. Das, Use of ligand-based pharmacophore modeling and docking approach to find novel acetylcholinesterase inhibitors for treating Alzheimer's, Biomedicine & Pharmacotherapy, 71 (2015) 146-152.
[13] J. Lee, M. Bogyo, Target deconvolution techniques in modern phenotypic profiling, Current Opinion in Chemical Biology, 17 (2013) 118-126.
[14] C.H. Wong, K.W. Siah, A.W. Lo, Estimation of clinical trial success rates and related parameters, Biostatistics, (2018) 1-14.
[15] J.A. DiMasi, H.G. Grabowski, R.W. Hansen, Innovation in the pharmaceutical industry: New estimates of R&D costs, Journal of Health Economics, 47 (2016) 20-33.
[16] G.C. Terstappen, C. Schlüpen, R. Raggiaschi, G. Gaviraghi, Target deconvolution strategies in drug discovery, Nature Reviews Drug Discovery, 6 (2007) 891-903.
[17] M. Rask-Andersen, M.S. Almén, H.B. Schiöth, Trends in the exploitation of novel drug targets, Nature Reviews Drug Discovery, 10 (2011) 579.
[18] I. Kola, J. Landis, Can the pharmaceutical industry reduce attrition rates?, Nature Reviews Drug Discovery, 3 (2004) 711.
[19] F. Sams-Dodd, Target-based drug discovery: is something wrong?, Drug Discovery Today, 10 (2005) 139-147.
[20] A.M. Ghaemmaghami, M.J. Hancock, H. Harrington, H. Kaji, A. Khademhosseini, Biomimetic tissues on a chip for drug discovery, Drug Discovery Today, 17 (2012) 173-181.
[21] J.A. Lee, M.T. Uhlik, C.M. Moxham, D. Tomandl, D.J. Sall, Modern Phenotypic Drug Discovery Is a Viable, Neoclassic Pharma Strategy, Journal of Medicinal Chemistry, 55 (2012) 4527-4538.

[22] P.A. Clemons, Complex phenotypic assays in high-throughput screening, Current Opinion in Chemical Biology, 8 (2004) 334-338.
[23] M. Schenone, V. Dančík, B.K. Wagner, P.A. Clemons, Target identification and mechanism of action in chemical biology and drug discovery, Nature Chemical Biology, 9 (2013) 232-240.
[24] S. Ziegler, V. Pries, C. Hedberg, H. Waldmann, Target Identification for Small Bioactive Molecules: Finding the Needle in the Haystack, Angewandte Chemie International Edition, 52 (2013) 2744-2792.
[25] B. Lomenick, R. Hao, N. Jonai, R.M. Chin, M. Aghajan, S. Warburton, J. Wang, R.P. Wu, F. Gomez, J.A. Loo, Target identification using drug affinity responsive target stability (DARTS), Proceedings of the National Academy of Sciences, 106 (2009) 21984-21989.
[26] J.N. Chan, D. Vuckovic, L. Sleno, J.B. Olsen, O. Pogoutse, P. Havugimana, J.A. Hewel, N. Bajaj, Y. Wang, M.F. Musteata, Target identification by chromatographic co-elution: monitoring of drug-protein interactions without immobilization or chemical derivatization, Molecular & Cellular Proteomics, 11 (2012).
[27] G.M. West, L. Tang, M.C. Fitzgerald, Thermodynamic analysis of protein stability and ligand binding using a chemical modification-and mass spectrometry-based strategy, Analytical Chemistry, 80 (2008) 4175-4185.
[28] W.P. Blackstock, M.P. Weir, Proteomics: quantitative and physical mapping of cellular proteins, Trends in Biotechnology, 17 (1999) 121-127.
[29] J.S. Cottrell, Protein identification using MS/MS data, Journal of Proteomics, 74 (2011) 1842-1851.
[30] A. McFedries, A. Schwaid, A. Saghatelian, Methods for the Elucidation of Protein-Small Molecule Interactions, Chemistry & Biology, 20 (2013) 667-673.
[31] G.M. West, C.L. Tucker, T. Xu, S.K. Park, X. Han, J.R. Yates, M.C. Fitzgerald, Quantitative proteomics approach for identifying protein–drug interactions in complex mixtures using protein stability measurements, Proceedings of the National Academy of Sciences, 107 (2010) 9078-9082.
[32] E.C. Strickland, M.A. Geer, D.T. Tran, J. Adhikari, G.M. West, P.D. DeArmond, Y. Xu, M.C. Fitzgerald, Thermodynamic analysis of protein-ligand binding interactions in complex biological mixtures using the stability of proteins from rates of oxidation, Nature Protocols, 8 (2012) 148.
[33] P. Cuatrecasas, Protein purification by affinity chromatography derivatizations of agarose and polyacrylamide beads, Journal of Biological Chemistry, 245 (1970) 3059-3065.
[34] S.-M.A. Huang, Y.M. Mishina, S. Liu, A. Cheung, F. Stegmeier, G.A. Michaud, O. Charlat, E. Wiellette, Y. Zhang, S. Wiessner, Tankyrase inhibition stabilizes axin and antagonizes Wnt signalling, Nature, 461 (2009) 614-620.
[35] M. Bantscheff, D. Eberhard, Y. Abraham, S. Bastuck, M. Boesche, S. Hobson, T. Mathieson, J. Perrin, M. Raida, C. Rau, V. Reader, G. Sweetman, A. Bauer, T. Bouwmeester, C. Hopf, U. Kruse, G. Neubauer, N. Ramsden, J. Rick, B. Kuster, G. Drewes, Quantitative chemical proteomics reveals mechanisms of action of clinical ABL kinase inhibitors, Nature Biotechnology, 25 (2007) 1035.
[36] S. Hildonen, E. Skarpen, T.G. Halvorsen, L. Reubsaet, Isolation and mass spectrometry analysis of urinary extraexosomal proteins, Scientific Reports, 6 (2016) 36331.
[37] P.L. Coleman, M.M. Walker, D.S. Milbrath, D.M. Stauffer, J.K. Rasmussen, L. R. Krepski, S.M. Heilmann, Immobilization of Protein A at high density on azlactone-functional polymeric beads and their use in affinity chromatography, Journal of Chromatography A, 512 (1990) 345-363.
[38] M. Bantscheff, A. Scholten, A.J.R. Heck, Revealing promiscuous drug–target interactions by chemical proteomics, Drug Discovery Today, 14 (2009) 1021-1029.

[39] G.L. Rosano, E.A. Ceccarelli, Recombinant protein expression in Escherichia coli: advances and challenges, Frontiers in Microbiology, 5 (2014) 172-172.
[40] D.A. Jeffery, M. Bogyo, Chemical proteomics and its application to drug discovery, Current Opinion in Biotechnology, 14 (2003) 87-95.
[41] D. Josić, H. Schwinn, A. Štrancar, A. Podgornik, B. Miloš, Y.-P. Lim, M. Vodopivec, Use of compact, porous units with immobilized ligands with high molecular masses in affinity chromatography and enzymatic conversion of substrates with high and low molecular masses. Presented at the 1997 International Symposium on Preparative Chromatography, Washington, DC, 1–4 June 1997., Journal of Chromatography A, 803 (1998) 61-71.
[42] H. Kataoka, New trends in sample preparation for clinical and pharmaceutical analysis, TrAC Trends in Analytical Chemistry, 22 (2003) 232-244.
[43] J. Pan, C. Zhang, Z. Zhang, G. Li, Review of online coupling of sample preparation techniques with liquid chromatography, Analytica Chimica Acta, 815 (2014) 1-15.
[44] L. Nováková, H. Vlčková, A review of current trends and advances in modern bio-analytical methods: Chromatography and sample preparation, Analytica Chimica Acta, 656 (2009) 8-35.
[45] S.R. Wilson, T. Vehus, H.S. Berg, E. Lundanes, Nano-LC in proteomics: recent advances and approaches, Bioanalysis, 7 (2015) 1799-1815.
[46] E. Lundanes, L. Reubsaet, T. Greibrokk, Chromatography: basic principles, sample preparations and related methods, John Wiley & Sons, 2013.
[47] S. Ehlert, T. Rösler, U.J.J.o.s.s. Tallarek, Packing density of slurry-packed capillaries at low aspect ratios, Journal of Separation Science, 31 (2008) 1719-1728.
[48] H. Minakuchi, K. Nakanishi, N. Soga, N. Ishizuka, N. Tanaka, Octadecylsilylated Porous Silica Rods as Separation Media for Reversed-Phase Liquid Chromatography, Analytical Chemistry, 68 (1996) 3498-3501.
[49] A. Al-Hussin, R.I. Boysen, K. Saito, M.T.W. Hearn, Preparation and electrochromatographic characterization of new chiral β-cyclodextrin poly(acrylamidopropyl) porous layer open tubular capillary columns, Journal of Chromatography A, 1358 (2014) 199-207.
[50] C. Kulsing, R. Knob, M. Macka, P. Junor, R.I. Boysen, M.T.W. Hearn, Molecular imprinted polymeric porous layers in open tubular capillaries for chiral separations, Journal of Chromatography A, 1354 (2014) 85-91.
[51] O.K. Brandtzaeg, B.-T. Røen, S. Enger, E. Lundanes, S.R. Wilson, Multichannel Open Tubular Enzyme Reactor Online Coupled with Mass Spectrometry for Detecting Ricin, Analytical Chemistry, 89 (2017) 8667-8673.
[52] J. Krenkova, F. Svec, Less common applications of monoliths: IV. Recent developments in immobilized enzyme reactors for proteomics and biotechnology, Journal of Separation Science, 32 (2009) 706-718.
[53] F. Svec, Porous polymer monoliths: Amazingly wide variety of techniques enabling their preparation, Journal of Chromatography A, 1217 (2010) 902-924.
[54] R.D. Arrua, M.C. Strumia, C.I. Alvarez Igarzabal, Macroporous Monolithic Polymers: Preparation and Applications, Materials, 2 (2009) 2429-2466.
[55] S. Hjertén, J.-L. Liao, R. Zhang, High-performance liquid chromatography on continuous polymer beds, Journal of Chromatography A, 473 (1989) 273-275.
[56] F. Svec, J.M.J. Frechet, Continuous rods of macroporous polymer as high-performance liquid chromatography separation media, Analytical Chemistry, 64 (1992) 820-822.
[57] G.A. Platonova, T.B. Tennikova, Affinity processes realized on high-flow-through methacrylate-based macroporous monoliths, Journal of Chromatography A, 1065 (2005) 19-28.

[58] L. Geiser, S. Eeltink, F. Svec, J.M. Fréchet, In-line system containing porous polymer monoliths for protein digestion with immobilized pepsin, peptide preconcentration and nano-liquid chromatography separation coupled to electrospray ionization mass spectroscopy, Journal of Chromatography A, 1188 (2008) 88-96.
[59] M. Motokawa, H. Kobayashi, N. Ishizuka, H. Minakuchi, K. Nakanishi, H. Jinnai, K. Hosoya, T. Ikegami, N. Tanaka, Monolithic silica columns with various skeleton sizes and through-pore sizes for capillary liquid chromatography, Journal of Chromatography A, 961 (2002) 53-63.
[60] N. Tanaka, H. Kobayashi, N. Ishizuka, H. Minakuchi, K. Nakanishi, K. Hosoya, T. Ikegami, Monolithic silica columns for high-efficiency chromatographic separations, Journal of Chromatography A, 965 (2002) 35-49.
[61] J.C. Masini, F. Svec, Porous monoliths for on-line sample preparation: A review, Analytica Chimica Acta, 964 (2017) 24-44.
[62] M. Safdar, J. Sproß, J. Jänis, Microscale immobilized enzyme reactors in proteomics: Latest developments, Journal of Chromatography A, 1324 (2014) 1-10.
[63] F. Svec, T.B. Tennikova, Z. Deyl, Monolithic Materials: Preparation, Properties and Applications, Elsevier Science B. V., 2003.
[64] A. Premstaller, H. Oberacher, W. Walcher, A.M. Timperio, L. Zolla, J.-P. Chervet, N. Cavusoglu, A. van Dorsselaer, C.G. Huber, High-Performance Liquid Chromatography−Electrospray Ionization Mass Spectrometry Using Monolithic Capillary Columns for Proteomic Studies, Analytical Chemistry, 73 (2001) 2390-2396.
[65] J.M.G. Cowie, V. Arrighi, Polymers : chemistry and physics of modern materials, 3rd ed. ed., Taylor & Francis, Boca Raton, Fla, 2008.
[66] C.K. Zacharis, E.A. Kalaitzantonakis, A. Podgornik, G. Theodoridis, Sequential injection affinity chromatography utilizing an albumin immobilized monolithic column to study drug–protein interactions, Journal of Chromatography A, 1144 (2007) 126-134.
[67] J. Krenkova, N.A. Lacher, F. Svec, Highly efficient enzyme reactors containing trypsin and endoproteinase LysC immobilized on porous polymer monolith coupled to MS suitable for analysis of antibodies, Analytical Chemistry, 81 (2009) 2004-2012.
[68] C. Ericson, J.-L. Liao, K.i. Nakazato, S. Hjertén, Preparation of continuous beds for electrochromatography and reversed-phase liquid chromatography of low-molecular-mass compounds, Journal of Chromatography A, 767 (1997) 33-41.
[69] J. Du, Y. Chen, Atom-Transfer Radical Polymerization of a Reactive Monomer: 3-(Trimethoxysilyl)propyl Methacrylate, Macromolecules, 37 (2004) 6322-6328.
[70] X. Liu, M. He, B. Chen, B. Hu, Polymer monolithic capillary microextraction on-line coupled with inductively coupled plasma-mass spectrometry for the determination of trace Au and Pd in biological samples, Spectrochimica Acta Part B: Atomic Spectroscopy, 101 (2014) 254-260.
[71] D. Lee, F. Svec, J.M.J. Fréchet, Photopolymerized monolithic capillary columns for rapid micro high-performance liquid chromatographic separation of proteins, Journal of Chromatography A, 1051 (2004) 53-60.
[72] O.K.M. Brandtzæg, Online Sample Preparation Platforms for Targeted Nano Liquid Chromatography Mass Spectrometry Bioanalysis, in: Department of Chemistry, University of Oslo, 2018, pp. 96.
[73] C.M. Dobson, Protein folding and misfolding, Nature, 426 (2003) 884.
[74] W.J. Wedemeyer, E. Welker, M. Narayan, H.A. Scheraga, Disulfide Bonds and Protein Folding, Biochemistry, 39 (2000) 4207-4216.
[75] S. Jones, J.M. Thornton, Protein-protein interactions: A review of protein dimer structures, Progress in Biophysics and Molecular Biology, 63 (1995) 31-65.

[76] I.M. Klotz, N. Langebman, D. Dahnall, Quaternary structure of proteins, Annual Review of Biochemistry, 39 (1970) 25-62.
[77] R. Aebersold, A.L. Burlingame, R.A. Bradshaw, Western blots versus selected reaction monitoring assays: time to turn the tables?, Molecular & Cellular Proteomics, 12 (2013) 2381-2382.
[78] S.C. Alley, N.M. Okeley, P.D. Senter, Antibody–drug conjugates: targeted drug delivery for cancer, Current Opinion in Chemical Biology, 14 (2010) 529-537.
[79] A.L. Nelson, E. Dhimolea, J.M. Reichert, Development trends for human monoclonal antibody therapeutics, Nature Reviews Drug Discovery, 9 (2010) 767.
[80] R. O'Kennedy, S. Fitzgerald, C. Murphy, Don't blame it all on antibodies – The need for exhaustive characterisation, appropriate handling, and addressing the issues that affect specificity, TrAC Trends in Analytical Chemistry, 89 (2017) 53-59.
[81] H. Towbin, T. Staehelin, J. Gordon, Electrophoretic transfer of proteins from polyacrylamide gels to nitrocellulose sheets: procedure and some applications, Proceedings of the National Academy of Sciences, 76 (1979) 4350-4354.
[82] W.N. Burnette, "Western Blotting": Electrophoretic transfer of proteins from sodium dodecyl sulfate-polyacrylamide gels to unmodified nitrocellulose and radiographic detection with antibody and radioiodinated protein A, Analytical Biochemistry, 112 (1981) 195-203.
[83] C. Burrell, C.R. Howard, F.A. Murphy, Fenner and white's medical virology, Fifth edition. ed., Academic Press, Amsterdam, Netherlands, 2017.
[84] A.K. Bhuyan, On the mechanism of SDS-induced protein denaturation, Biopolymers, 93 (2010) 186-199.
[85] J.A. Reynolds, C. Tanford, Binding of dodecyl sulfate to proteins at high binding ratios. Possible implications for the state of proteins in biological membranes, Proceedings of the National Academy of Sciences of the United States of America, 66 (1970) 1002-1007.
[86] A.L. Shapiro, E. Viñuela, J. V. Maizel, Molecular weight estimation of polypeptide chains by electrophoresis in SDS-polyacrylamide gels, Biochemical and Biophysical Research Communications, 28 (1967) 815-820.
[87] A. Voronkov, D.D. Holsworth, J. Waaler, S.R. Wilson, B. Ekblad, H. Perdreau-Dahl, H. Dinh, G. Drewes, C. Hopf, J.P. Morth, Structural basis and SAR for G007-LK, a lead stage 1, 2, 4-triazole based specific tankyrase 1/2 inhibitor, Journal of Medicinal Chemistry, 56 (2013) 3012-3023.
[88] L. Ornstein, Disc Electrophoresis- I Background and Theory*, Annals of the New York Academy of Sciences, 121 (1964) 321-349.
[89] D.E. Williams, R.A. Reisfeld, Disc Electrophoresis in Polyacrylamide gels: Extention to new Conditions of pH and Buffer, Annals of the New York Academy of Sciences, 121 (1964) 373-381.
[90] T. Mahmood, P.C. Yang, Western blot: technique, theory, and trouble shooting, North American journal of medical sciences, 4 (2012) 429-434.
[91] E.R. Tovey, B.A. Baldo, Protein binding to nitrocellulose, nylon and PVDF membranes in immunoassays and electroblotting, Journal of Biochemical and Biophysical Methods, 19 (1989) 169-183.
[92] J. Kyhse-Andersen, Electroblotting of multiple gels: a simple apparatus without buffer tank for rapid transfer of proteins from polycrylamide to nitrocellulose, Journal of Biochemical and Biophysical Methods, 10 (1984) 203-209.
[93] B.T. Kurien, R.H. Scofield, Western blotting, Methods, 38 (2006) 283-293.
[94] M.W. Bolt, P.A. Mahoney, High-Efficiency Blotting of Proteins of Diverse Sizes Following Sodium Dodecyl Sulfate–Polyacrylamide Gel Electrophoresis, Analytical Biochemistry, 247 (1997) 185-192.

[95] J.V. Olsen, S.-E. Ong, M. Mann, Trypsin Cleaves Exclusively C-terminal to Arginine and Lysine Residues, Molecular & Cellular Proteomics, 3 (2004) 608-614.
[96] R. Aebersold, M. Mann, Mass-spectrometric exploration of proteome structure and function, Nature, 537 (2016) 347.
[97] J. Abian, A.J. Oosterkamp, E. Gelpí, Comparison of conventional, narrow-bore and capillary liquid chromatography/mass spectrometry for electrospray ionization mass spectrometry: practical considerations, Journal of Mass Spectrometry, 34 (1999) 244-254.
[98] A. Michalski, E. Damoc, J.-P. Hauschild, O. Lange, A. Wieghaus, A. Makarov, N. Nagaraj, J. Cox, M. Mann, S. Horning, Mass spectrometry-based proteomics using Q Exactive, a high-performance benchtop quadrupole Orbitrap mass spectrometer, Molecular & Cellular Proteomics, (2011).
[99] P.E. Miller, M.B. Denton, The quadrupole mass filter: basic operating concepts, Journal of Chemical Education, 63 (1986) 617.
[100] M. Scigelova, A. Makarov, Orbitrap Mass Analyzer – Overview and Applications in Proteomics, Proteomics, 6 (2006) 16-21.
[101] J.K. Eng, B. Fischer, J. Grossmann, M.J. MacCoss, A Fast SEQUEST Cross Correlation Algorithm, Journal of Proteome Research, 7 (2008) 4598-4602.
[102] H. Clevers, Wnt/β-catenin signaling in development and disease, Cell, 127 (2006) 469-480.
[103] C.Y. Logan, R. Nusse, The Wnt signaling pathway in development and disease, Annual Review of Cell and Developmental Biology 20 (2004) 781-810.
[104] P. Polakis, Wnt signaling and cancer, Genes & Development, 14 (2000) 1837-1851.
[105] R.A. Mook, X.-R. Ren, J. Wang, H. Piao, L.S. Barak, H.K. Lyerly, W. Chen, Benzimidazole inhibitors from the Niclosamide chemotype inhibit Wnt/β-catenin signaling with selectivity over effects on ATP homeostasis, Bioorganic & Medicinal Chemistry, 25 (2017) 1804-1816.
[106] T. Vehus, Nano-liquid chromatography-tandem mass spectrometry platforms for determination of low-abundant Wnt/beta-catenin proteins in cancer research, in: Department of Chemistry, University in Oslo, 2018, pp. 102.
[107] S. Guettler, J. LaRose, E. Petsalaki, G. Gish, A. Scotter, T. Pawson, R. Rottapel, F. Sicheri, Structural Basis and Sequence Rules for Substrate Recognition by Tankyrase Explain the Basis for Cherubism Disease, Cell, 147 (2011) 1340-1354.
[108] M. De Rycker, C.M. Price, Tankyrase Polymerization Is Controlled by Its Sterile Alpha Motif and Poly(ADP-Ribose) Polymerase Domains, Molecular and Cellular Biology, 24 (2004) 9802-9812.
[109] H.S. Berg, K.E. Seterdal, T. Smetop, R. Rozenvalds, O.K. Brandtzaeg, T. Vehus, E. Lundanes, S.R. Wilson, Self-packed core shell nano liquid chromatography columns and silica-based monolithic trap columns for targeted proteomics, Journal of Chromatography A, 1498 (2017) 111-119.
[110] M. Rogeberg, T. Vehus, L. Grutle, T. Greibrokk, S.R. Wilson, E. Lundanes, Separation optimization of long porous-layer open-tubular columns for nano-LC–MS of limited proteomic samples, Journal of Separation Science, 36 (2013) 2838-2847.
[111] H.K. Hustoft, O.K. Brandtzaeg, M. Rogeberg, D. Misaghian, S.B. Torsetnes, T. Greibrokk, L. Reubsaet, S.R. Wilson, E. Lundanes, Integrated enzyme reactor and high resolving chromatography in “sub-chip” dimensions for sensitive protein mass spectrometry, Scientific Reports, 3 (2013) 3511.
[112] M.C.S. Levernæs, O.K. Brandtzaeg, S.F. Amundsen, L. Reubsaet, E. Lundanes, T.G. Halvorsen, S.R. Wilson, Selective Fishing for Peptides with Antibody-Immobilized Acrylate Monoliths, Coupled Online with NanoLC-MS, Analytical Chemistry, 90 (2018) 13860-13866.

[113] L.D. Taylor, C.K. Chiklis, T.E. Platt, Synthesis and polymerization of 2-vinyl-4,4-dimethyl-5-oxazolone, Journal of Polymer Science Part B: Polymer Letters, 9 (1971) 187-190.
[114] S.M. Heilmann, J.K. Rasmussen, L.R. Krepski, H.K. Smith, Chemistry of alkenyl azlactones. VII. Preparation and properties of multiazlactones derived from mercaptan-functional compounds and oligomers, Journal of Polymer Science Part A: Polymer Chemistry, 24 (1986) 1-14.
[115] L.D. Taylor, T.E. Platt, The synthesis of vinyl peptide monomers, Journal of Polymer Science Part C: Polymer Letters, 7 (1969) 597-603.
[116] C. Olsen, Ethylene dimethacrylate-co-vinyl azlactone monolithic polymer immobilized with trypsin for on-line digestion of proteins., in, University of Oslo, Unpublished Bachelor Thesis, 2016. Available upon request.
[117] B. Chen, M.E. Dodge, W. Tang, J. Lu, Z. Ma, C.-W. Fan, S. Wei, W. Hao, J. Kilgore, N.S. Williams, M.G. Roth, J.F. Amatruda, C. Chen, L. Lum, Small molecule–mediated disruption of Wnt-dependent signaling in tissue regeneration and cancer, Nature Chemical Biology, 5 (2009) 100-107.
[118] H. Tong, D. Bell, K. Tabei, M.M. Siegel, Automated data massaging, interpretation, and e-mailing modules for high throughput open access mass spectrometry, Journal of the American Society for Mass Spectrometry, 10 (1999) 1174-1187.
[119] T. Furuya, A.S. Kamlet, T. Ritter, Catalysis for fluorination and trifluoromethylation, Nature, 473 (2011) 470.
[120] D. O'Hagan, Understanding organofluorine chemistry. An introduction to the C–F bond, Chemical Society Reviews, 37 (2008) 308-319.
[121] J.K. Rasmussen, R.M. Gleason, D.S. Milbrath, R.L. Rasmussen, Derivatization of Azlactone-Functional Supports with Small Ligands. Strategies for Control of Ligand Density, Industrial & Engineering Chemistry Research, 44 (2005) 8554-8559.
[122] L.M. Harwood, C.J. Moody, J.M. Percy, Experimental organic chemistry : standard and microscale, 2nd ed. ed., Blackwell Science, Oxford, 1999.
[123] E. Valeur, M. Bradley, Amide bond formation: beyond the myth of coupling reagents, Chemical Society Reviews, 38 (2009) 606-631.
[124] T.I. Al-Warhi, H.M.A. Al-Hazimi, A. El-Faham, Recent development in peptide coupling reagents, Journal of Saudi Chemical Society, 16 (2012) 97-116.
[125] J.R. Dunetz, J. Magano, G.A. Weisenburger, Large-Scale Applications of Amide Coupling Reagents for the Synthesis of Pharmaceuticals, Organic Process Research & Development, 20 (2016) 140-177.
[126] A. Nathubhai, T. Haikarainen, P.C. Hayward, S. Muñoz-Descalzo, A.S. Thompson, M.D. Lloyd, L. Lehtiö, M.D. Threadgill, Structure-activity relationships of 2-arylquinazolin-4-ones as highly selective and potent inhibitors of the tankyrases, European Journal of Medicinal Chemistry, 118 (2016) 316-327.
[127] S. Xie, F. Svec, J.M. Fréchet, Design of reactive porous polymer supports for high throughput bioreactors: Poly (2-vinyl-4, 4-dimethylazlactone-co-acrylamide-co-ethylene dimethacrylate) monoliths, Biotechnology and Bioengineering, 62 (1999) 30-35.
[128] D.S. Peterson, T. Rohr, F. Svec, J.M. Fréchet, Enzymatic microreactor-on-a-chip: protein mapping using trypsin immobilized on porous polymer monoliths molded in channels of microfluidic devices, Analytical Chemistry, 74 (2002) 4081-4088.

7 Appendix

7.1 Production of ethylene dimethacrylate-co-vinyl azlactone monoliths in different sizes of capillaries using old and new replacement chemicals

During polymerization the capillaries filled with polymerization solution was kept in the oven in a horizontal straight position to reduce possible effects of movement in the polymerization solution. This was solved as shown in **Figure 52**.

Figure 52: The capillaries filled with polymerization solution were kept in a close to horizontal straight position using aluminum foil (Left) instead of the bent shape (Right).

For the individually prepared EDMA-co-VDM monoliths, the measured backpressure corrected for the length of the monoliths and the contribution from the LC set-up, are given in the following tables. The backpressure of the monoliths prepared in 180 µm ID capillaries using the old chemicals are given in **Table 8** and the 250 µm ID capillaries in **Table 9**. The backpressure of the monoliths prepared in 250 µm ID capillaries after the chemicals were replaced with new ones are given in **Table 10**. To determine if replacing the chemicals used for preparation of monoliths produced significantly different monoliths, single factor ANOVA was used to compare the measured backpressure at different flow rates of the monoliths prepared with old and new chemicals. For all of the six different flow rates, the backpressure was not significantly different between the monoliths prepared with old and new chemicals, calculated

F was smaller than critical F value of the F-test. The ANOVA are presented from **Table 11** to **Table 16**.

Table 8: Backpressure measured on seven individually prepared EDMA-co-VDM monoliths in 180 µm ID capillaries using "old chemicals". The backpressure was corrected for length and pressure on the system without monolith attached, and is presented with as bar per meter [bar m^{-1}].

Flow rate [µLmin^{-1}] / Monolith	0.2	0.4	0.5	0.6	0.8	1.0
1	77	154	200	248	321	413
2	60	136	164	202	260	298
3	73	155	180	223	302	378
4	14	28	30	30	46	54
5	19	46	52	64	77	94
6	27	60	79	96	131	171
7	33	70	85	101	141	175
Average	43	93	113	138	182	226
STD	26	54	67	85	110	139

Table 9: Backpressure measured on seven individually prepared EDMA-co-VDM monoliths in 250 µm ID capillaries using "old chemicals". The backpressure was corrected for length and pressure on the system without monolith attached, and is presented with as bar per meter [bar m^{-1}].

Flow rate [µLmin^{-1}] / Monolith	0.2	0.4	0.5	0.6	0.8	1.0
1	9	17	22	27	37	67
2	4	9	13	16	20	34
3	5	14	18	22	20	25
4	4	10	12	14	18	23
5	5	8	10	12	17	21
6	8	14	15	19	19	46
7	11	16	9	11	11	56
Average	6	13	14	17	20	36
STD	3	4	5	6	8	14

Table 10: Backpressure measured on eight individually prepared EDMA-co-VDM monoliths in 180 µm ID capillaries using "new chemicals". The backpressure was corrected for length and pressure on the system without monolith attached, and is presented with as bar per meter [bar m^{-1}].

Flow rate [µLmin^{-1}] / **Monolith**	**0.2**	**0.4**	**0.5**	**0.6**	**0.8**	**1.0**
1	3	5	7	9	11	16
2	4	8	9	11	14	23
3	4	8	8	10	13	18
4	5	9	12	14	19	31
5	3	11	13	18	24	31
6	8	18	22	26	26	43
7	3	8	10	12	12	19
8	4	10	10	12	12	21
Average	4	10	11	14	16	25
STD	2	4	5	6	6	9

Table 11: Single factor ANOVA test of the backpressure corrected for monolith length at 0.2 µLmin^{-1} flow between EDMA-co-VDM monoliths prepared in 250 µm ID capillaries with old and new chemicals. The test established the total standard deviation, and the variance within monoliths prepared with the same chemicals and between the monoliths prepared with different chemicals. By an F-test, the test determines if the change in chemicals creates monoliths that are significantly different from each other, this is the case when $F > F_{crit}$.

Groups	*Count*	*Sum*	*Average*	*Variance*
Old	7	45.5	6.5	8.3
New	8	34.5	4.3	3.1

ANOVA

Source of Variation	*SS*	*df*	*MS*	*F*	*P-value*	*F crit*
Between Groups	17.8	1	17.8	3.3	0.09	4.7
Within Groups	71.1	13	5.5			
Total	88.9	14				

Table 12: Single factor ANOVA test of the backpressure corrected for monolith length at 0.4 µLmin^{-1} flow between EDMA-co-VDM monoliths prepared in 250 µm ID capillaries with old and new chemicals. The test established the total standard deviation, and the variance within monoliths prepared with the same chemicals and between the monoliths prepared with different chemicals. By an F-test, the test determines if the change in chemicals creates monoliths that are significantly different from each other, this is the case when $F > F_{crit.}$

Groups	*Count*	*Sum*	*Average*	*Variance*
Old	7	87.7	12.5	14.2
New	8	77.3	9.7	13.3

ANOVA

Source of Variation	*SS*	*df*	*MS*	*F*	*P-value*	*F crit*
Between Groups	30.7	1	30.7	2.2	0.2	4.7
Within Groups	178.5	13	13.7			
Total	209.2	14				

Table 13: Single factor ANOVA test of the backpressure corrected for monolith length at 0.5 µLmin^{-1} flow between EDMA-co-VDM monoliths prepared in 250 µm ID capillaries with old and new chemicals. The test established the total standard deviation, and the variance within monoliths prepared with the same chemicals and between the monoliths prepared with different chemicals. By an F-test, the test determines if the change in chemicals creates monoliths that are significantly different from each other, this is the case when $F > F_{crit.}$

Groups	*Count*	*Sum*	*Average*	*Variance*
Old	7	99.3	14.2	21.5
New	8	90.4	11.3	21.8

ANOVA

Source of Variation	*SS*	*df*	*MS*	*F*	*P-value*	*F crit*
Between Groups	31.2	1	31.2	1.4	0.3	4.7
Within Groups	281.6	13	21.7			
Total	312.7	14				

Table 14: Single factor ANOVA test of the backpressure corrected for monolith length at 0.6 µLmin^{-1} flow between EDMA-co-VDM monoliths prepared in 250 µm ID capillaries with old and new chemicals. The test established the total standard deviation, and the variance within monoliths prepared with the same chemicals and between the monoliths prepared with different chemicals. By an F-test, the test determines if the change in chemicals creates monoliths that are significantly different from each other, this is the case when $F > F_{crit.}$

Groups	*Count*	*Sum*	*Average*	*Variance*
Old	7	121.3	17.3	34.5
New	8	112.4	14.1	32.8

ANOVA

Source of Variation	*SS*	*df*	*MS*	*F*	*P-value*	*F crit*
Between Groups	40.1	1	40.1	1.2	0.3	4.7
Within Groups	436.7	13	33.6			
Total	476.8	14				

Table 15: Single factor ANOVA test of the backpressure corrected for monolith length at 0.8 µLmin^{-1} flow between EDMA-co-VDM monoliths prepared in 250 µm ID capillaries with old and new chemicals. The test established the total standard deviation, and the variance within monoliths prepared with the same chemicals and between the monoliths prepared with different chemicals. By an F-test, the test determines if the change in chemicals creates monoliths that are significantly different from each other, this is the case when $F > F_{crit.}$

Groups	*Count*	*Sum*	*Average*	*Variance*
Old	7	141.8	20.3	62.2
New	8	130.6	16.3	36.2

ANOVA

Source of Variation	*SS*	*df*	*MS*	*F*	*P-value*	*F crit*
Between Groups	57.9	1	57.9	1.2	0.3	4.7
Within Groups	626.3	13	48.2			
Total	684.2	14				

Table 16: Single factor ANOVA test of the backpressure corrected for monolith length at 1.0 µLmin^{-1} flow between EDMA-co-VDM monoliths prepared in 250 µm ID capillaries with old and new chemicals. The test established the total standard deviation, and the variance within monoliths prepared with the same chemicals and between the monoliths prepared with different chemicals. By an F-test, the test determines if the change in chemicals creates monoliths that are significantly different from each other, this is the case when $F > F_{crit.}$

Groups	*Count*	*Sum*	*Average*	*Variance*
Old	7	250.7	35.8	189.7
New	8	203.4	25.4	82.6

ANOVA

Source of Variation	*SS*	*df*	*MS*	*F*	*P-value*	*F crit*
Between Groups	402.2	1	402.2	3.0	0.1	4.7
Within Groups	1715.9	13	132.0			
Total	2118.1	14				

7.1.1 Chemicals evaluated by proton nuclear magnetic resonance

The ^{1}H-NMR spectra of the liquid chemicals (new and old) used for production of EDMA-co-VDM monoliths (i.e. DMF, γ-MAPS, VDM, EDMA, 1-propanol and 1,4-butanediol) are shown in **Figure 53** to **Figure 64**. Using DMSO-D^{6} as solvent gave rise to signal at 2.5 and 3.3 ppm. From the integral of the numerated peaks, the new and old chemicals are quite similar in composition. The old 1,4-butanediol had impurities (not numerated peaks) which were not present in the new 1,4-butanediol. Also, the new VDM appears to be less pure than the old VDM (which has been stored at -80 degrees since 2009); this observation is based on the impurity peaks having higher integrals in the spectrum of the new VDM compared to the same peaks in the spectrum of the old VDM.

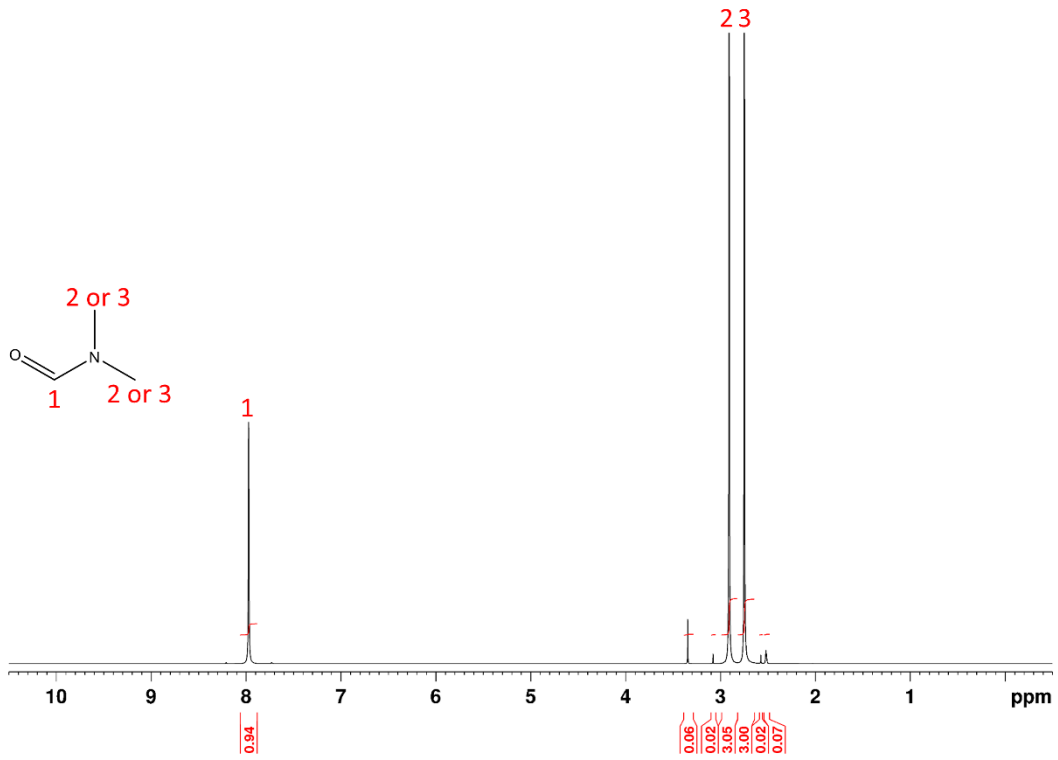

Figure 53: ^{1}H-NMR spectrum of "new" DMF dissolved 1+9 in DMSO-D^{6}, 16 scans on AVII400 (400 MHz).

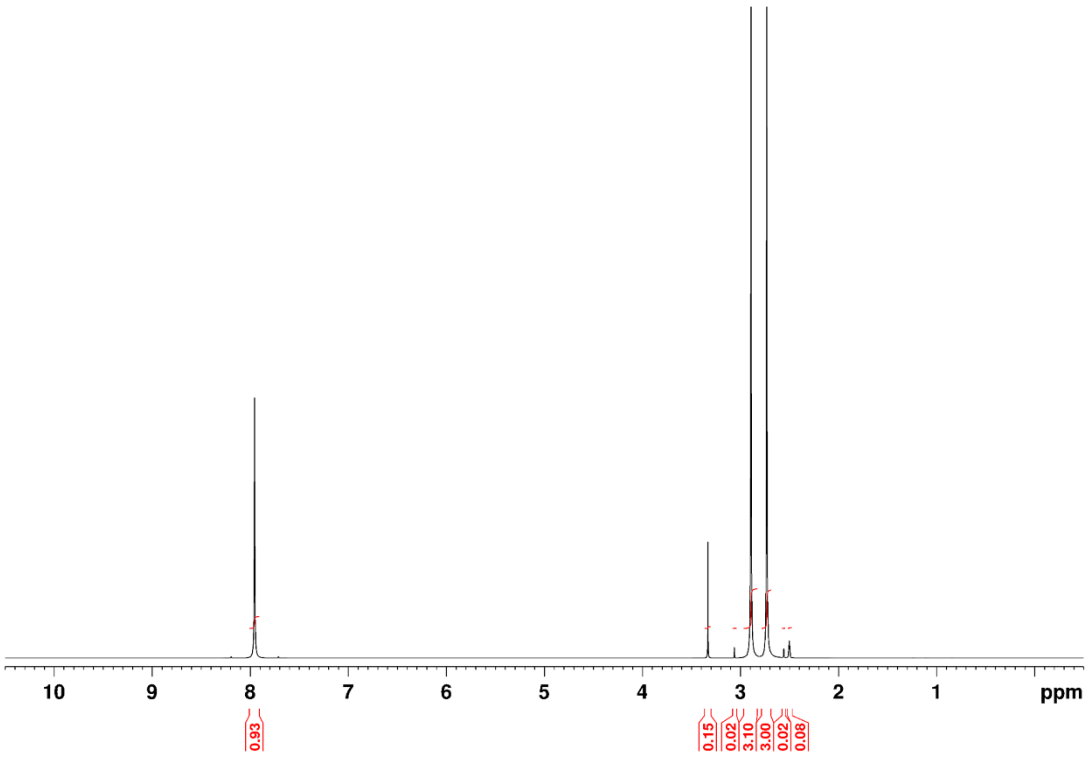

Figure 54: ^{1}H-NMR spectrum of "old" DMF dissolved 1+9 in DMSO-D^{6}, 16 scans on AVII400 (400 MHz).

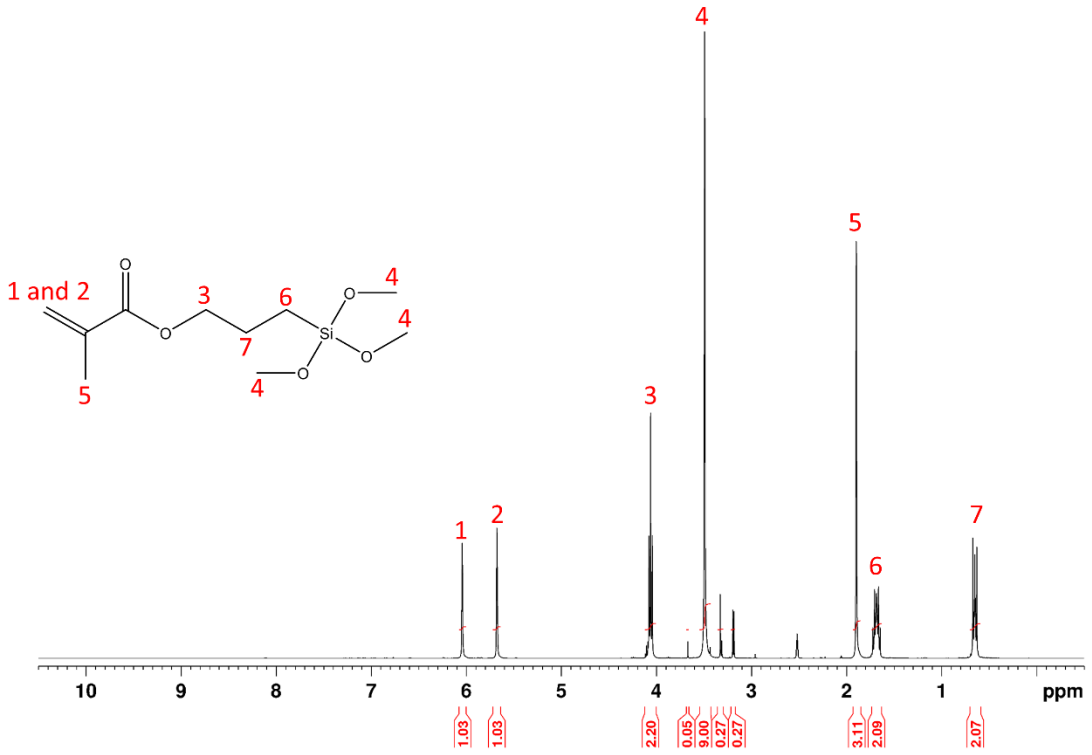

Figure 55: ^{1}H-NMR spectrum of "new" ɣ-MAPS dissolved 1+9 in DMSO-D^{6}, 16 scans on AVII400 (400 MHz).

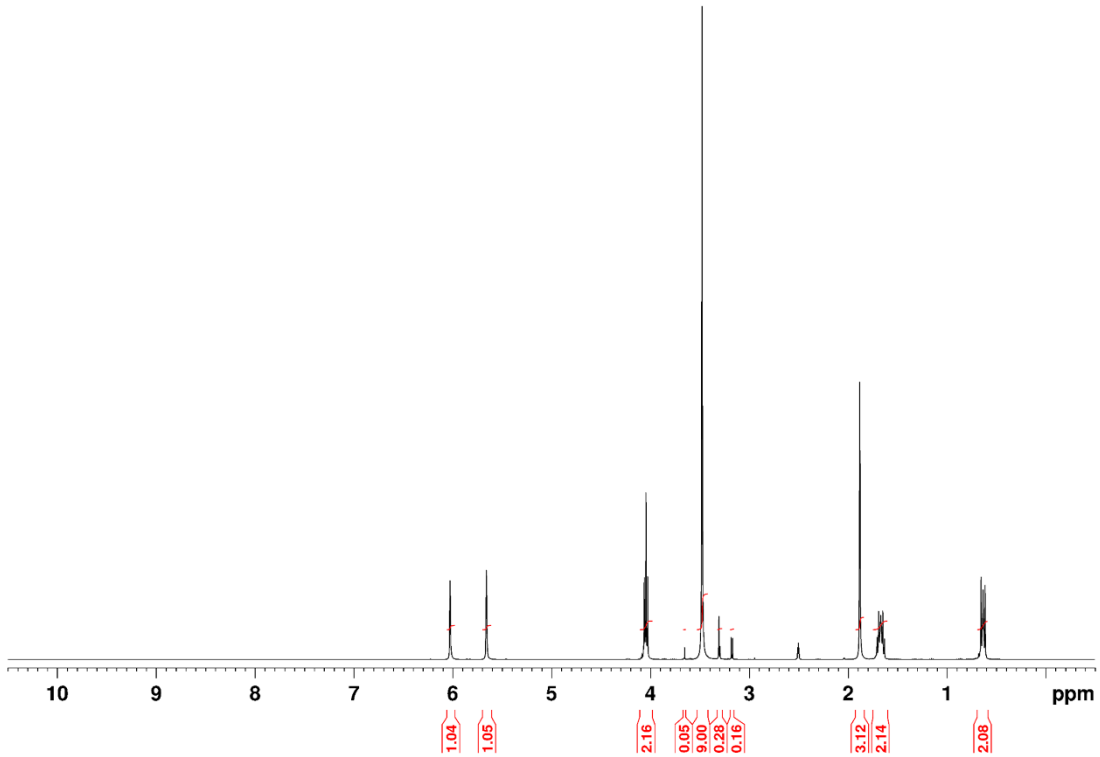

Figure 56: ^{1}H-NMR spectrum of "old" ɣ-MAPS dissolved 1+9 in DMSO-D^{6}, 16 scans on AVII400 (400 MHz).

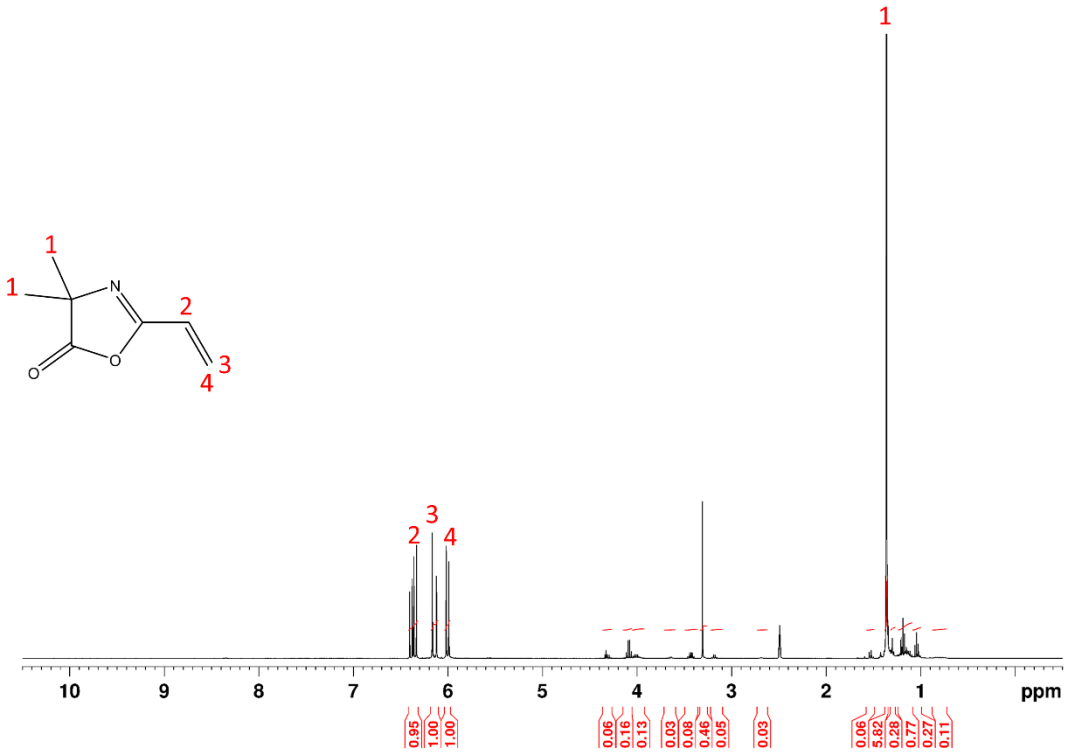

Figure 57: ^{1}H-NMR spectrum of "new" VDM dissolved 1+9 in DMSO-D^{6}, 16 scans on AVII400 (400 MHz).

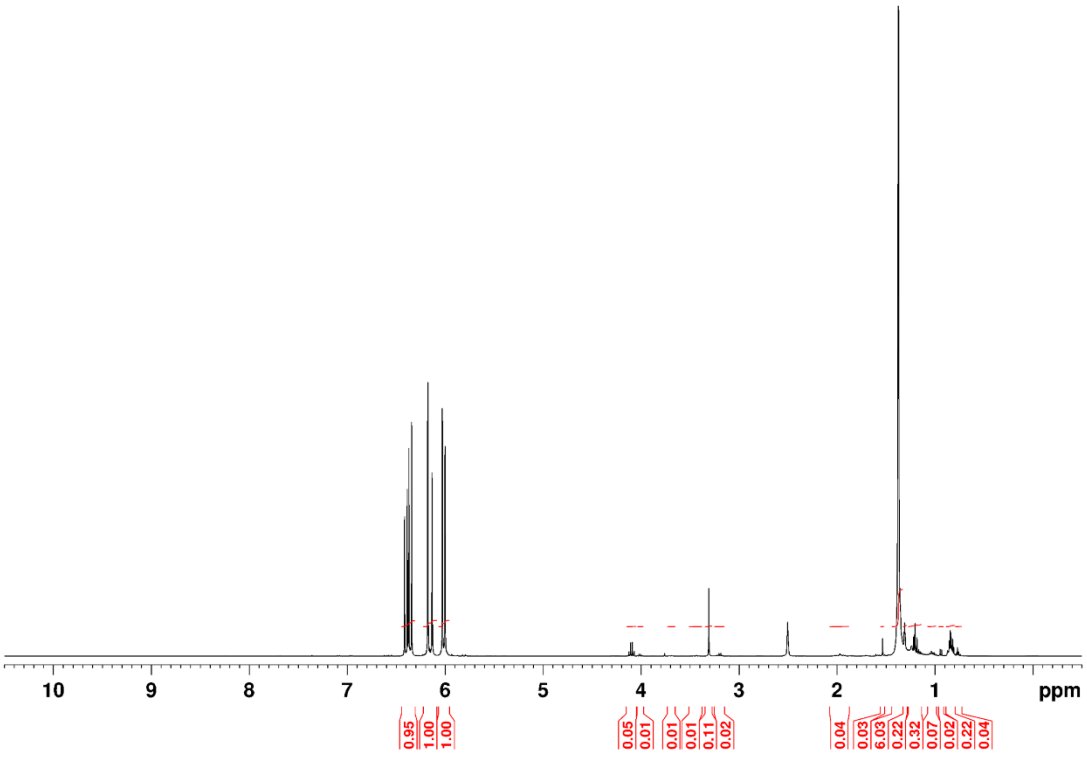

Figure 58: ^{1}H-NMR spectrum of "old" VDM dissolved 1+9 in DMSO-D^{6}, 16 scans on AVII400 (400 MHz).

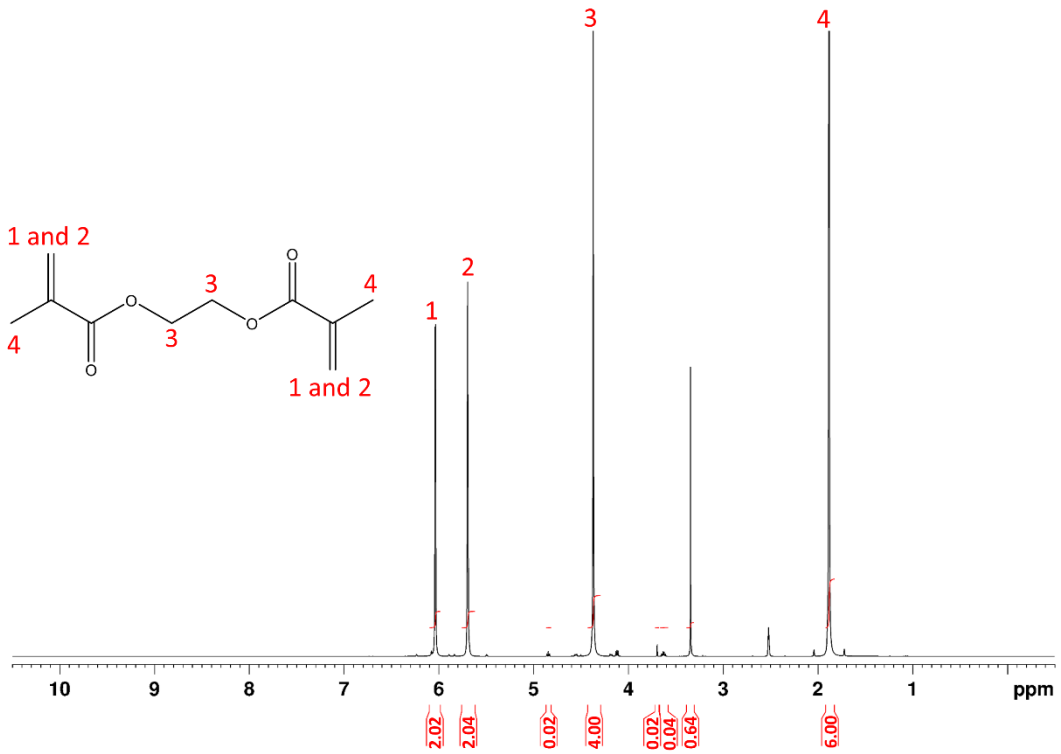

Figure 59: ^{1}H-NMR spectrum of "new" EDMA dissolved 1+9 in DMSO-D^{6}, 16 scans on AVII400 (400 MHz).

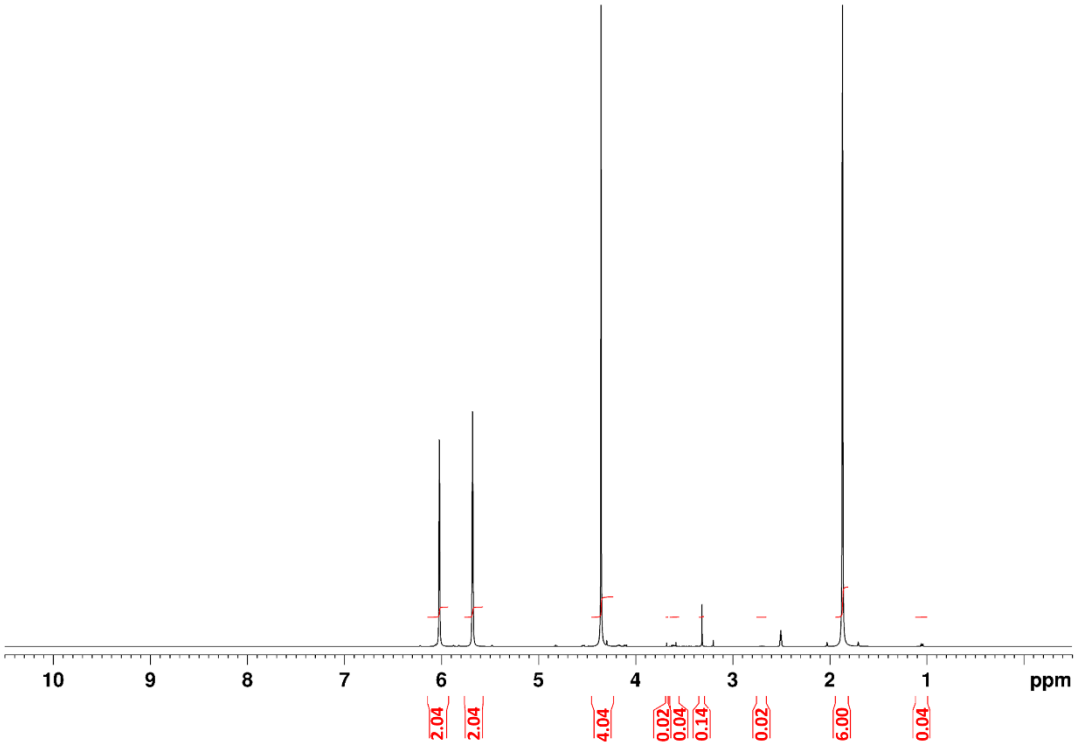

Figure 60: ^{1}H-NMR spectrum of "old" EDMA dissolved 1+9 in DMSO-D^{6}, 16 scans on AVII400 (400 MHz).

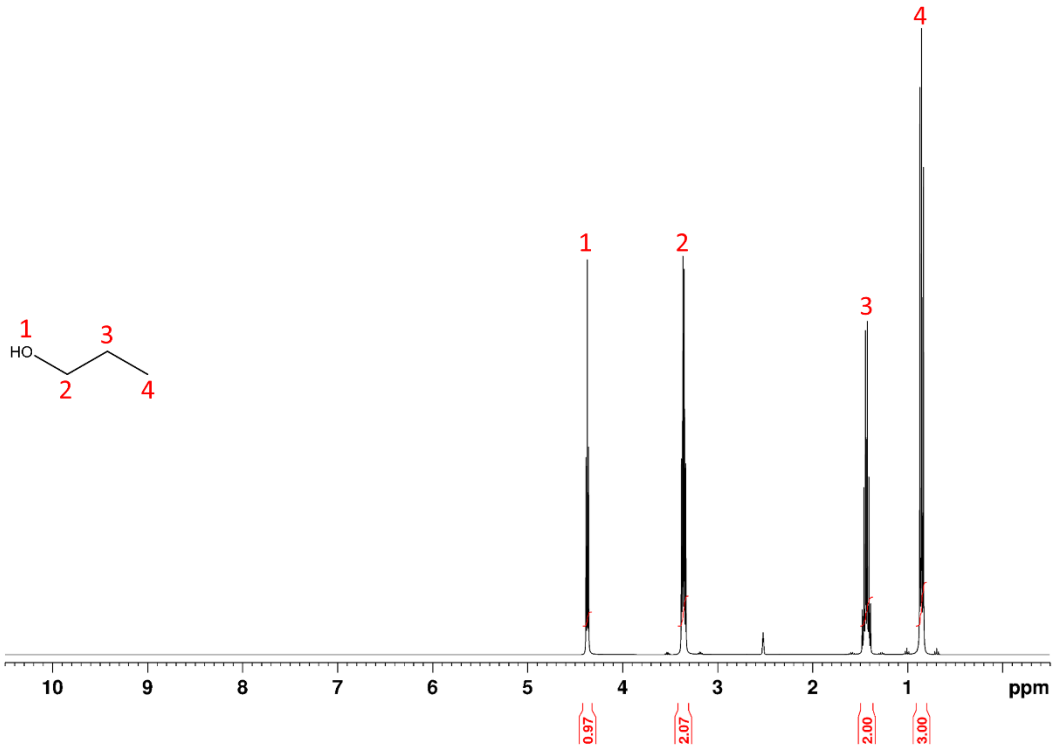

Figure 61: ^{1}H-NMR spectrum of "new" 1-propanol dissolved 1+9 in DMSO-D^{6}, 16 scans on AVII400 (400 MHz).

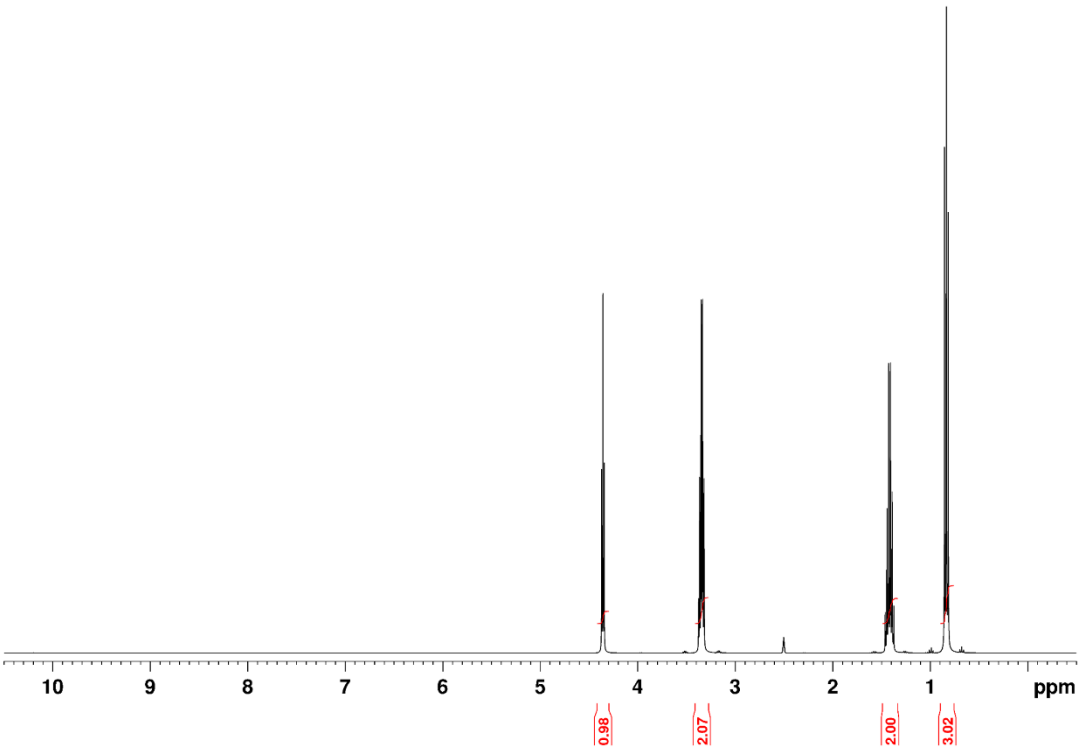

Figure 62: ^{1}H-NMR spectrum of "old" 1-propanol dissolved 1+9 in DMSO-D^{6}, 16 scans on AVII400 (400 MHz).

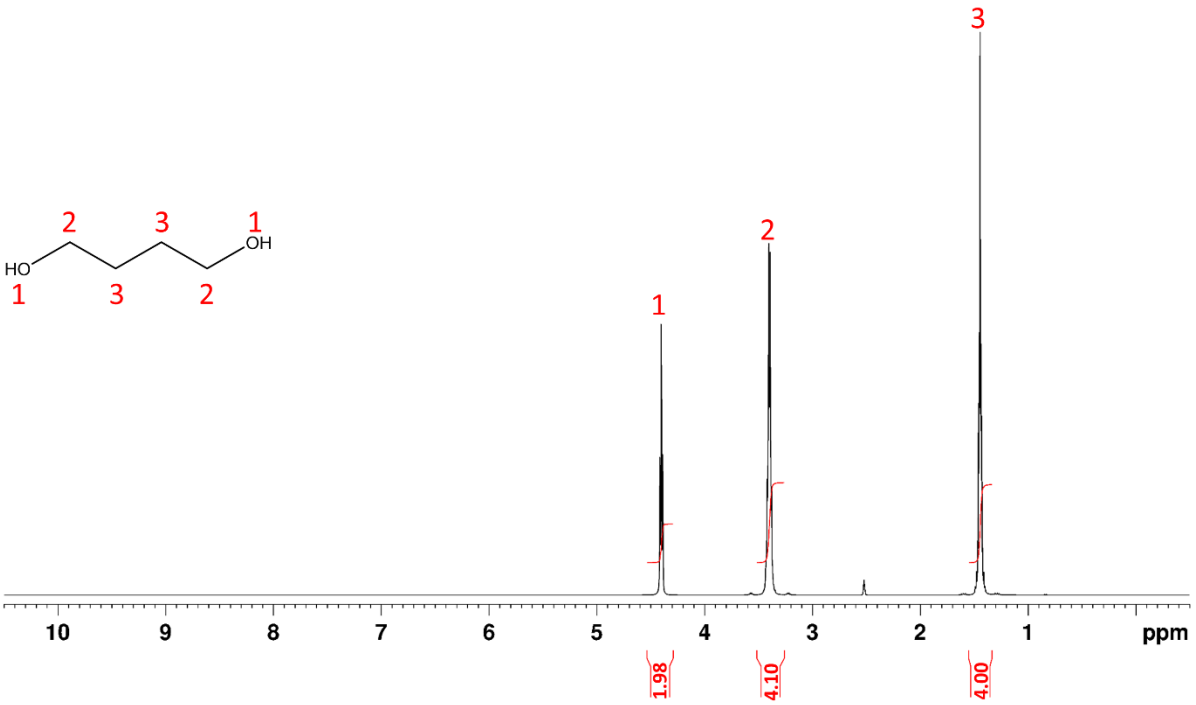

Figure 63: ^{1}H-NMR spectrum of "new" 1,4-butanediol dissolved 1+9 in DMSO-D^{6}, 16 scans on AVII400 (400 MHz).

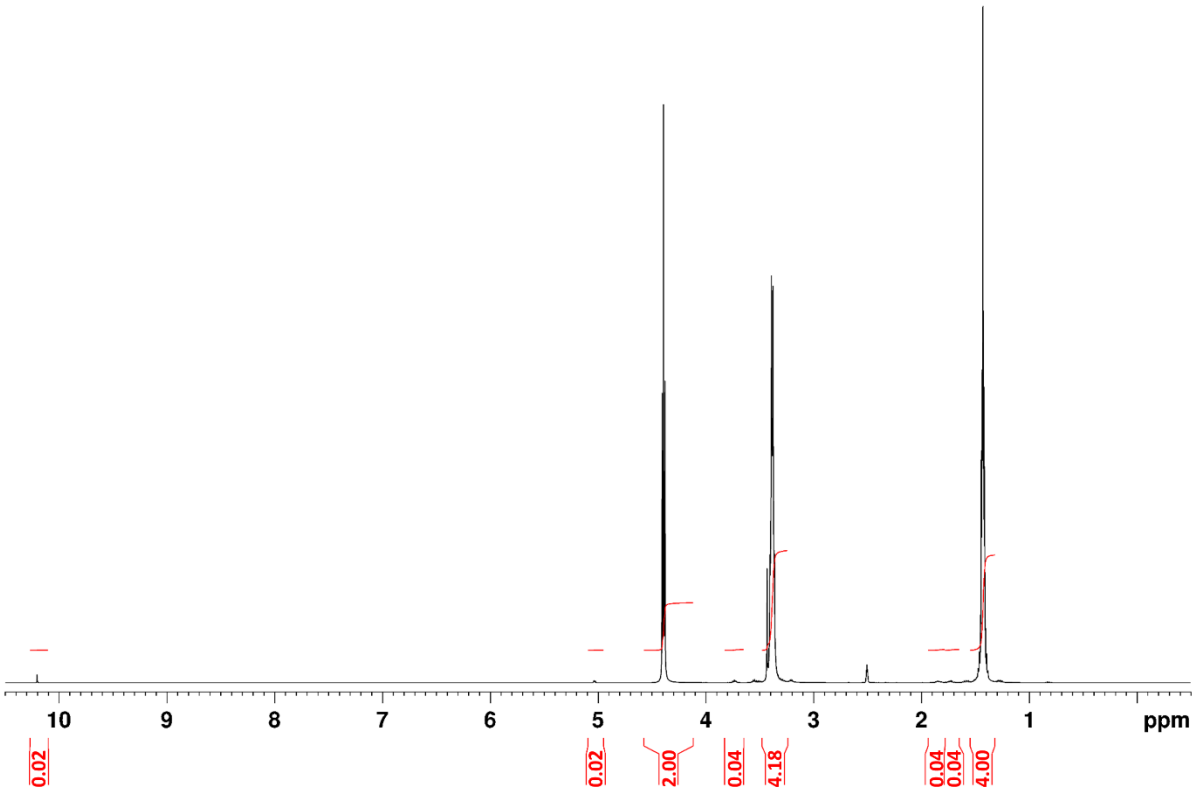

Figure 64: ^{1}H-NMR spectrum of "old" 1,4-butanediol dissolved 1+9 in DMSO-D^{6}, 16 scans on AVII400 (400 MHz).

7.2 The initially selected Wnt-signaling pathway inhibitor 161

To determine if the amount of inhibitor 161 was sufficient for the planned testing, the UV-Vis absorbance of the inhibitor solution was measured by nanodrop. It was expected that 161 would show a complex UV-Vis absorption spectrum due to the conjugated double bonds. However, as shown in **Figure 65**, there was only one sharp peak at 230 nm.

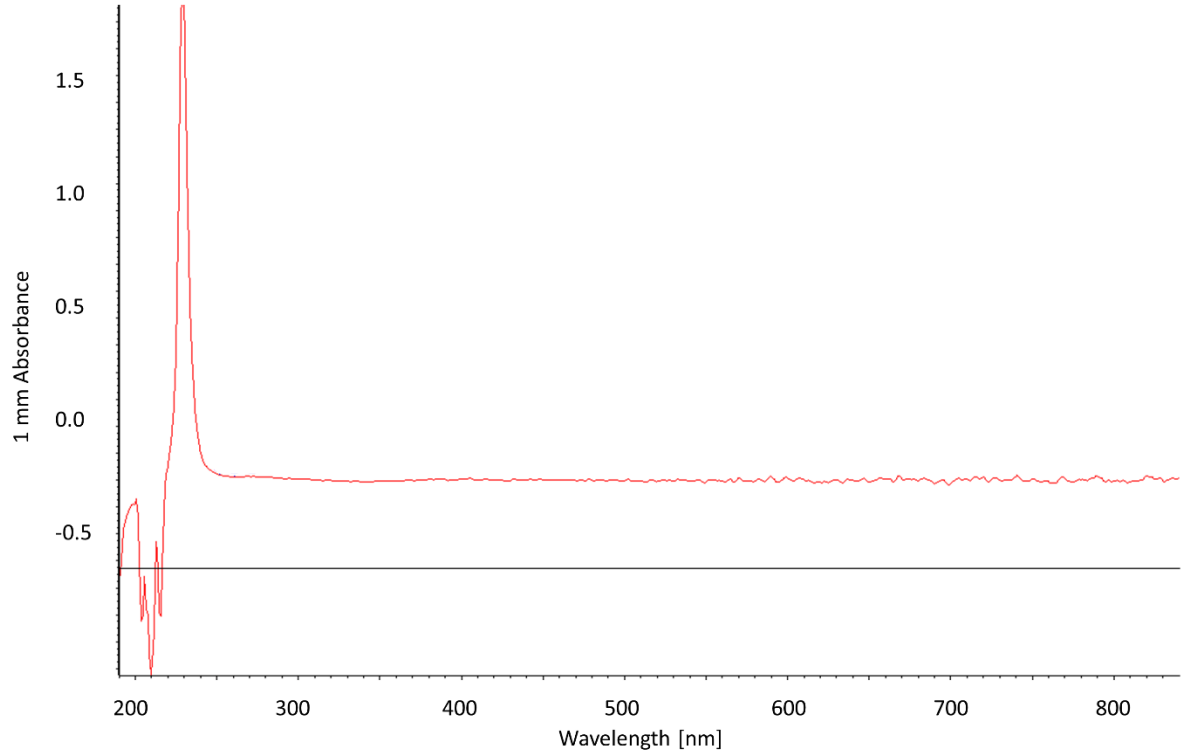

Figure 65: Absorbance spectrum for Wnt-signaling pathway inhibitor 161 diluted 1+9 in 0.1% FA. Spectrum recorded in UV-Vis spectral region (190 nm to 840 nm) by nanodrop.

7.3 Additional procedures for the synthesis of linked LDW639

The procedures that was not part of the final synthesis path is given in this section.

7.3.1 Purification of *tert*-butyloxycarbonyl protected linked drug

The first attempt of purifying the crude material gathered from the peptide coupling, third step of the synthesis, was done using an Armen Flashmaster by Armen Instruments (Saint-Ave,

France), with a 24 mm ID x 150 mm silica gel 60 flash column cartridge from Götec labortechnik GmbH (Bickenbach, Germany). The solvent used for elution was 5% MeOH in DCM. The flow was restricted to 4 bar, and UV-reactive fractions were collected following UV detection at 254 nm.

The fraction was then reanalyzed by TLC, and the product spot was found in fraction number 4 and 5. Fraction 4 also contained some starting reagent. ^{1}H-NMR of the crude material is given in **Figure 66** and that of fraction 5 is given in **Figure 67**. The purified product had a less assembly of peaks in the range from 2.7 to 4.4, and a contaminant disturbing the peaks at 7.4 and 8.0 form the benzene ring is not present. This contaminant was most probably a residue of hydrochloric LDW639 salt that was not coupled to the linker.

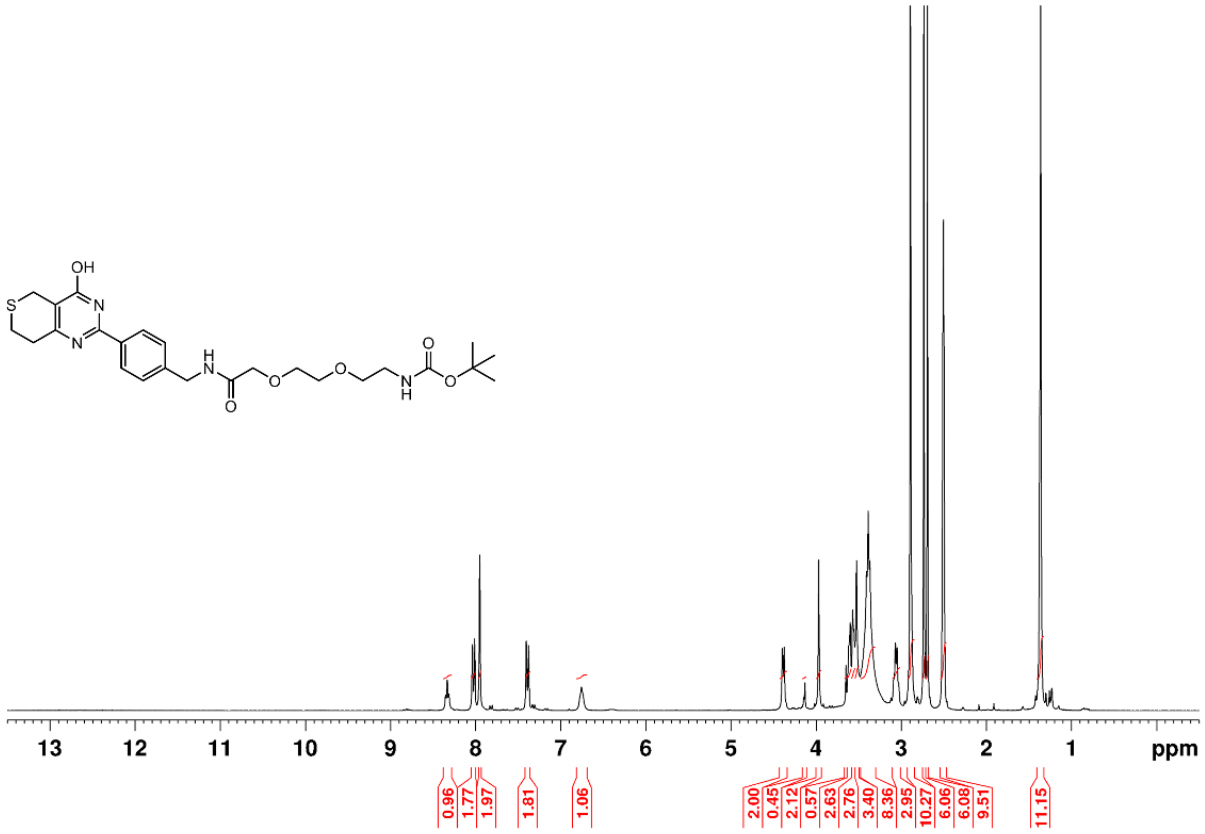

Figure 66: ^{1}H-NMR spectrum of crude material dissolved in DMSO-D^{6}, 16 scans on DPX300 (300 MHz).

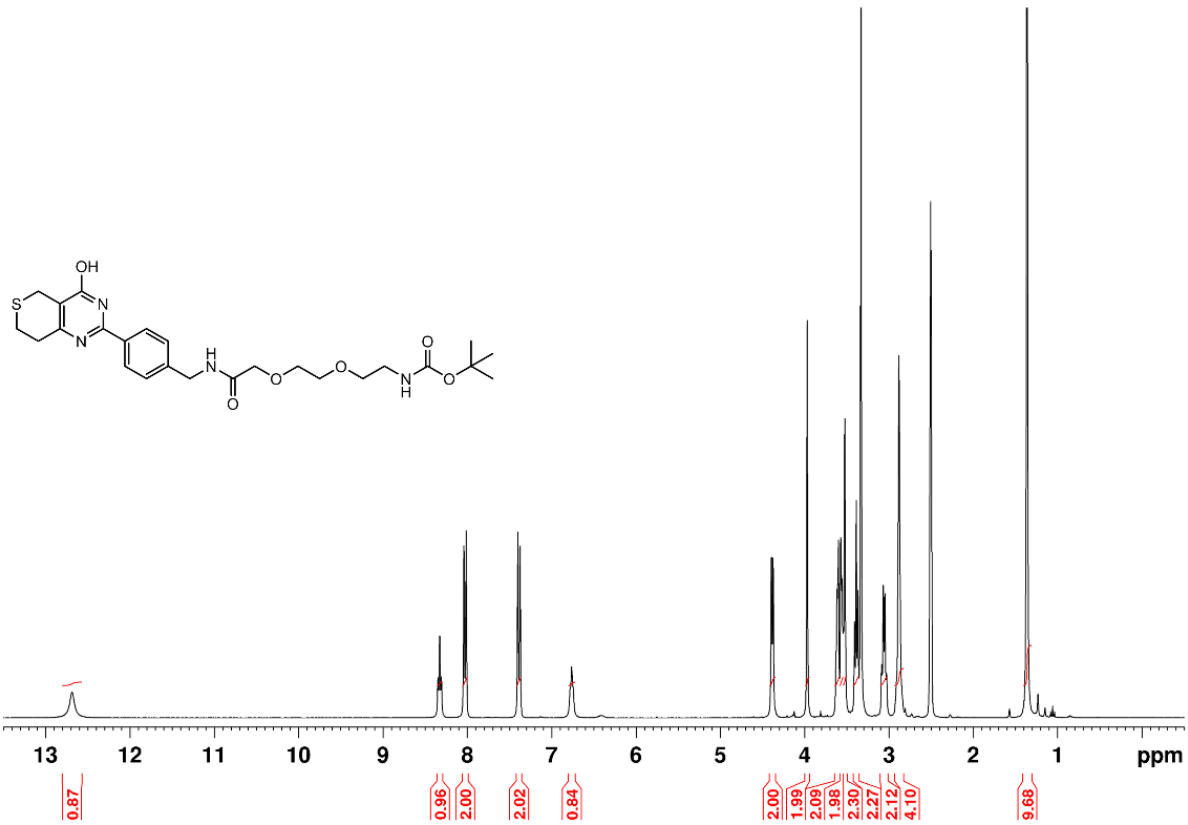

Figure 67: ^{1}H-NMR spectrum of purified material from Flashmaster dissolved in DMSO-D^{6}, 16 scans on DPX300 (300 MHz).

7.3.2 Extraction of free amine group of linked LDW639

To see if it was possible to achieve a free amino group instead of a hydrochloric salt of linked LDW639, 53 mg of this salt was attempted to be extracted with 3 times 20 mL DCM with 5 mL saturated NaCl premade by Christian Schnaars. Saturated NaCl was added to separate the water and organic phases more efficiently. The product was found in the organic phase by TLC testing, and 9 mg of product were collected after removal of solvent. The extraction yield was 18 %, and the entire sample was used to record the proton spectrum shown in **Figure 68**.

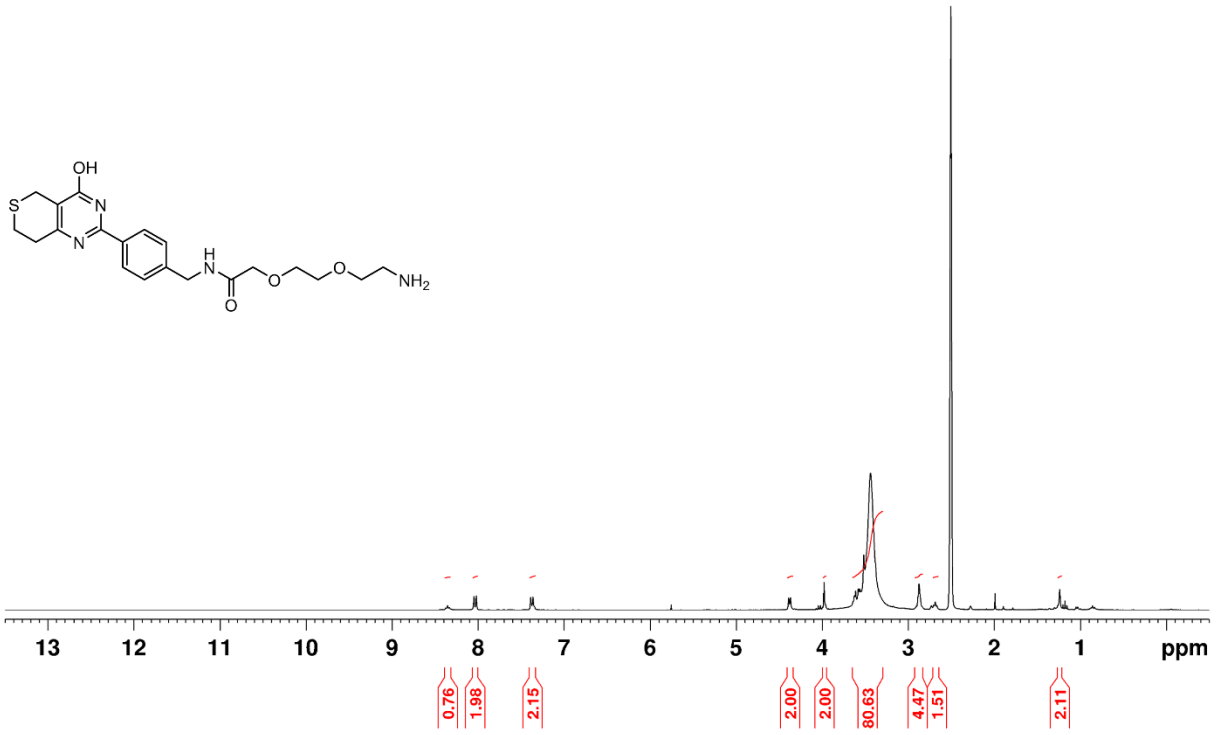

Figure 68: ^{1}H-NMR spectrum of free amine from extraction dissolved in DMSO-D^{6}, 16 scans on DPX300 (300 MHz).

7.4 Composition analysis

In this section, a short description of the MS settings used for composition analysis by Engineer Osamu Sekiguchi is given and the two analyses are presented. The MS spectra were obtained by ESI-MS in positive mode, with a scan range from *m/z* 50 to 1500. The voltage applied on the capillary was 3.5 kV. The data analysis was done using Bruker Compass DataAnalysis version 4.3.

Element analysis of purified BOC protected linked LDW639

The fifth fraction from the automatic flash was analysed, and the *m/z* values found are presented in **Table 17**, while data analysis of different formula compared to deviation from the exact mass is given in **Table 18**. The sample had a concentration of 1.8 mg/mL dissolved in MeOH. The monoisotopic mass of the intended structure, $C_{25}H_{34}N_4O_6S$, is 518.2191 Da.

Table 17: *m/z* values in the mass spectrum found by ESI-MS positive mode, scanning from *m/z* 50 to 1500. The relative intensities are given for each *m/z* value.

m/z	% Intensity	*m/z*	% Intensity	*m/z*	% Intensity
185.115	1.3	514.639	1.7	557.183	4.4
285.142	1.3	524.045	1.8	558.186	1.3
313.173	2.9	541.209	100.0	942.847	2.3
360.324	3.6	542.201	28.6	944.845	1.4
413.266	5.7	543.210	6.5	1006.289	2.3
414.270	1.5	544.210	1.5	1059.430	1.6
466.087	2.0	553.459	1.4		

Table 18: Comparison of possible composition formulas of the synthesis drug with the *m/z* value 541.2091.

Ion formula	*m/z*	Deviation [ppm]	Ion formula	*m/z*	Deviation [ppm]
$C_{23}H_{29}N_{10}O_4S$	541.2088	-0.5	$C_{30}H_{29}N_4O_6$	541.2082	-1.8
$C_{25}H_{34}N_4NaO_6S$	541.2091	0.0	$C_{31}H_{25}N_8O_2$	541.2095	0.7
$C_{26}H_{37}O_{10}S$	541.2102	2.0	$C_{33}H_{30}N_2NaO_4$	541.2098	1.2
$C_{24}H_{25}N_{14}S$	541.2102	1.9	$C_{31}H_{33}N_4OS_2$	541.2090	-0.2

Element analysis of hydrochloric linked LDW639 salt

The deprotected linked LDW639 was analysed and the *m/z* values found are presented in **Table 19**, while data analysis of different formula compared to deviation from the exact mass is given in **Table 20**. The sample had a concentration of 1.0 mg/mL dissolved in MeOH. The monoisotopic mass of the intended structure, $C_{20}H_{27}N_4O_4S$, is 419.1748 Da.

Table 19: *m/z* values in the mass spectrum found by ESI-MS positive mode, scanning from *m/z* 50 to 1500. The relative intensities are given for each *m/z* value.

m/z	% Intensity	*m/z*	% Intensity	*m/z*	% Intensity
107.041	100.0	242.955	2.6	420.178	20.2
109.037	5.0	274.101	4.1	421.173	4.5
120.987	4.4	360.324	6.9	441.157	50.2
133.003	4.8	408.309	3.3	442.160	11.6
164.921	3.6	413.266	12.8	443.155	2.6
178.107	4.8	414.270	3.5	553.459	3.5
185.115	2.6	419.175	86.9		

Table 20: Comparison of possible composition formulas of the synthesis drug with the *m/z* value 419.1748.

Ion formula	*m/z*	Deviation [ppm]	Ion formula	*m/z*	Deviation [ppm]
$C_{19}H_{24}N_8NaS$	419.1737	-2.6	$C_{23}H_{24}ClN_6$	419.1745	-0.5
$C_{20}H_{27}N_4O_4S$	419.1748	0.0	$C_{25}H_{29}ClNaO_2$	419.1748	0.2
$C_{15}H_{31}O_{13}$	419.1759	2.8	$C_{15}H_{28}ClN_8O_2S$	419.1739	-2.1
$C_{15}H_{32}N_4NaO_4S_2$	419.1757	2.3	$C_{18}H_{29}ClN_6NaS$	419.1755	1.8
$C_{28}H_{23}N_2O_2$	419.1754	1.5	$C_{17}H_{33}ClN_2NaO_4S$	419.1742	-1.4

7.5 Ultraviolet-visible absorbance measurements of immobilization solutions

The UV-vis measurements of immobilization solutions by both capillary cell and pedestal on nanodrop are presented in this section. The differences found between an immobilization solutions before and after flushing of a monolith was analysed by ANOVA, to determine if the absorbance was significant different or not.

7.5.1 Measurements by capillary cell on SpectraSystem

The measurements using a capillary cell for the immobilization solutions used to immobilize drug on three 250 µm ID monoliths are given in **Table 21** and visualized in **Figure 69**. For determination of significant difference in absorbance of the immobilization solution before and after flushing in a monolith, single factor ANOVA was calculated using EXCEL. The findings are given in **Table 22**, and it is clear that $F_{crit} < F$ meaning that UV-Vis absorbance at 254 nm of the immobilization solution before and after flushing a monolith are not significantly different.

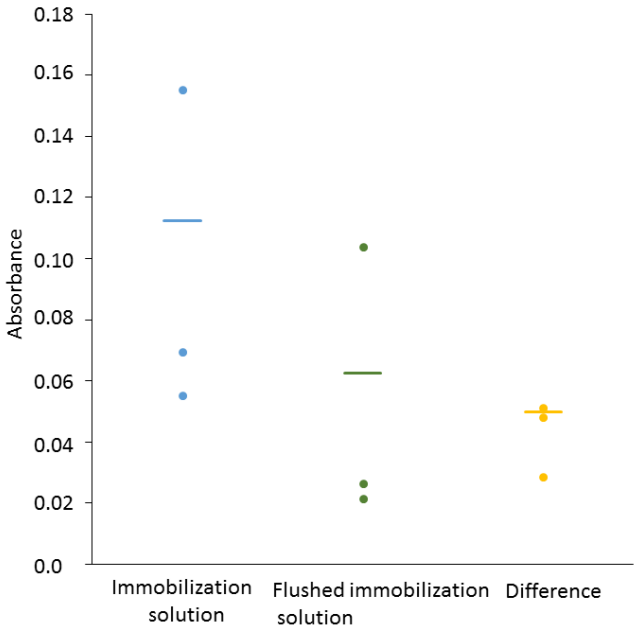

Figure 69: The absorbance at 254 nm by "Immobilization solution" (blue): 0.25 mg/mL drug dissolved in 50 mM phosphate buffer (pH 7.2), "Flushed immobilization solution" (green) the same solution after flushing through a monolith, and the difference (yellow). Three replicates have been reported, and the bars represent the averages. Corrected for attribution from 50 mM phosphate buffer.

Table 21: Measured absorbance at 254 nm of: "Immobilization solution": 0.25 mg/mL drug dissolved in 50 mM phosphate buffer (pH 7.2), and "Flushed immobilization solution" the same solution after flushing through a 14 cm, 250 µM ID EDMA-co-VDM monolith. Corrected for attribution from 50 mM phosphate buffer. For each monolith replicate, three measuring replicates were carried out.

Monolith replicate	Immobilization solution	Flushed immobilization solution
#1	0.16	0.10
#2	0.07	0.02
#3	0.06	0.03
Average	0.11	0.06
STD	0.05_7	0.04_5
%STD	52%	75%

Table 22: Single factor ANOVA test of absorbance of UV-Vis from 0.25 mg/mL immobilization solution before and after flushing through a monolith. The test established the total standard deviation, and the variance within same solution and between the two solutions. By an F-test, the test determines if the two solutions are significantly different from each other, this is the case when $F > F_{crit.}$

Groups	*Count*	*Sum*	*Average*	*Variance*
Immobilization solution	3	0.28	0.093	0.003
Flushed immobilization solution	3	0.15	0.051	0.002

ANOVA

Source of Variation	*SS*	*df*	*MS*	*F*	*P-value*	*F crit*
Between Groups	0.003	1	0.002_7	1.1	0.36	7.7
Within Groups	0.010	4	0.002_5			
Total	0.013	5				

7.5.2 Measurements by nanodrop

The UV-Vis absorbance measurements of the immobilization solutions used to immobilize drug on five 250 µm ID monoliths are shown in **Table 23** and **Table 25** for 243 nm and 285 nm, respectively. For determination of possible significant difference in absorbance of immobilization before and after flushing in a monolith, single factor ANOVA was calculated using EXCEL. The findings are given in **Table 24** for 243 nm and for 285 nm in **Table 26**.

Table 23: Measured absorbance at 243 nm of: "Immobilization solution": 0.25 mg/mL drug dissolved in 50 mM phosphate buffer (pH 7.2), and "Flushed immobilization solution" the same solution after flushing through a 14 cm, 250 µM ID EDMA-co-VDM monolith. Corrected for 50 mM phosphate buffer absorbance by blank. For each monolith replicate, three measuring replicates were carried out.

Wavelength 243 nm	**Immobilization solution**	**Flushed immobilization solution**
Monolith 1	0.649	0.569
Monolith 2	0.635	0.562
Monolith 3	0.662	0.589
Monolith 4	0.653	0.578
Monolith 5	0.643	0.593
Average	0.649	0.58
STD	0.01	0.01
%STD	1.6%	2.2%

Table 24: Single factor ANOVA test of absorbance of UV-Vis at 243 nm from 0.25 mg/mL immobilization solution before and after flushing through a monolith. The test established the total standard deviation, and the variance within same solution and between the two solutions. By an F-test, the test determines if the two solutions are significantly different from each other, this is the case when $F > F_{crit}$.

Groups	*Count*	*Sum*	*Average*	*Variance*
Immobilization solution	5	3.24	0.65	1.0E-04
Flushed immobilization solution	5	2.89	0.58	1.7E-04

ANOVA

Source of Variation	*SS*	*df*	*MS*	*F*	*P-value*	*F crit*
Between Groups	0.012	1	0.012	91.7	1.2E.05	5.3
Within Groups	0.001	8	1.3E-04			
Total	0.013	9				

Table 25: Measured absorbance at 285 nm of: "Immobilization solution": 0.25 mg/mL drug dissolved in 50 mM phosphate buffer (pH 7.2), and "Flushed immobilization solution" the same solution after flushing through a 14 cm, 250 µM ID EDMA-co-VDM monolith. Corrected for 50 mM phosphate buffer absorbance by blank. For each monolith replicate, three measuring replicates were carried out.

Wavelength 285 nm	Immobilization solution	Flushed immobilization solution
Monolith 1	0.471	0.413
Monolith 2	0.461	0.408
Monolith 3	0.482	0.429
Monolith 4	0.478	0.422
Monolith 5	0.468	0.432
Average	0.472	0.421
STD	0.008	0.01
%STD	1.8%	2.4%

Table 26: Single factor ANOVA test of absorbance of UV-Vis at 285 nm from 0.25 mg/mL immobilization solution before and after flushing through a monolith. The test established the total standard deviation, and the variance within same solution and between the two solutions. By an F-test, the test determines if the two solutions are significantly different from each other, this is the case when $F > F_{crit}$.

Groups	*Count*	*Sum*	*Average*	*Variance*
Immobilization solution	5	2.36	0.47	6.9E-05
Flushed immobilization solution	5	2.10	0.42	1.0E-04

ANOVA

Source of Variation	*SS*	*df*	*MS*	*F*	*P-value*	*F crit*
Between Groups	0.007	1	0.0066	76.8	2.25E.05	5.3
Within Groups	0.0007	8	8.6E-05			
Total	0.007	9				

7.6 Adopting liquid chromatography mass spectrometry method for tankyrase 2 measurement

Initially the CRAM reactors was evaluated for trapping of recombinant TNKS2 by measuring TNKS2 with LC-MS. This was done to find a suitable elution solution for TNKS2 trapped on the CRAM reactors. The first comparison of the trapping potential of the CRAM reactors and a monolith not immobilized with drugs, was also evaluated by LC-MS.

Concerning the recombinant TNKS2, the protein was a shorter version of the native TNKS2, expressed by the amino acids sequence from 667 to 1166 missing the first 666 amino acids compared to the native TNKS2. Due to this reduced length, it is not certain that it has the identical characteristics and behavior as native TNKS2.

7.6.1 Preliminary search for elution solution to elute trapped tankyrase 2 on CRAM reactor

A preliminary experiment using a single CRAM reactor to find a suitable elution solution for TNKS2 after it was trapped on the reactor was carried out as described in **Experimental 2.9**, with the following specifics: The solution consisting of 0.028 mg/mL recombinant TNKS2 was dissolved in 50 mM ammonium acetate. The washing steps with 50 mM ammonium acetate (*i.e.* the fractions called Wash1 and Wash2) were not executed. For elution of TNKS2, all of the elution solutions mentioned in **Experimental 2.9**, **Table 1** was flushed through the CRAM reactor and collected, no washing step was executed in between elution. The CRAM reactor was immobilized by the linked LDW639 in a solution with a concentration of 0.25 mg/mL.

After collection, the samples were digested with trypsin as described in **Experimental 2.12.2**(In-solution digestion of proteins), and at the end of the procedure the samples were resolved in 15 µL 0.1% FA in HPLC-grade water. The samples was measured by LC-MS, and it was observed that salts gathered on the emitter and that the backpressure on the system increased. A pre-made trypsinated HSA sample from PhD candidate Henriette Engen Berg was measured by LC-MS to check if there were any other problems, the measurement of HSA proceeded without problems. The correlation scores and percentage coverage of the TNKS2 flush on the CRAM reactor and the trypsinated HSA sample are shown in **Table 27**. The samples were therefore desalted by Zip-tip prior to another injection, and the HSA sample was adopted as a control for loss of peptides during desalting procedure described in **Experimental 2.12.2**(Desalting of peptide sample). The correlation scores and percentage coverage of the desalted samples are shown in **Table 28**.

From the correlation score and percentage coverage of TNKS and HSA, in the samples before and after desalting by Zip-tip, it is clear that the LC-MS system shows some carry over of proteins. An indication of carry over is that the TNKS2 sample in **Table 27** shows a score of 4.6 and 35.6 % coverage of HSA, even though HSA was not part of the sample preparation in this experiment. Also, the HSA control showed a 36.6% coverage of TNKS2. The score of TNKS2 was reduced from 37.7 prior to desalting, to a score of 25.0 after desalting, meaning the concentration of TNKS2 correlating peptides in the samples had been reduced due to the Zip-tip procedure. The concentration of the TNKS2 sample was not further diluted during desalting procedure, as the volume before and after desalting was 10 µL. However, a

contradicting observation was that the HSA sample showed a higher coverage and score after desalting compared to before desalting.

The HSA sample was the first to be introduced into the LC-MS system, and the LC-MS system had been washed after the previous injection of samples consisting of TNKS2 had been analysed (making carry over from old samples highly unlikely). As it is difficult to pin-point the carry over to the LC-MS system, the desalting by Zip-tip may give an explanation for the presence of TNKS2 in the HSA sample. The entire procedure for all of the samples was completed with a single Zip-tip, and the last samples to be desalted was the HSA sample. Besides human error, it is quite probable that peptides belonging to TNKS2 was transferred from the Zip-tip to the HSA sample. Based on this it is important for later sample preparation by Zip-tip, that Zip-tips are used only one time for one sample.

The purpose of this experiment was to find a possible elution solvent for trapped TNKS2 from the CRAM reactor. Two solutions appeared to be most promising: 10% ACN and 0.1 M NaOH, showing scores of 1.89 and 2.19, respectively. However, as the following solvents consisted of 20% to 50% ACN and did not have scores above 0 for TNKS2, the actual elution potential of 10% ACN was unclear. Most probably, as 10% ACN was the first solvent flushed through the CRAM reactor after the TNKS2 solution was applied, the findings of TNKS2 was due to residual TNKS2 being washed out of the reactor (not trapped TNKS2). Another explanation of the findings of TNKS2 in 10% ACN was that this sample was desalted following Tankyrase2 Flush, meaning TNKS2 most probably also has been transferred to the sample by the Zip-Tip. The elution with 0.1 M NaOH showed an elution of TNKS2, but it is also uncertain if this is only due to transfer of TNKS2 from the Zip-tip procedure.

The adopted LC-MS method was successful at measuring and detecting TNKS2 in concentration ranges below 0.028 mg/mL. As desalting was executed with only one Zip-tip for all of the samples, it is difficult to conclude which elution solution showed the highest potential for eluting TNKS2. However, as 0.1 M NaOH showed a score of TNKS2 this was selected for further testing.

Table 27: The correlation score and the percentage coverage of TNKS2 and HSA found in flush of TNKS2 on CRAM reactor and pre-digested HSA control prior to Zip-tip.

Description of sample	Score of HSA	%Coverage of HSA	Score of TNKS2	%Coverage of TNKS2
Tankyrase2 Flush	4.6	35.6	37.7	32.2
Trypsinated HSA	2582.6	80.8	0	36.6

Table 28: The correlation score and the percentage coverage of TNKS2 and HSA found in samples, shown in the first column, all samples were collected from a CRAM reactor except from the sample called Trypsinated HSA.

Description of sample	Score of HSA	%Coverage of HSA	Score of TNKS2	%Coverage of TNKS2
Trypsinated HSA	3238.8	93.6	0	35.0
Blank	980.8	86.4	0	33.4
Tankyrase2 Flush	175.8	75.2	25.0	36.6
Blank1	328.9	83.7	0	31.0
Elution 10%ACN	169.4	80.0	1.9	32.0
Blank2	180.8	80.1	Not present	Not present
Elution 20%ACN	138.4	66.0	Not present	Not present
Blank3	113.0	77.8	0	15.8
Elution 30%ACN	101.9	79.6	0	25.0
Blank4	72.5	71.1	0	21.2
Elution 40%ACN	60.1	68.1	0	33.6
Blank5	48.0	72.2	0	15.4
Elution 50%ACN	44.3	71.8	0	32.2
Blank6	43.6	67.8	0	8.0
Elution 0,1M NaOH	25.3	65.4	2.2	31.8
Blank7	43.1	64.7	Not present	Not present
Elution 0,1M NaOH 30%ACN	38.7	71.3	0	32.0
Blank8	30.4	67.6	0	11.0
Elution 0,3M NaOH	30.2	63.0	0	32.8
Blank9	23.3	70.1	0	5.8
Elution (4/96, v/v) isopropanol/AmAc	39.0	67.8	Not present	Not present
Blank10	45.0	63.9	0	7.4

7.6.2 Preliminary experiment for selective elution of tankyrase 2 in a mixture with cytochrome C and myoglobin

To see if the reactors could differentiate between TNKS2, cytochrome C and myoglobin a preliminary experiment using two CRAM reactors and a monolith without immobilized drugs was carried out as described in **Experimental 2.9**, with the following specifics: The solution consisting of 0.035 mg/mL recombinant TNKS2, cytochrome C and myoglobin was dissolved in 50 mM ammonium acetate. For elution of TNKS2 from CRAM reactor number 1 0.1 M NaOH was used and from CRAM reactor number 2 isopropanol/AmAc (4/96, *v/v*) was used.

The CRAM reactors were immobilized by the linked LDW639 in a solution with a concentration of 0.25 mg/mL. The monolith that was not immobilized with linked LWD639, was flushed with 50 mM phosphate buffer. The elution fractions collected from the monolith was a 0.1 M NaOH solution followed by a wash of 50 mM ammonium acetate and then elution with isopropanol/AmAc (4/96,v/v). The collected fractions were prepared for LC-MS measurement by the procedure described in **Experimental 2.12.2**. For control of the trypsination, two samples of HSA were used. The correlation scores of the proteins are shown in **Table 29**, and the percentage coverage are shown in **Table 30**.

Only one monolith was used in this experiment, as a consequence of a shortage of VDM. For comparison of the two elution solutions, it would have been optimal to have two monolith that was subjected to elution solution in the same manner as their counterpart CRAM reactor.

The conclusion from the previous experiment that each sample should be desalted by a single use Zip-tip was discovered after this experiment. Meaning all of the sample in this experiment was also desalted by the same Zip-tip, and as a consequence only the percentage coverage and correlation score of the TNKS2 Flush on the CRAM reactors and the monolith was assessed. Comparison of the CRAM reactors with the monolith showed that the fractions collected from the monolith had lower coverage and score for TNKS2 than the CRAM reactors, indicating that the monolith exhibited some secondary interactions towards the protein. Due to the high percentage coverage of TNKS2 in the Flush collected for both CRAM reactors, it was assumed that dissolving TNKS2 in 50 mM AmAc reduced the binding of TNKS2 to the immobilized drug.

As the monolith used as CRAM reactors (immobilized or not) contains VDM, it is probable that the proteins have undergone covalent binding to VDM as proteins contains reactive groups (NH_2, OH and SH groups). To be able to assess the CRAM reactor ability of trapping TNKS2 based on bonding with the immobilize drug, the secondary interactions due to the monolith needed to be resolved.

As the monoliths displayed secondary interactions with proteins, a modification of the EDMA-co-VDM monolith need to be examined to reduce interactions with proteins. A solution of 50 mM AmAc was presumed to reduce the binding between TNKS2 and immobilized drug, and was selected for further examinations as a possible elution solution for trapped TNKS2 on the CRAM reactors.

Table 29: The correlation score of HSA, TNKS2, cytochrome C and myoglobin found in the samples, type of sample is described in the first column.

Description of sample	HSA	TNKS2	Cytochrome C	Myoglobin
3µg HSA	1784.3	17.2	0	96.0
Blank	66.2	Not present	0	Not present
0,7µg HSA	1793.5	4.9	0	Not present
Blank	176.9	0	0	Not present
Protein mix control	4.6	227.0	277.3	527.4
Blank	64.0	4.2	2.7	64.3
Flush CRAM reactor 1	0	78.9	29.4	441.8
Blank	22.9	0	3.7	29.4
Wash 1	120.1	22.1	46.5	220.6
Blank	11.2	0	0	7.9
Wash 2	116.3	15.4	115.5	90.3
Blank	1.9	0	0	0
Elution 0.1 M NaOH	5.7	9.8	160.6	61.3
Blank	9.6	0	0	0
Flush CRAM reactor 2	80.3	146.5	121.3	386.5
Blank	32.0	0	0	10.8
Wash 1	49.3	167.1	159.1	311.0
Blank	26.9	0	0	11.6
Wash 2	44.3	37.2	118.7	107.3
Blank	20.4	0	0	0
Elution (4/96, v/v) isopropanol/AmAc	18.7	7.3	119.2	94.9
Blank	7.3	0	0	0
Flush monolith 1	Not present	33.2	47.0	215.7
Blank	8.6	0	0	0
Wash 1	19.7	25.1	59.4	175.2
Blank	3.9	0	0	0
Wash 2	8.7	53.8	74.4	93.2
Blank	11.1	Not present	14.3	54.6
Elution 0.1 M NaOH	10.0	45.4	177.2	63.2
Blank	2.1	0	0	0
Wash 3	Not present	1.9	48.9	6.0
Blank	4.2	Not present	0	0
Elution (4/96, v/v) isopropanol/AmAc	9.6	0	21.0	9.7
Blank	2.2	0	0	0

Table 30: The coverage percentage of HSA, TNKS2, cytochrome C and myoglobin found in the samples, type of sample is described in the first column.

Description of sample	%HSA	%TNKS2	%Cytochrome C	%Myoglobin
3µg HSA	95.7	52.2	64.8	85.1
Blank	83.2	Not present	60.0	Not present
0,7µg HSA	95.2	48.4	46.7	Not present
Blank	81.1	11.6	43.8	Not present
Protein mix control	48.8	69.2	71.4	85.1
Blank	85.4	57.0	70.5	75.4
Flush CRAM reactor 1	51.7	65.8	75.2	87.0
Blank	71.1	45.8	60.9	85.1
Wash 1	77.7	41.0	86.7	89.0
Blank	83.1	30.2	58.1	81.2
Wash 2	64.9	47.0	77.1	74.7
Blank	56.7	31.2	64.8	70.8
Elution 0.1 M NaOH	25.0	28.0	80.9	87.7
Blank	51.2	17.8	36.2	48.0
Flush CRAM reactor 2	44.3	57.8	82.9	100.0
Blank	62.4	54.6	60.9	83.1
Wash 1	53.2	68.2	94.3	89.0
Blank	57.0	41.8	36.2	87.0
Wash 2	51.6	38.0	79.0	77.3
Blank	42.0	15.8	54.3	70.1
Elution (4/96, v/v) isopropanol/AmAc	47.6	35.2	77.1	74.0
Blank	29.7	11.0	28.6	47.4
Flush monolith 1	Not present	41.0	71.4	100.0
Blank	36.0	12.4	27.6	81.2
Wash 1	47.8	53.2	59.0	89.0
Blank	40.7	10.2	49.5	48.0
Wash 2	43.8	36.8	60.9	79.2
Blank	39.2	Not present	0	55.5
Elution 0.1 M NaOH	41.9	37.0	93.3	77.9
Blank	26.1	6.8	40.0	50.0
Wash 3	Not present	31.4	60.9	75.3
Blank	25.6	Not present	40.0	29.9
Elution (4/96, v/v) isopropanol/AmAc	52.9	29.0	80.9	54.6
Blank	35.6	2.8	46.7	9.7

7.7 Detection of recombinant tankyrase 2 by western blot

Another method for detection of TNKS2 was needed, as during the study the Q-Exactive MS was not operational due to technical issues. The assessment of the trapping ability of the CRAM reactor and a monolith was repeated using WB as detection. The experiment was repeated as both the detection system and the set-up for application of TNKS2 on the reactor was replaced.

Two CRAM reactors and one monolith were applied 0.7 µg TNKS2 using the procedure described in **Experimental 2.10**. The manual application system (**Experimental 2.9**) was replaced with the semi-automatic application set-up as it was easier, faster and offered a more similar application of TNKS2 on the reactors. TNKS2 was dissolved in HPLC-grade water instead of 50 mM ammonium acetate in this experiment. The reason for the change of solvent was the suspicion that salt disrupt the interaction between LDW639 and TNKS2. The CRAM reactors had been immobilized with 0.25 mg/mL drug, and the monolith was "fake-immobilized" by flushing with storage solution 50 mM phosphate buffer. The elution step was completed with isopropanol/AmAc (4/96, *v/v*), solution "**#a**" in **Experimental 2.10**, **Table 2**. In addition, a control consisting of 0.7 µg of TNKS2 standard was used.

The procedure described for WB in **Experimental 2.11** was followed with the following deviations: An LDS loading buffer was used, and the samples were heated at 92 °C for 2.5 min after addition of loading buffer in a pre-heated GC-oven. For the gel electrophoresis a 4-12% bis-tris gel and MOPS running buffer were used. The primary antibody dilution of mouse-antiTNKS1/2 was a factor of 1:1000. A loading control was not run for this experiment as only recombinant TNKS2 was present in the standard.

For the recombinant TNKS2, WB was expected to show a single band for TNKS2 at approx. $8x10^4$ g/mol (80 kDa). However, the bands from the control and flush of TNKS2 from the two CRAM reactors and the monolith in **Figure 70** revealed problems with the quality of the standard. The band at $1.4x10^5$ g/mol (140 kDa) can be due to dimer formation and the two bands at $4x10^4$ g/mol (40 kDa) can be due to degradation of the protein. If this occurred during sample preparation or if it has been this way since the purchased vial was opened is impossible to say. The additional samples from each CRAM reactor and the monolith (*i.e.* two collected wash fractions and one elution fraction) did not show any visible bands after 2000 s exposure,

Appendix 7.10, **Figure 79 (to the right)**, when visualizing with the lanes of the control and the TNKS2 flushes covered.

As the lanes were visualized at the same time, the intensity of the bands are proportional to the amount of TNKS2 present. That the band in the lane of the flushed TNKS2 collected from the monolith is weaker than the band in the lane of the control adds to the suspicion that the EDMA-co-VDM monolith displays secondary interactions towards TNKS2.

Another question which arose as a consequence of the questionable quality of the standard of TNKS2 was whether or not the TNKS2 trapping capability of the CRAM reactors was affected. To be able to assess the trapping capability of the CRAM reactors a purer TNKS2 should be used.

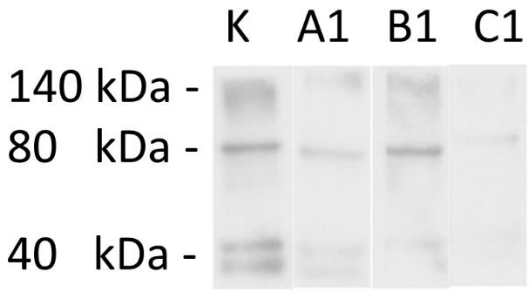

Figure 70: Western blot of tankyrase 2 standard. The gel was loaded with 0.7 µg pure standard in lane K. Lane A1 and B1 are collected fractions after 0.7 µg of standard flushed through a 14 cm, 250 µm ID monolith with immobilized drug. Lane C1 are a collected fraction after 0.7 µg of standard flushed through a 14 cm, 250 µm ID monolith not immobilized with drug. Exposure time was 1 s. The primary antibody anti-TNKS1/2 had a dilution factor of 1/1000 and the secondary antibody donkey anti-mouse a dilution factor of 1/5000. Raw file are given in Appendix 7.10, Figure 79.

TNKS2 was detected in the flush from both CRAM reactors and the monolith, the weaker signal of TNKS2 flush from the monolith compared to the control increased the suspicion of secondary interactions on the EDMA-co-VDM monolith. For further assessment of the CRAM reactors, a purer TNKS2 should be used.

7.8 Detection of tankyrases 1 and 2 from cell lysate applied on CRAM reactors by western blot

Based on the previous chapter, the source of TNKSs was replaced by HEK293 and HEK293-EGFP-TNKS1 cells. The HEK-EGFP-TNKS1 cell line was a regular HEK293 cell line treated with a fusion protein to stabilize and overexpress TNKS1, giving a higher concentration of TNKS1 in the cells compared to the regular HEK293 cell line. By using cells as the source of

tankyrase, the proteins needed to be extracted by cell lysis. Additionally, the WB procedure needed to be optimized for detection of full-length TNKS2 and TNKS1. WB was expected to show a band of TNKS1 at $1.3x10^5$ g/mol (130 kDa), while a band for TNKS2 was expected at $1.1x10^5$ g/mol (110 kDa).

The initial WB procedure used for the recombinant TNKS2 (previous chapter) is summarized in **Figure 71**, showing which points of the procedure that would be adjusted during the optimization. The first change made to the procedure was utilizing actin as a loading control (point 1 in **Figure 71**). A loading control was used to be certain that cell lysate had been applied on the CRAM reactors, and also to confirm that loading of the gel and blotting from gel to membrane occurred without problems. Actin was expected to have a band at $4.2x10^4$ g/mol (42 kDa).

WB was in all the following experiments used as a detection of TNKS1/2 to assess whether or not a CRAM reactor could trap TNKS1/2, and release TNKS1/2 after trapping by a suitable elution solution.

1. No loading control.
2. LDS loading buffer.
3. Samples heated at 92 °C for 2.5 min.
4. 4-12% bis-tris gel.
5. MOPS running buffer.
6. Primary antibody mouse-antiTNKS1/2 dilution factor 1:1000.

Figure 71: Overview of the initial WB procedure that would be exchanged during WB for full length TNKS1/2 from cell lysate.

First attempt at detection of tankyrase by western blot

For the first attempt at detecting full-length TNKS1/2 from cell lysate, the cell lysis was executed with ultrasonication in the presence of urea and ABC buffer. The ultrasonication procedure was based on the bachelor project by Master's student Binish Arshad at the Bioanalytical Chemistry research group. The total amount of proteins extracted from the approx. 1 million HEK293 and HEK293-EGFP-TNKS1 cells is given in **Table 31**. The purpose of the first WB examination was to get an indication at which amount of cell lysate TNKS1/2 was detectable by WB. Three replicates of 9 µg, 6 µg, 3 µg and 1.5 µg of total amount of protein were examined and presented in **Figure 72**.

Form the visualization, TNKS1/2 appears smeared in the lanes of 9 µg protein and 6 µg protein, and not detectable at 3 µg protein or below. Actin was detectable at 1.5 µg protein in one replicate, but was not detected in one of the replicates consisting of 9 µg protein. Due to actin not being detected in all samples, it was assumed that denaturation by the loading buffer was insufficient.

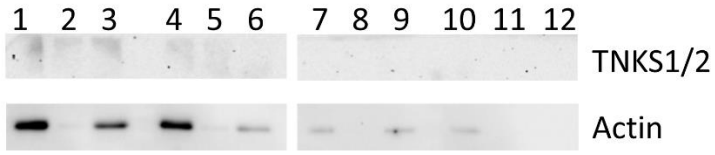

Figure 72: Western blot of: (1-3) lane of 9 µg protein from HEK293, (4-6) lane of 6 µg protein from HEK293, (7-9) lane of 3 µg protein from HEK293, (10-12) lane of 9 µg protein from HEK293. The raw file from WB is given in Appendix 7.10, Figure 80. The exposure time was 3600 s for TNKS1/2 and 150 s for actin.

Changes made to the WB procedure based on the first attempt

As a consequence of the suspicion that the denaturation by the loading buffer was insufficient, the loading buffer was replaced by an in-house buffer belonging to the Unit of Cell Signaling. The procedure of heating the samples after addition of loading buffer was executed at 70 °C for 10 min, (point 2 and 3 in **Figure 71**).

As the bands of TNKS1/2 appeared smeared in the first attempt at detection by WB, the 4-12% bis-tris gel and the MOPS running buffer (point 4 and 5 in **Figure 71**) was replaced by a 3-8% tris acetate gel and a tris acetate running buffer. By exchanging the gel and the running buffer, a better separation is achieved around the expected range of TNKS1/2, this is shown by the protein ladder in **Appendix 7.10**, **Figure 78**.

The last change to the WB procedure was an increase in the dilution factor of primary antibody for TNKS1/2 from 1:1000 to 1:250, to achieve a higher coverage of TNKS1/2 present on the membrane, (point 6 in **Figure 71**).

In addition to changes in the WB method, cell lysis was completed with ultrasonication with the cells dissolved in water and the total amount of protein extracted is given in **Table 31**. The urea and ABC buffer was removed from the procedure as this cell lysate was planned to be applied on CRAM reactors, and based on the assessment of the CRAM reactor by LC-MS (**Appendix 7.6.2)**, salt disrupts the interaction between LDW639 and TNKS2. Additionally,

ultrasonication with water extracted over 2 times the amount protein from both HEK293 cells and HEK293-EGFP-TNKS1 cells.

In addition to the changes made to the WB procedure, a comparison of the trapping of TNKS1/2 and elution by 50 mM AmAc solution from three types of reactors was carried out. One CRAM reactor (immobilized with 0.25 mg/mL immobilization solution), a CRAM reactor flushed with MEA and one MEA monolith.

From visualization in **Figure *73***, *the bands of TNKS1/2 in cell lysate from both HEK293 and HEK293-EGFP-TNKS1 appears smeared, and only the Wash 1 from the CRAM reactor flushed with MEA shows a smeared band of TNKS1/2. No eluate from the CRAM reactor, the MEA monolith or the CRAM reactor flushed with MEA contained TNKS1/2 detectable by WB.*

The CRAM reactor once again showed an interaction with proteins besides TNKS1/2, actin was not detected in the flush of cell lysate collected of the CRAM reactor. The interactions do not appear to be of a covalent nature, as actin is present in the first wash with water.

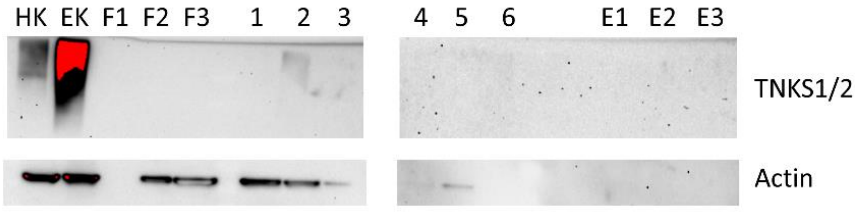

Figure 73: Western blot of: (HK) lane of 30 µg protein from HEK293 and (EK) lane of 30 µg protein from HEK293-EGFP-TNKS1. Samples collected from CRAM reactor: (F1) Flush of 54 µg protein from HEK293, (1) Wash 1 with water, (4) Wash 2 with water and (E1) eluted with 50 mM AmAc. Samples collected from MEA reactor: (F2) Flush of 54 µg protein from HEK293, (2) Wash 1 with water, (5) Wash 2 with water and (E2) eluted with 50 mM AmAc. Samples collected from CRAM reactor flushed with MEA: (F3) Flush of 54 µg protein from HEK293, (3) Wash 1 with water, (6) Wash 2 with water and (E3) eluted with 50 mM AmAc. The raw file from WB is given in Appendix 7.10, Figure 81 and Figure 82. The exposure time for TNKS1/2 (was 1800 s on the membrane to the left, and 3600 s to the left) and 320 s for actin on both membranes.

Changing the elution solution

In the following attempt of detecting TNKS1/2 by WB, a new range of elution solutions was examined for the possibility of eluting trapped TNKS1/2. The examined solutions was "**#b**" to "**#f**" in **Experimental 2.10**, **Table 2** (50 mM AmAc, 200 mM AmAc, 500 mM AmAc and 1 M AmAc and 2% FA).

The reactors used in the previous attempt was eluted with 1 M AmAc and 2% FA. In addition, a new CRAM reactor was prepared with a 5 mg/mL immobilization solution. The

immobilization solution was increased from 0.25 mg/mL to 5 mg/mL to achieve a higher coverage of the VDM groups on the monolith, as described in **Chapter 3.5**. The new CRAM reactor was applied 70 µg protein from HEK293 cell lysate.

*From visualization in **Figure 74**, no lane displayed a band for TNKS1/2, and only the cell lysate of HEK293 and the Flush from the new CRAM reactor showed a band of actin. That actin was present in the Flush of the new CRAM reactor and not in the subsequent fractions indicated that increasing the concentration of drug in the immobilization solution was successful in reducing secondary interactions. The following CRAM reactors were prepared with a 5 mg/mL immobilization solution. The reason why TNKS1/2 was not present in any of the eluates were difficult to answer, but a suspicion was that the method for cell lysis did not give free native TNKS1/2 in the solution.*

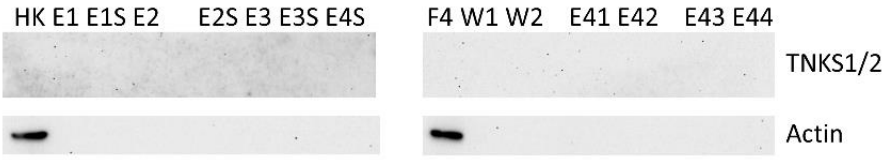

Figure 74: Western blot of: (HK) lane of 30 µg protein from HEK293. Elutes collected from CRAM reactor: (E1) eluted with 1 M AmAc and (E1S) 2% FA. Elutes collected from MEA reactor: (E2) eluted with 1 M AmAc and (E2S) 2% FA. Elutes collected from CRAM reactor flushed with MEA: (E3) eluted with 1 M AmAc and (E3S) 2% FA. Samples collected from new CRAM reactor (5 mg/mL immobilization solution): (F4) Flush of 70 µg protein from HEK293, (W1) Wash 1 with water, (W2) Wash 2 with water and (E41) eluted with 50 mM AmAc, (E42) eluted with 200 mM AmAc (E43) eluted with 500 mM AmAc (E44) eluted with 1 M AmAc (E4S) eluted with 2% FA. The raw file from WB is given in Appendix 7.10, Figure 83 and Figure 84. The exposure time was 2400 s for TNKS1/2 and 600 s for actin.

Introducing a positive control for tankyrases 1 and 2

A positive control for TNKS1/2 was received from Dr. Nina Therese Solberg. This control consisted of HEK293 cells treated with Wnt-inhibitor 007-LK, which causes TNKS1/2 to be stabilized during cell lysis. This control was used to assess if the smeared bands of TNKS1/2 was a due to the cell lysis method or the WB procedure, or if the issue was due to the antibodies for TNKS1/2. The 007-LK control was expected to have a band for TNKS1 and a band for TNKS2.

Another control treated with DMSO was also received, and by comparison to the 007-LK this would display weaker bands of TNKS1/2. Cell lysis had been executed using RIPA buffer by Dr. Nina Therese Solberg.

Additionally, a CRAM reactor was assessed for trapping of TNKS1/2 by applying cell lysate of HEK293-EGFP-TNKS1 (contains larger amounts of TNKS1 than regular HEK293). A total of 85 µ of protein was applied over two injections of 20 µL of cell lysate.

*From visualization in **Figure 75**, both positive controls (007-LK and DMSO) showed bands of TNKS1/2. For cell lysate of HEK293-EGFP-TNKS1 the band of TNKS1/2 was still smeared, and TNKS1/2 was not present in any of the fractions collected from the CRAM reactor. Another method for cell lysis needed to be examined to see if bands without smear could be obtained.*

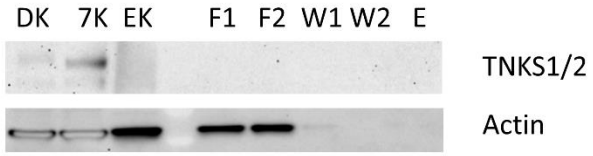

Figure 75: Western blot of: (DK) lane of 21 µg of protein from DMSO control, (7K) lane of 21 µg of protein from 007-LK control, and (EK) lane of 30 µg protein from HEK293-EGFP-TNKS1. Samples collected from CRAM reactor: (F1) Flush of 42.5 µg protein from HEK293, (F2) Flush of 42.5 µg protein from HEK293, (W1) Wash 1 with water, (W2) Wash 2 with water and (E) eluted with 2% FA. The raw file from WB is given in Appendix 7.10, Figure 85. The exposure time was 4500 s for TNKS1/2 and 600 s for actin.

Cell lysis by non-denaturing buffer

In the following experiment, cell lysis of HEK293 cells was completed with a non-denaturing buffer based on Voronkov *et al.*[87]. The non-denaturing buffer had prepared cell lysate that showed bands (without smear) of TNKS1/2. Compared to buffer used by Voronkov, the DNase was added to the non-denaturing buffer used in this study as DNase was not obtainable at the time. Samples of HEK293 and HEK293-EGFP-TNKS1 was also examined for cell lysis by a denaturing RIPA buffer. Denatured proteins were not suited for assessing the CRAM reactors trapping capabilities of TNKS1/2, but was used as an extra control to see if bands of TNKS1/2 could be obtained from the cell material used in the study.

The total amount of protein extracted from approx. 1 million HEK293 and HEK-EGFP-TNKS1 cells are given in **Table 31**, which shows that cell lysis by non-denaturing buffer gives 1.6 times the amount of proteins compared to ultrasonication with water. The RIPA buffer extracted approx. the same amount of proteins from the cells as ultrasonication with water.

In the experiment, both buffers were evaluated concerning their ability to extract TNKS1/2 in an amount and shape that allowed detection of TNKS1/2 bands by WB. Additionally, a CRAM reactor was applied 77.6 µg of protein from HEK293 cells lysed by a non-denaturing buffer.

As elution solvent, 2% FA was selected from the previous experiments and a new denaturing solution consisting of 2% SDS (solution "**#g**" in **Experimental 2.10**, **Table 2**) was used to evaluate the elution of possibly trapped TNKS1/2. If TNKS1/2 was trapped by binding to the LDW639, it was expected that denaturing the protein would release TNKS1/2 from LDW639.

*From visualization in **Figure 76**, TNKS1/2 bands was visible in the cell lysate controls from both HEK293 and HEK293-EGFP-TNKS1 using both a non-denaturing buffer and a RIPA buffer. However, concerning the CRAM reactor, none of the collected fractions showed the presence of TNKS1/2. Actin behaves as expected from previous experiments, and are not present after Wash 2.*

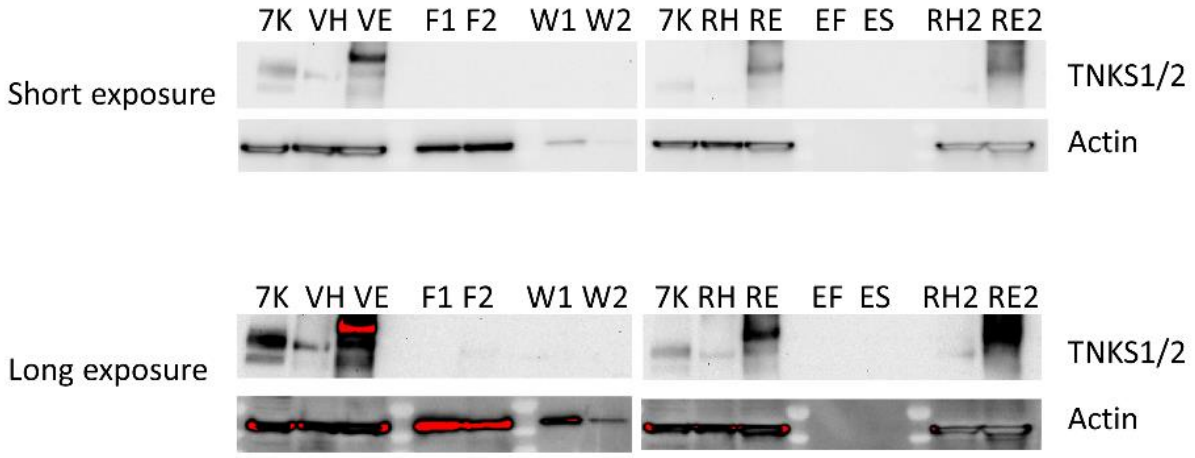

Figure 76: Western blot of: (7K) lane of 21 µg of protein from 007-LK control, (VH) lane of 29 µg of protein from HEK293 and (VE) lane of 23 µg protein from HEK293-EGFP-TNKS1. Samples collected from CRAM reactor in the following lanes: (F1) Flush of 38.8 µg protein from HEK293, (F2) Flush of 38.8 µg protein from HEK293, (W1) Wash 1 with water, (W2) Wash 2 with water, (EF) eluted with 2% FA and (ES) eluted with 2% SDS. Controls from a denaturing buffer: (RH) lane of 18 µg of protein from HEK293 (RE) lane of 10.5 µg of protein from HEK293-EGFP-TNKS1, (RH2) lane of 30 µg of protein from HEK293 and (RE2) lane of 30 µg of protein from HEK293-EGFP-TNKS1. The raw files from WB is given in Appendix 7.10, Figure 86 and Figure 87. The exposure time was 530 s (short exposure) and 5400 s (long exposure) for TNKS1/2 and 150 s (short exposure) and 3600 s (long exposure) for actin.

Table 31: Overview of extracted material from HEK293 and HEK293-EGFP-TNKS1 cell lines with different methods and solvent described in Experimental 2.8.

Method	Solvent	Cell line	#Replicates	Total amount of protein
Ultrasonication	6 M urea in 100 mM ABC	HEK293	3	138 µg ± 13 µg
Ultrasonication	Water	HEK293	3 6 Total 9	274 µg ± 14 µg 310 µg ± 69 µg 298 µg ± 58 µg
Lysis buffer	Non-denaturing	HEK293	3	478 µg ± 19 µg
Lysis buffer	Denaturing RIPA buffer	HEK293	1	312 µg
Ultrasonication	6 M urea in 100 mM ABC	HEK293-EGFP-TNKS1	3	104 µg ± 4 µg
Ultrasonication	Water	HEK293-EGFP-TNKS1	3	217 µg ± 22 µg
Lysis buffer	Non-denaturing	HEK293-EGFP-TNKS1	3	398 µg ± 4 µg
Lysis buffer	Denaturing RIPA buffer	HEK293-EGFP-TNKS1	1	180 µg

7.8.1 Examining loss of proteins due to application by syringe and polyetheretherketone sample loop

In a final attempt to assess why TNKS1/2 was not present in any of the collected fractions from the CRAM reactors or the MEA reactors; the total amount of protein was examined at different parts of the application system. The experiment was carried out to assess if TNKS1/2 could be lost prior to application onto the reactors.

The system used for application, described in **Experimental 2.10** was a closed system. The points where TNKS1/2 could be lost was in the syringe, the 6-ports valve and the PEEK sample loop. To evaluate if TNKS1/2 was lost, cell lysate was collected, from the first and second time the syringe was filled with cell lysate. Additionally, during filling of the sample loop with the syringe, cell lysate was collected. Lastly, a fraction was collected when the sample loop was filled with cell lysate and flushed with water from the syringe. The amount of protein found in the samples is given in **Table 32**, showing that the concentration of the samples is reduced after being in the syringe compared to the cell lysate transferred with a pipette (samples used as

controls in the WB procedure were prepared with a pipette). The concentration is not affected by the sample loop.

The syringe used in the experiments with cell lysate was a 250 µL glass syringe. Approx. 70 µL of cell lysate was filled in the syringe the second time, and the concentration of protein in the sample collected was 1.28 µg/µL. Compared to the concentration in the cell lysate transferred with a pipette 1.41 µg/µL, the sample from the syringe was diluted with 10% equivalent to 7 µL. The 0.50 mm outer diameter x 50 mm needle tip equals a maximum volume of 9.8 µL. The actual volume is not known as the inner diameter of the tip was not stated. However, it makes it probable that the measured dilution was due to the volume of the needle tip. WB of the same type of samples could have been examined for TNKS1/2 to be certain TNKS1/2 was not lost during application.

Table 32: Amount of protein found per µL sample. Method for sample collection is described in the first column.

Description of sample	Amount of protein found per µL sample
Cell lysate transferred by pipette.	1.41 µg/µL
Cell lysate collected from syringe after wash with MeOH and water.	1.15 µg/µL
Cell lysate collected from syringe after wash with cell lysate.	1.28 µg/µL
Cell lysate collected from loop, letting 20 µL pass first and collected the next 20 µL. Total of 60 µL cell lysate applied onto loop.	1.25 µg/µL
Cell lysate collected from loop, by flushing out with water.	1.27 µg/µL

7.9 Measuring total amount of protein in cell samples after cell lysis

The amount of protein in a lysed cell sample was measured using a calibration curve. The absorbance at 562 nm for BCA, a standard protein, was measured at six different total amounts of protein as shown in **Table 33**. The calibration curve was established as shown in **Figure 77**. The equation of the curve was found by extrapolation (*i.e.* adding a trendline in EXCEL), and the amount of protein in the unknown samples was calculated from the equation.

Table 33: The measured absorbance of the BSA, at different total amount of protein, at 562 nm. Number of replicates was three.

Replicate µg protein	1	2	3
0	-0.006	-0.009	-0.01
2	0.059	0.097	0.103
4	0.184	0.206	0.198
6	0.277	0.278	0.262
8	0.354	0.338	0.334
10	0.421	0.398	0.399

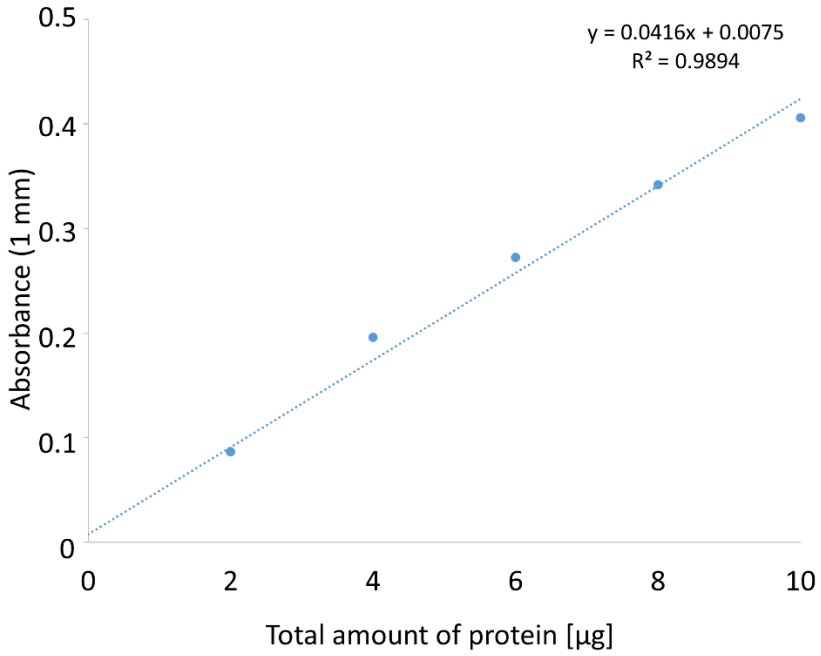

Figure 77: Calibration curve found by plotting total amount of protein against absorbance and adding a trendline, with equation and R-squared value.

7.10 Raw files from western blot analysis

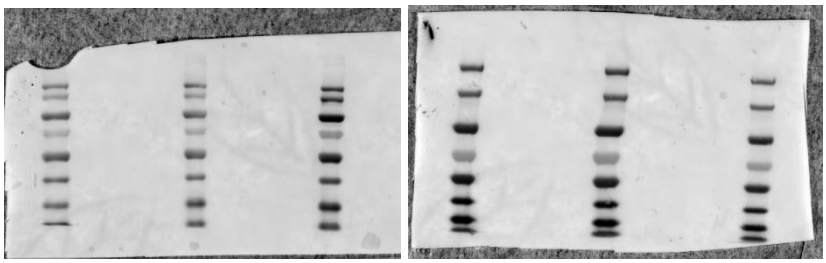

Figure 78: Protein ladder run on: (Left) a 4-12% bis-tris gel with MOPS running buffer, from the top the bars marks 140, 115, 80, 65, 50, 40, 30 and 25 kDa. (Right) a 3-8% tris acetate gel with tris acetat running buffer, from the top the bars marks 150, 120, 85, 65, 50, 40, 30, 25 kDa.

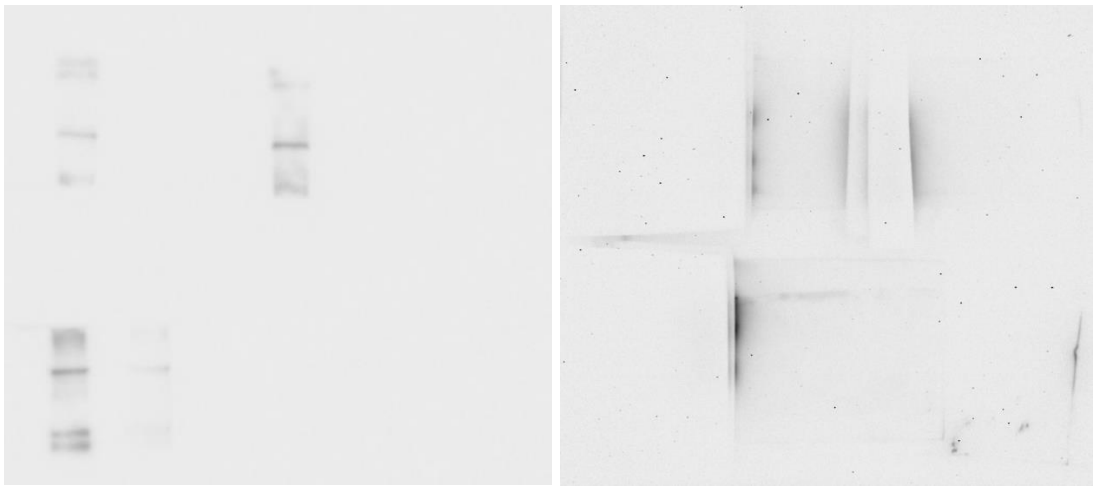

Figure 79: Western blot of recombinant TNKS2 standard: (Left) Short exposure) and (Right) long exposure). The membrane on top was blotted upside down. (Figure 70).

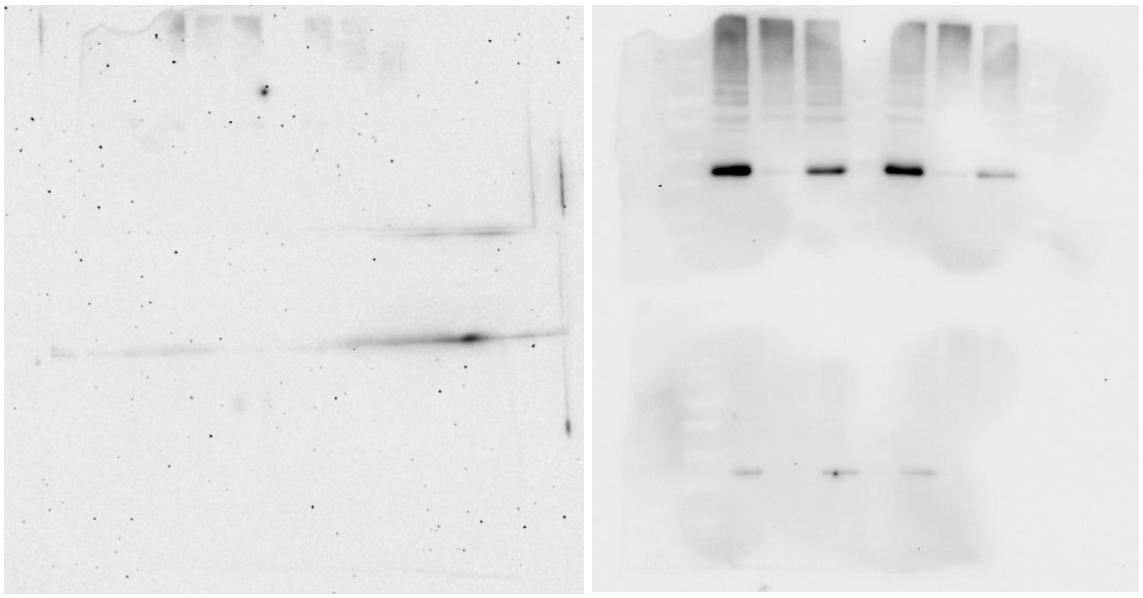

Figure 80: Western blot of cell lysate of HEK293, visualized for TNKS1/2 (Left) and for actin (Right). (Figure 72).

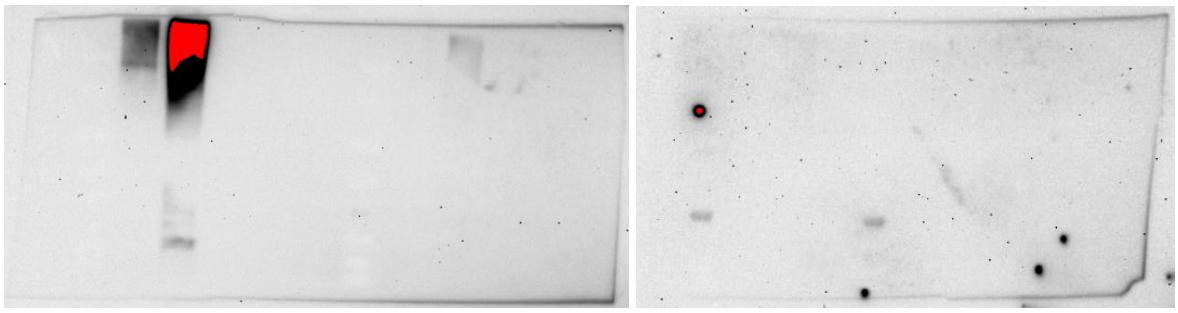

Figure 81: Western blot of cell lysate of HEK293 and HEK293-EGFP-TNKS1. Additionally HEK293 was applied on three types of reactors: CRAM reactor, MEA reactor and CRAM reactor flushed with MEA. Visualized for TNKS1/2, (Figure 73).

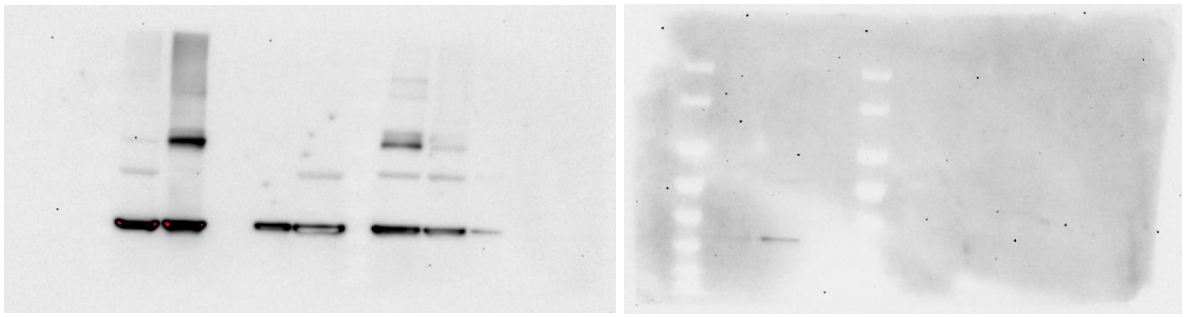

Figure 82: Western blot of cell lysate of HEK293 and HEK293-EGFP-TNKS1. Additionally, HEK293 was applied on three types of reactors: CRAM reactor, MEA reactor and CRAM reactor flushed with MEA. Visualized for actin, (Figure 73).

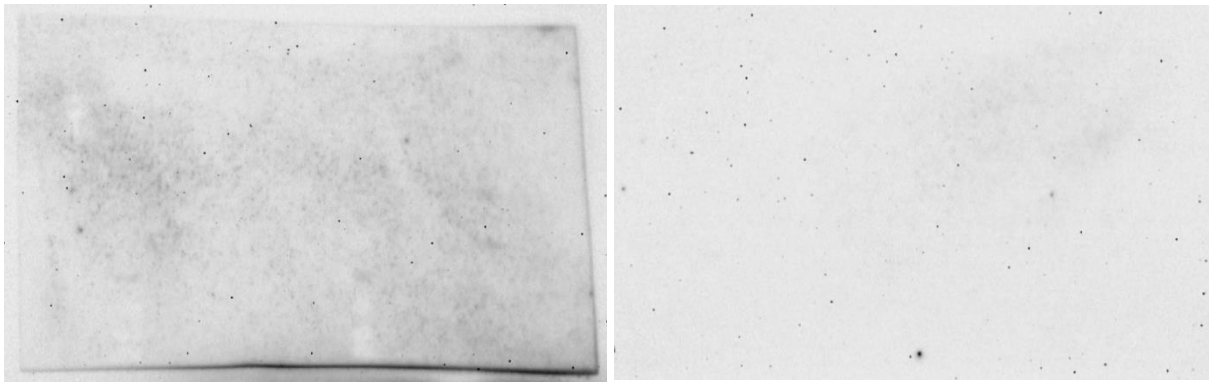

Figure 83: Western blot of cell lysate of HEK293. Additionally, HEK293 was applied on new CRAM reactor and TNKS1/2 was attempted eluted from old reactors (from Figure 81) and the new reactor with different elution solutions. Visualized for TNKS1/2, (Figure 74).

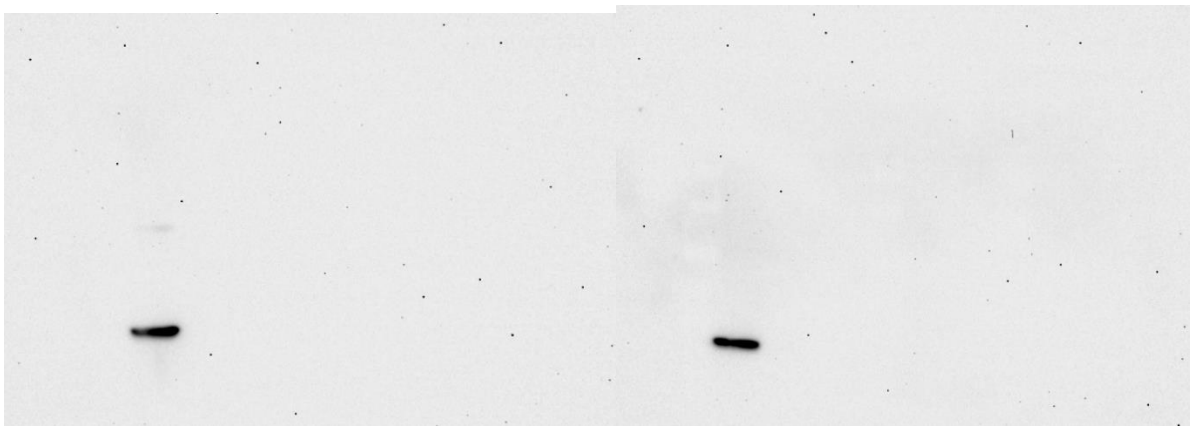

Figure 84: Western blot of cell lysate of HEK293. Additionally, HEK293 was applied on new CRAM reactor and TNKS1/2 was attempted eluted from old reactors (from Figure 81) and the new reactor with different elution solutions. Visualized for actin, (Figure 74).

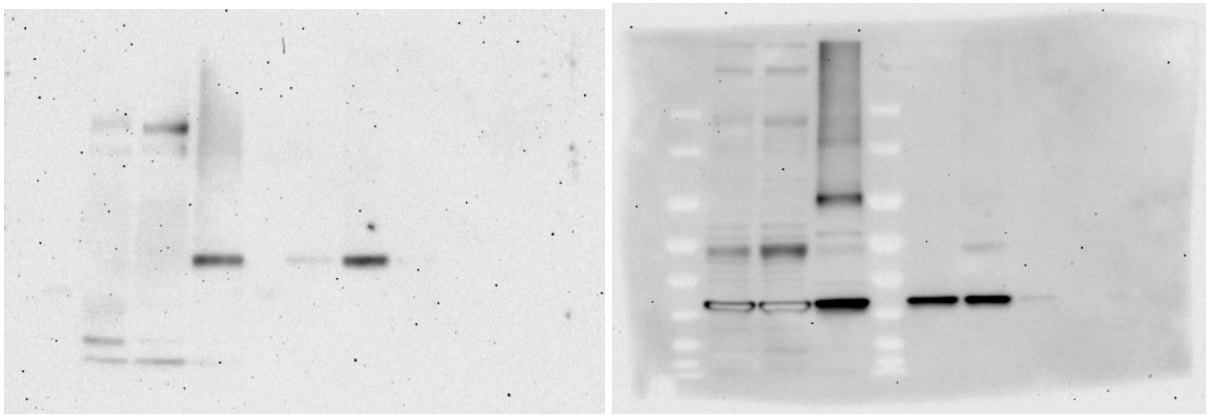

Figure 85: Western blot of cell lysate of HEK293-EGFP-TNKS1 with positive controls DMSO and 007-LK. Additionally, HEK293-EGFP-TNKS1 was applied on new CRAM reactor. Visualized for TNKS1/2 (Left) and actin (Right), (Figure 75).

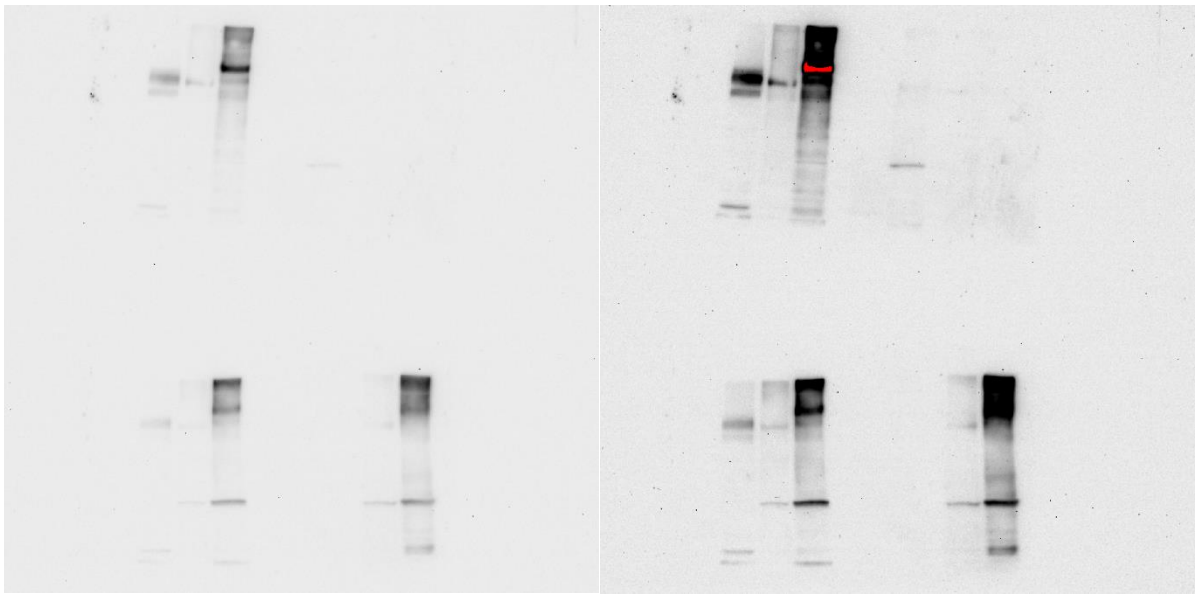

Figure 86: Western blot of cell lysate of HEK293 and HEK293-EGFP-TNKS1 with positive control 007-LK and control over cell lysis with RIPA buffer. Additionally, HEK293 was applied on new CRAM reactor. Visualized for TNKS1/2, short exposure (Left) and long exposure (Right), (Figure 76).

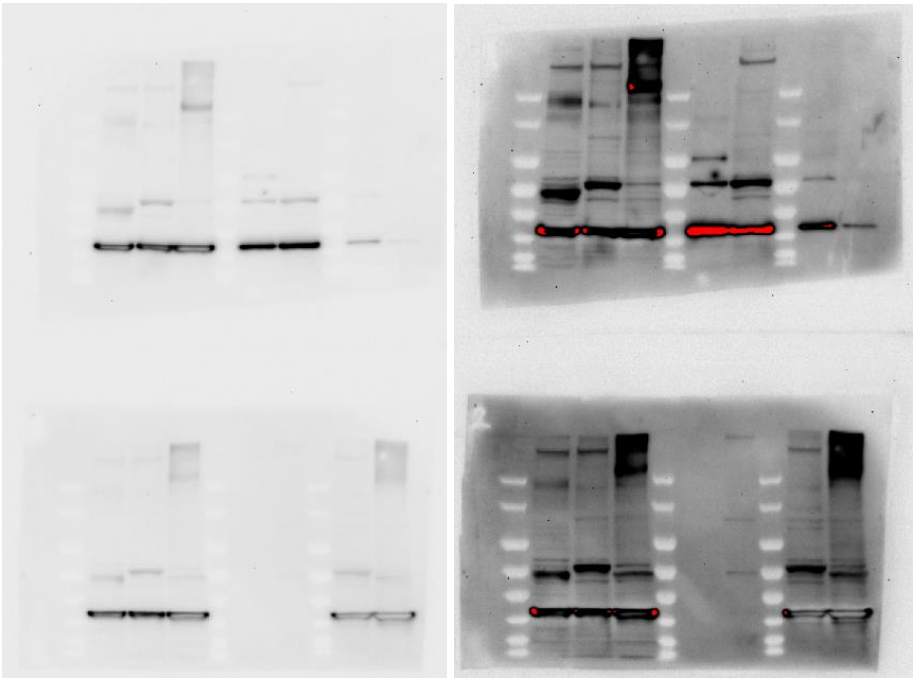

Figure 87: Western blot of cell lysate of HEK293 and HEK293-EGFP-TNKS1 with positive control 007-LK and control over cell lysis with RIPA buffer. Additionally, HEK293 was applied on new CRAM reactor. Visualized for actin, short exposure (Left) and long exposure (Right), (Figure 76).

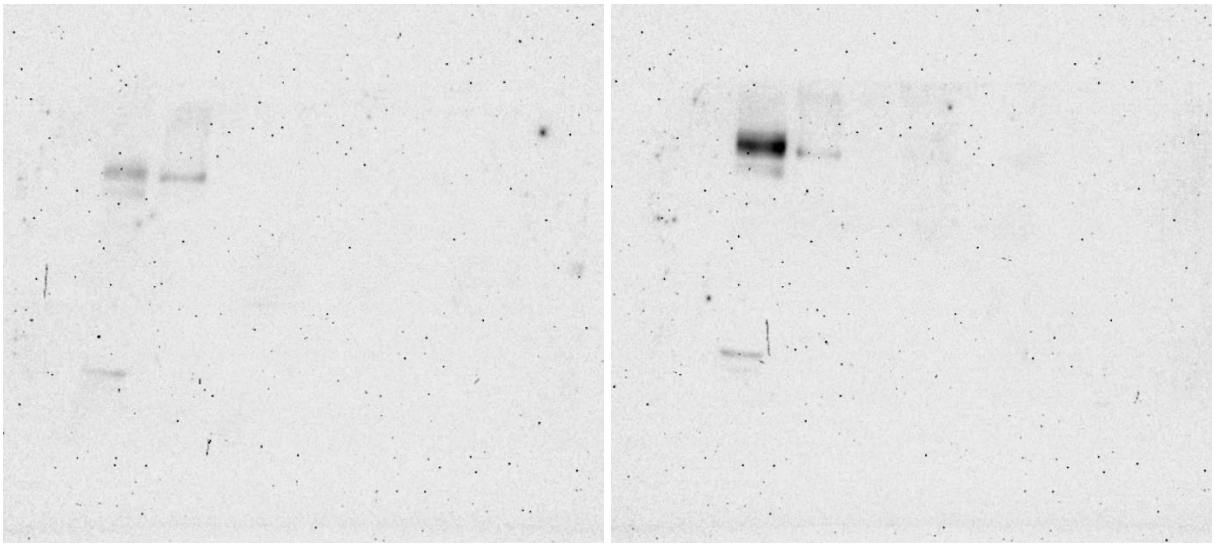

Figure 88: Western blot of cell lysate of HEK293 and positive control 007-LK Additionally, HEK293 was applied on new CRAM reactor and a MEA monolith. Visualized for TNKS1/2: (Left) CRAM reactor and (Right) MEA monolith, (Figure 51).

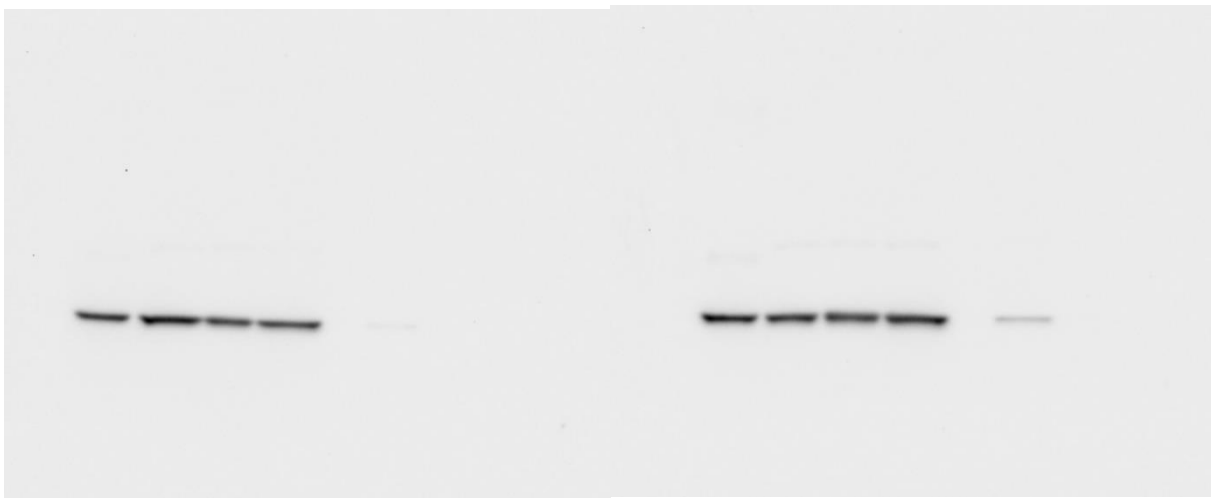

Figure 89: Western blot of cell lysate of HEK293 and positive control 007-LK Additionally, HEK293 was applied on new CRAM reactor and a MEA monolith. Visualized for actin (short exposure): (Left) CRAM reactor and (Right) MEA monolith, (Figure 51).

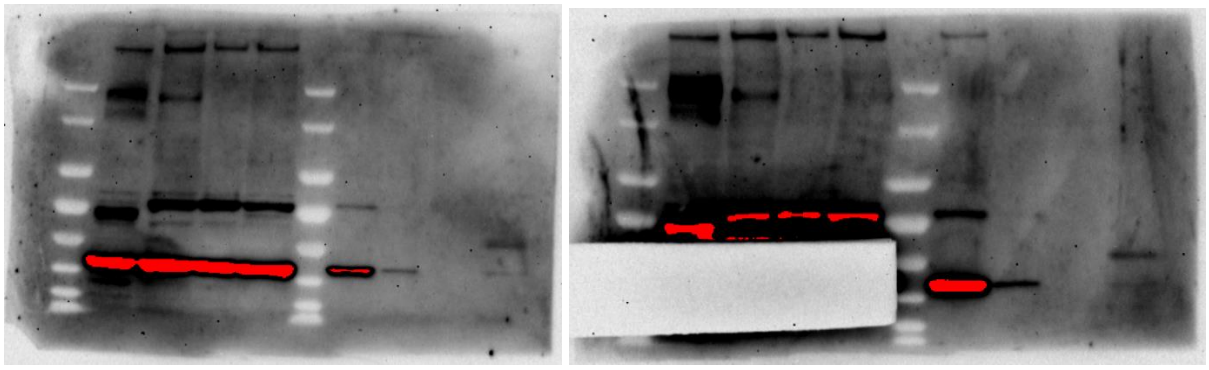

Figure 90: Western blot of cell lysate of HEK293 and positive control 007-LK Additionally, HEK293 was applied on new CRAM reactor and a MEA monolith. For the MEA monolith the following lanes were covered: positive controls of 007-LK and cell lysate, and Flush 1 and 2. Visualized for actin (long exposure): (Left) CRAM reactor and (Right) MEA monolith, (Figure 51).